THE IMPROVEMENT OF WIND TUNNEL DIFFUSER CHARACTERISTICS

By

HENRY G. WEBB JR.

B.Ae.E., Rensselaer Polytechnic Institute
1942

and

JOSEPH E. ZUPANICK

B.S. University of Pittsburgh
1943

SUBMITTED IN PARTIAL FULFILLMENT OF THE
REQUIREMENTS FOR THE DEGREE OF
MASTER OF SCIENCE
IN
AERONAUTICAL ENGINEERING

From the
MASSACHUSETTS INSTITUTE OF TECHNOLOGY
1949

Signature of Authors:

Henry G. Webb Jr.

Joseph E. Zupanick

Certified by:

Department of Aeronautical
Engineering, Sept. 2, 1949

Chairman, Department Committee on
Graduate Students

Sept. 2, 1949

Prof. Joseph S. Newell
Secretary of the Faculty
Massachusetts Institute of Technology
Cambridge 39, Massachusetts.

Dear Professor Newell:

In accordance with the requirements of the faculty, we hereby submit a thesis entitled,

THE IMPROVEMENT OF WIND TUNNEL
DIFFUSER CHARACTERISTICS

in partial fulfillment of the requirements for the Degree of Master of Science in Aeronautical Engineering.

Henry G. Webb, Jr.

Joseph E. Zupanick

ACKNOWLEDGMENT

The authors wish to express their appreciation and sincere thanks to the following persons who were of assistance in the preparation of this thesis.

To Professor Joseph Bicknell for giving us the opportunity of working on the project and his suggestions during the course of the work.

To Mr. Harry Hilberg of the Wright Brothers Wind Tunnel Staff for his aid in the construction of the equipment and in obtaining necessary test equipment. Also to Mr. J.R. Maddox of the Aeronautical Machine Shop for his splendid cooperation on the machine work involved during the project.

To the sponsors of the Diffuser Research Project for making the funds available for the construction of the equipment.

To the typist Eleanor Mugnai for her work performed on the Vari-Typer.

TABLE OF CONTENTS

I PURPOSE

This experimental investigation was conducted primarily to determine the effect of freely rotating windmills on the space and time variations of velocity in a model of the Wright Brothers Wind Tunnel diffuser. It is required to determine both the optimum position and blade configuration of the windmill to give the lowest turbulence level and most uniform velocity distribution at the diffuser exit.

A further characteristic to be considered is the energy loss associated with each diffuser windmill. Thus a comparison of windmills with damping screens or other devices capable of producing the improvements mentioned above may be made.

II SUMMARY

The installation of several types of freely rotating windmills in two positions in a model of the Wright Brothers Wind Tunnel diffuser was tested. It was found that the velocity distribution, turbulence, and energy losses could all be reduced by the proper selection of windmill location and blade form. No single configuration was optimum for the simultaneous achievement of all three effects.

A description of the methods employed to study the diffuser characteristics is given. Data are presented for the velocity distributions in the form of contour plots of the q ($\frac{1}{2}\rho U^2$) variation at the tailpipe exit, and also as a weighted variation with duct radius. Turbulence measurements are given as quantitative results, but attention is called to the inaccuracies involved in their determination. Diagrams illustrating the behavior of tufts placed on the diffuser and tailpipe walls are included. The interpretation of a modified diffuser efficiency, used to estimate energy losses, is explained.

Specific conclusions to be drawn from these tests are made and recommendations for further investigation are given.

III INTRODUCTION

The work contained herein is an experimental investigation of the effects of a windmill, placed in a diffuser, on the velocity distribution and turbulence level of the stream.

The existing problem that brought the work in this thesis about was that the flow in the Wright Brothers Wind Tunnel is of such a nature as to produce undesirable eddies. It is these eddies that make it impossible to have the uniform and steady stream required for the testing of flutter models, although the flow is satisfactory for the present type of testing in which a rigid model is completely restrained. This problem is discussed by R.A. Summers, ref. 5.

The standard method of attacking the problem is by placing a honeycomb or a series of damping screens at or near the maximum section. The damping screen with a uniform pressure drop coefficient reduces the velocity variations of the stream of fluid passing through it, since the resistance is proportional to the square of the local wind velocity, the high speed areas therefore losing more total head than the low speed regions. The flow is thereby improved in two respects, the variation in velocity across the section is reduced along with decreasing the turbulent motions of large scale by reducing them to motions of smaller scale. The effect of damping screens on wind tunnel turbulence has been investigated by H.L. Dryden and G.B. Schubauer, ref. 6.

Since the speed in the maximum section is relatively low, the amount of energy dissipated by the screen is reduced to a minimum. Nevertheless, it is more efficient to adopt a device which transfers excess energy from high speed regions to the low speed regions as required. In addition to 'smoothing' out the flow in this manner the velocity in the boundary layer can be speeded-up to delay and possibly prevent seperation where the flow is subjected to a positive pressure gradient, such as in a diffuser.

A windmill of appropriate design, placed in a diffuser and allowed to rotate freely is one such device capable of producing the same effects as the damping screen. The windmill is driven by the high speed regions and drives the low speed regions producing an even velocity distribution. It acts on the turbulence in a manner analogous to a rotating cutter. If a piece of wire fed into the cutter were such that the blade came around at the same time the cut in the wire did the resulting pieces would be the same as the ones fed in. If the same rate of feed was kept and the cutter rotated faster the resulting pieces would be smaller. Similarly, in the case of the windmill the resulting turbulence is a function of what goes into the windmill and the R.P.M. of the windmill

There occurs two classes of turbulence, generally termed 'coarse grained' and 'fine grained'. The wind mill reduces the 'coarse grained' turbulence but allows the 'fine grained' turbulence to pass through unaffected. The blade pitch of the windmill is analogous to the mesh of the damping screen in differentiating between the scale of turbulence which will be reduced and that which will not.

The use of a windmill to improve the flow has not been employed to any great extent. The only report available on the subject is by A.R. Collar, ref. 3. Most of the work is theoretical and assumes a small steady variation from a uniform velocity distribution. Very little test data is presented.

IV DESCRIPTION OF APPARATUS

A. The Tunnel and Diffuser.

The tunnel and diffuser, TD in notation, is comprised of and assembled in following order: the blower, the expansion section, the setting chamber, the bell mouth, the 15 inch constant section, the diffuser, and the 22.3 inch constant section tail pipe, figures 66, 56, 57 and 58.

The power source for the tunnel is a centrifugal blower. It is an American High Speed Blower, No. 245 and rated at 11,000 cubic feet per minute. The tunnel was run at a constant R.P.M. of 1780, since the driving motor is a 3 phase induction motor. The outlet of the blower is a rectangular section of 19 x $26\frac{1}{8}$ inches with the centrifugal impeller offset to the right viewing into the stream.

To prevent blower vibrations from being transmitted, a gap of ½ inch exists between the blower and the expansion section. The flexible seal, figure 57, between these two is made with a strip of $\frac{1}{8}$ inch by 4 inch rubber bolted to the flange of the blower and to the flange of the expansion section. To improve the irregular velocity distribution produced by the blower a series of 6 screens, 16 mesh and .009 inch dia, are evenly spaced in the expansion section, figure 66. A series of tufts were tied to the last screen in this section. The construction of the expansion section is of $\frac{3}{4}$ inch plywood and tapers from a 19 x $26\frac{1}{8}$ inch rectangular blower outlet to a regular octagon, 4 foot across flats at the settling chamber.

The settling chamber is also of $\frac{3}{4}$ inch plywood construction with a tuft observation port of 8 inches by 12 inches and a circular port on the top for the light source. The four static holes are located on the vertical and horizontal centerline of the regular octagon at station 1, given by figure 66.

The bell mouth and all of the tunnel aft is constructed of .042 inch gage steel with welded joints on each particular

section. The contraction cone surfaces are not completely satisfactory because of warping and generally poor fabrication.

The 15 inch constant section contains 4 static holes equally spaced on the periphery at station 2, given by figure 66.

This section and the 4½° half angle diffuser section are a scaled down model of the Wright Brothers Wind Tunnel. Due to the lack of rigidity of the gage of the metal a plywood frame was used to bring the diffuser section into round at the windmill.

B. Nacelles.

The forward nacelle, figures 59 and 67, is a scale model of the Wright Brothers Wind Tunnel fan drive motor fairing and supports. A scaled down model of the propeller in the full size tunnel is not present in this set up, since the blower produces the stream in this case. A cone at the end of the nacelle is removable to take the ½ inch shaft of the windmill hub, figure 66 and 71.

The aft, nacelle, figure 68, does not exist in the Wright Brothers Tunnel but is used here as a mount for the large aft windmill.

C. Windmills.

The forward and aft windmill are very similar except in chord and diameter of the blade figures 69 and 70. The blades are made of $\frac{1}{16}$ inch 17ST dural having a constant chord, with the leading edge rounded and the trailing edge tapered. The width of taper being about 15% of the chord. The blades are riveted to a threaded steel shank which in turn mounts into the wind mill hub, figure 71. This one hub is used for both the forward and aft windmills. The twist was put into the blades by the device shown in figure 65. This allows for a given increment of twist per inch of the blade. The total twist was then checked with the protractor arrangement of figure 60, which was also used to set the blade angle for the various configurations.

The windmills are tested with their respective nacelles.

D. Damping Screen.

An 18 mesh .010 inch diameter screen S was tacked to the $\frac{3}{4}$ inch plywood frame at the end of the tailpipe. One run was made with this configuration to determine the effects of screen on turbulence.

E. Instrumentation.

1. Pressure measurements.

The velocity distributions ahead of the forward nacelle were obtained by a pitot static tube mounted on the survey rake, pitot tube and wind direction indicator support, figure 66. The diffuser and tail pipe were removed for these readings. The data for the velocity distributions was obtained from a 31 tube survey rake, figure 63 and 72. The 29 total head tubes and 2 static tubes were connected to a vertical alcohol manometer board, all pressures being measured relative to atmospheric pressure. The scale is calibrated in inches of water. The average velocity was obtained from readings of the four static holes in the settling chamber, figure 66 and the four static holes in the 15 inch constant section, figure 66 and 58, connected to the same manometer board as the survey rake.

2. Wind Direction Indicator

By following the variations in flow direction, a vane direction indicator can be used to measure the large scale disturbance in the flow. The definition of turbulence shall, for the purposes of this report, be interpreted as including these large scale disturbances.

After several attempts to build a single vane indicator with an oil damper proved unsuccessful because of the large effect of temperature on the oil viscosity, an indicator employing only aerodynamic damping was decided upon. This would have the added advantage of a damping ratio independent of air speed. A disadvantage is that a low damping ratio must be used if the natural frequency is to be high

enough to respond to a reasonable range of disturbance frequencies.

The final design, fig. 73, described more fully in Sec. IX-C had stability up to a deflection of about 40°, above which the indicator was slightly unstable.

The three vanes are made of .005 inch brass shim stock while the supports are of hollow stainless steel tubing .034 inch outside diameter. The vertical pivot is .020 inch dia. piano wire with conical tips. The indicator is assembled by soldering and is mounted in a fork with two adjustable screws that hold, act as bearings for the pivot, fig. 64 and 73.

3. Tuft Studies

A series of 2 inch tufts were attached with scotch tape to the surface of the diffuser and tailpipe, fig. 62. With the large windmills installed on N_2 it was necessary to use the Strobotac-Strobolux apparatus to see the tufts in the diffuser, especially for the high windmill speeds.

4. Miscellaneous

The windmill speeds were measured with a General Radio Co. Strobotac-Strobolux for references purposes. For the same reason the ambient air temperature and atmospheric pressure were recorded for each run made. These data, together with all pressure measurements etc. are on file at the Wright Brothers Wind Tunnel.

V TEST PROCEDURE

A. Pressure Measurements and Windmill Speed

Before any runs were made all connections, from the tunnel static orifices, pitot tube, and rake, to the manometer board were checked for leaks.

With the single pitot tube installed on the support traverses in four directions were made for a complete survey of velocity at the end of the 15 inch dia. constant area section. Dynamic pressure heads were recorded and corrected for instrument error.

The variation of static pressure over the cross section of the tailpipe exit was checked with the single pitot tube. Since the variation was found to be small all subsequent runs were made with the survey rake incorporating two static pressure tubes. The position of the static holes was adjusted till the error caused by proximity to the adjacent total head tubes was eliminated.

After allowing the motor to accelerate to normal running speed on 220 V. the windmill rotational speed was taken with a Strobotac-Strobolux. The hub and one blade were marked to allow quick determination of the true speed. Pressure readings were then taken. The total head orifices on the rake were approximately 1 inch inside the tailpipe for most runs, but with the large downstream windmill installed some pressures were taken with the rake pushed inside the tailpipe up almost to the windmill. No trouble was experienced with vibration of the rake in either position due to the rigidity of the mount. The alcohol level in the manometer was adjusted till the tube connected to atmospheric pressure read zero. All heads were measured to the nearest .01 inch water. The rake was set at four angles from the horizontal, -45°, 0°, + 45°, and 90°, and pressure heads were read and recorded individually. Thus a time average pressure was measured. If the flow was very unsteady each reading might take as long as 10 seconds, but usually all heads were

read for each rake position in about 35 seconds. Since the centerline total head was read four times during each run the time variation of the average flow velocity could be checked over this time interval. The variation was found to be negligible. The pressure heads are not corrected for temperature variation of alcohol density, since the correction would be small, and the increased accuracy is not required.

B. Wind Direction Measurements

The axis of rotation of the indicator was vertical for all readings taken. The average and maximum angular deflections of the indicator were estimated visually. By viewing the instrument from above, with proper lighting, the movement can be read by reference to the protractor built into the instrument. The instrument oscillated most frequently at its natural frequency, although oscillations of lower frequency were readily detected.

To illustrate the reasoning behind finding a time average deflection the following simple case may be taken. If the vane oscillated sinusoidally with a constant amplitude of $\pm$ 10°, the time average deflection would be $(\frac{2}{\pi})(\pm 10°) \simeq \pm$ 6°. If the indicator movement is composed of many superposed and varying oscillations the process is not as simple, but with practice a fairly accurate estimate can be made. The time interval used for the averaging was approximately 10 seconds. As pointed out elsewhere in this report the deflections presented herein are not to be interpreted as true flow direction variations, but are useful only in comparing different configurations.

Readings were taken with the instrument at the following positions,

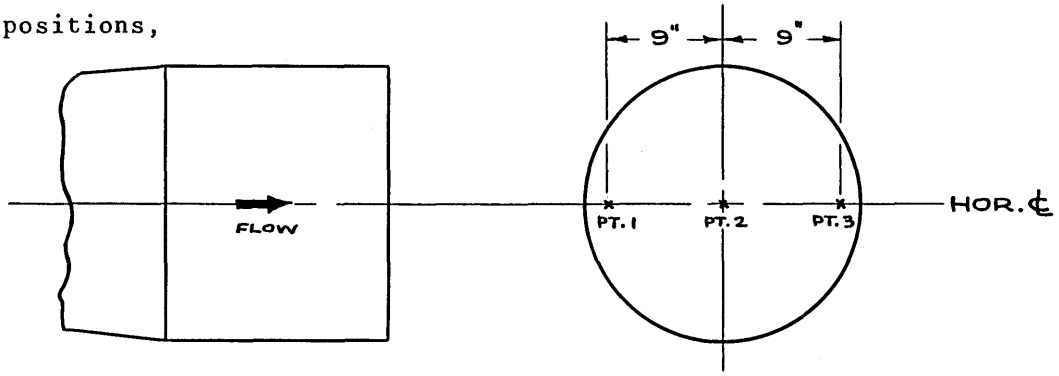

C. Tuft Studies

By means of tufts placed in the diffuser and tailpipe the type of flow along the wall was placed in one of the three following categories,

1. Relatively smooth
2. Rough, unseparated but with considerable large scale turbulence
3. Separated

VI TEST RESULTS AND DISCUSSION

A. Velocity Surveys

Fig. 1 shows a nearly uniform velocity distribution at the diffuser inlet. The velocity decreases more rapidly near the wall on the left side, facing upstream. Whether this is due to the slightly irregular fairing of the bell mouth or to the eccentric outlet from the centrifugal fan is uncertain. The result is that the flow tends to separate more readily on this side of the diffuser

The data obtained from the rake survey at the end of the tailpipe has been plotted directly on the curves in the Appendix. To show more readily the effect of the fans on the q distribution the data has been plotted on fig. 2 through fig. 6 as a ratio of a weighted, or average, q to the mean q. This weighted q or q_{2D} is a quantity dependent on the radius from the duct centerline, but not on an angular position from the horizontal reference line as is the data presented in the Appendix. The equation used to calculate q_{2D} at any radius r is,

$$q_{2D} = \left[\frac{\sum_n \left(h - \frac{\sum p}{n}\right)^{1/2}}{n} \right]^2 \qquad (1)$$

where n = 8, the number of pressure heads obtained at the radius r. This equation satisfies the continuity of mass, but introduces a slight error by not satisfying the equation for conservation of energy. The quantity $\bar{q}$, or the mean q is calculated from Eqn. 14.

Fig. 2 shows clearly the great change in the velocity distribution caused by the small windmill F_1. At the low blade angles considerable energy is transferred from the center of the duct to regions near the wall. Unfortunately the section of the blade near the hub is stalled at these high rotational speeds thus increasing the energy losses.

To reduce the energy loss caused by blade stalling the blades were twisted to give the small windmills F_3 and F_5, fig. 8.

With a twisted blade the effect of a change in blade angle setting is much less than that for an untwisted blade. This is shown clearly in fig. 4. The twist of F_5 is intermediate between a uniform twist, as for F_3, and a helical twist. The results obtained from F_3 and F_5 show that when the blade twist is close to that of a helix a change in pitch distribution has a smaller effect on the blade loading distribution than for an untwisted blade. For this reason an analysis of the windmill by any form of the blade element propeller theory will lead to large errors.

From a consideration of the weighted q distribution either of the three windmills mounted on the upstream nacelle N_1 will produce a fairly uniform average velocity distribution. The blade angle setting required for the best average distribution is such that the flow still separates or approaches separation in the diffuser and so the actual distribution is still not too satisfactory.

The action of the windmills mounted at the downstream end of the diffuser is quite different. Here the windmill operates in a flow having reached its greatest diviation from a uniform velocity, and the tailpipe following immediately behind the windmill helps further to give a uniform velocity distribution. Windmill F_2 has much the same effect as F_1 but the wake behind the hub and stalled section of the blades is more noticeable. With F_4 this loss is eliminated and a good velocity distribution is obtained both as a weighted average and as an actual distribution for a blade angle of about 20° as shown by fig. 6 and fig. 53.

B. Pressure Recovery

The pressure recovery is a measure of the efficiency of conversion of kinetic energy to potential energy. As such it reflects both the relative magnitude of the total head loss in the diffusion process, as well as the loss of static pressure head rise caused by a non-uniform velocity distribution at the tailpipe exit.

From fig. 7 it is seen that the tailpipe increases the pressure recovery by about 6%. This is due to the improvement in

velocity distribution. The possible further increase in pressure recovery if the velocity distribution were uniform is only about 3%. Thus the values of pressure recovery at the tailpipe exit reflect primarily the total head loss in the diffuser and tailpipe. This loss is caused by skin friction on the duct wall, eddy losses, and similar losses associated with the nacelle-fan group.

Windmill F_1 decreases the losses at large blade angle settings by reducing the eddy losses, but loses its effectiveness at low blade angles due to stalling of the fan. Since windmill F_2 has a limited effect on the diffuser flow it has an adverse effect at all blade angle settings due to stalling near the hub and blade root. All twisted blades on the other hand eliminate this windmill loss, and reduce the other losses considerably at low blade angles, F_4 having less effect than either F_3 or F_5.

The large drop in pressure recovery due to N_1 is apparent. This is caused by separation on the aft portion of the nacelle and by earlier separation of the flow on the diffuser wall. The windmill has little effect on the losses associated directly with the nacelle.

C. Turbulence

The direction indicator, fig. 73 which is described in Sect. IV-E-2 and IX-C gives a visual indication of low frequency turbulence. The intensity of turbulence can be reduced by eliminating separation in the diffuser wall, as well as by promoting dissipation of the turbulence by reducing its scale by means of the windmill. Furthermore by smoothing out large scale turbulence the action of the windmill might be compared to that of a flywheel in smoothing out an engine's torque.

By preventing separation in the diffuser, windmill F_1 reduces the turbulence up to a point where the blade stalling begins to increase it again. This latter effect is more apparent on the duct centerline, ref. fig. 10. Fig. 11 shows that the results obtained from F_5 are slightly better than with F_1, due chiefly to the absence of blade stalling. The damping screen added to the reduction of turbulence for the few configurations

tested. As shown in fig. 12, windmill F_2 at the end of the diffuser has little net effect on the turbulence since the decrease due to improved flow in the diffuser is offset by the increased turbulence generated by the blades. Windmill F_4, being twisted to a regular helix, gives a marked decrease in turbulence, although not as much as that given by F_1 or F_5, since the diffuser separation is not completely eliminated.

D. Tuft Studies

The flow along the diffuser and tailpipe wall can be studied by tufts. The motion of the tuft indicates whether the flow has separated from the surface or is about to separate.

The flow is quite good with the large nacelle N_1 out. With N_1 in the flow separates badly. This is improved greatly with the small windmill F_1 at low blade angles, no separation being seen. The flow is almost equally smooth at low blade angles with windmill F_5. The improvement in flow with F_2 and F_4 is not as great, considerable separation occurring on the left side of the diffuser.

From a consideration of the tuft studies, turbulence, and pressure recovery, it is apparent that the drag of nacelle N_1 is the largest component of the diffuser head loss. The use of windmills does not reduce this loss, but does decrease losses by reducing separation in the diffuser. The turbulence created by N_1 and that associated with flow separation in the diffuser can be reduced by the proper choice of windmill.

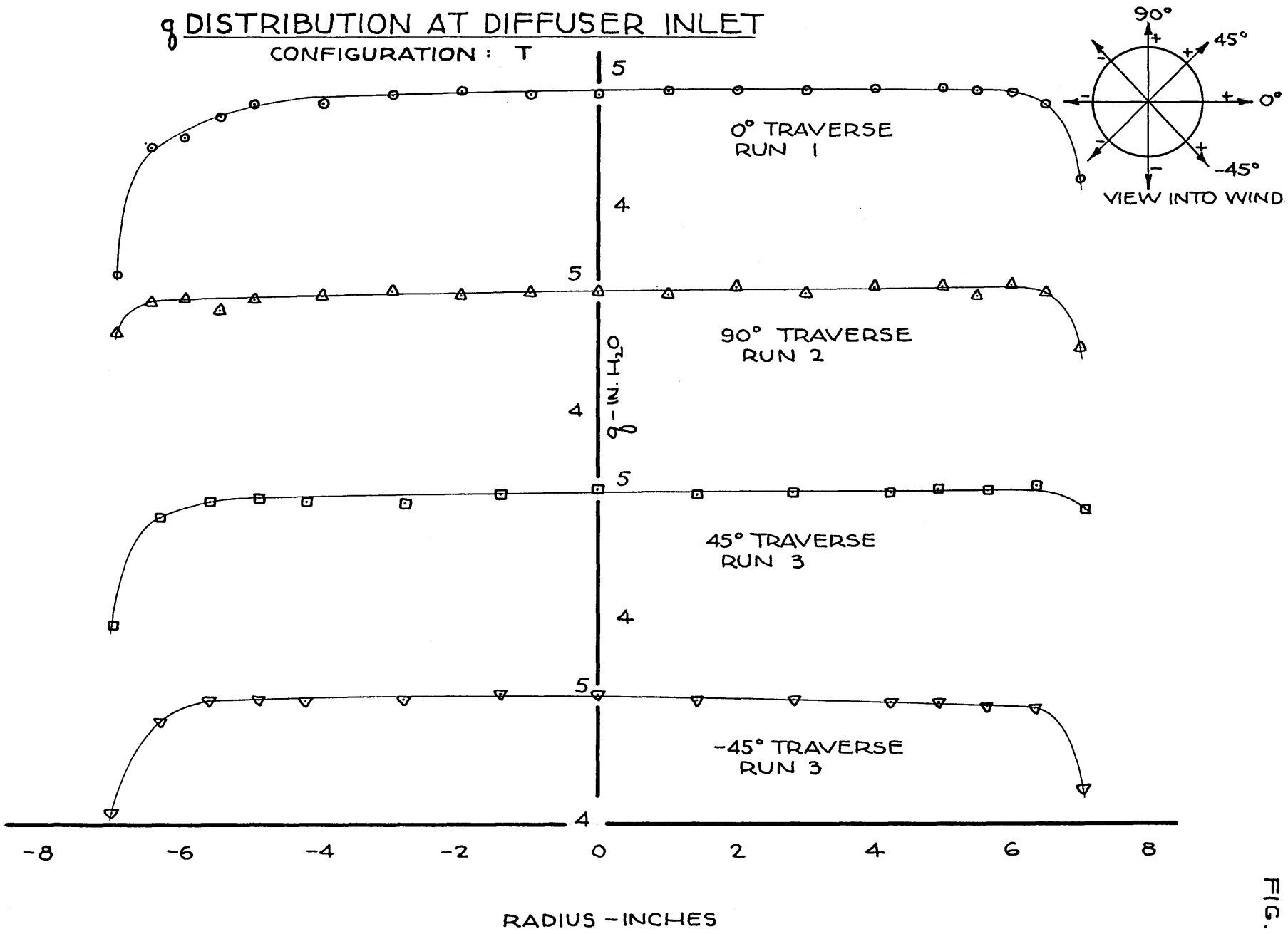
q DISTRIBUTION AT DIFFUSER INLET
CONFIGURATION : T
90°
45°
0°
-45°
VIEW INTO WIND
0° TRAVERSE
RUN 1
90° TRAVERSE
RUN 2
45° TRAVERSE
RUN 3
-45° TRAVERSE
RUN 3
q - IN. H2O
5
4
-8
-6
-4
-2
0
2
4
6
8
RADIUS - INCHES

FIG. 1

AVERAGE VELOCITY DISTRIBUTION AT END OF TAILPIPE

CONFIGURATION : TDN, F_1

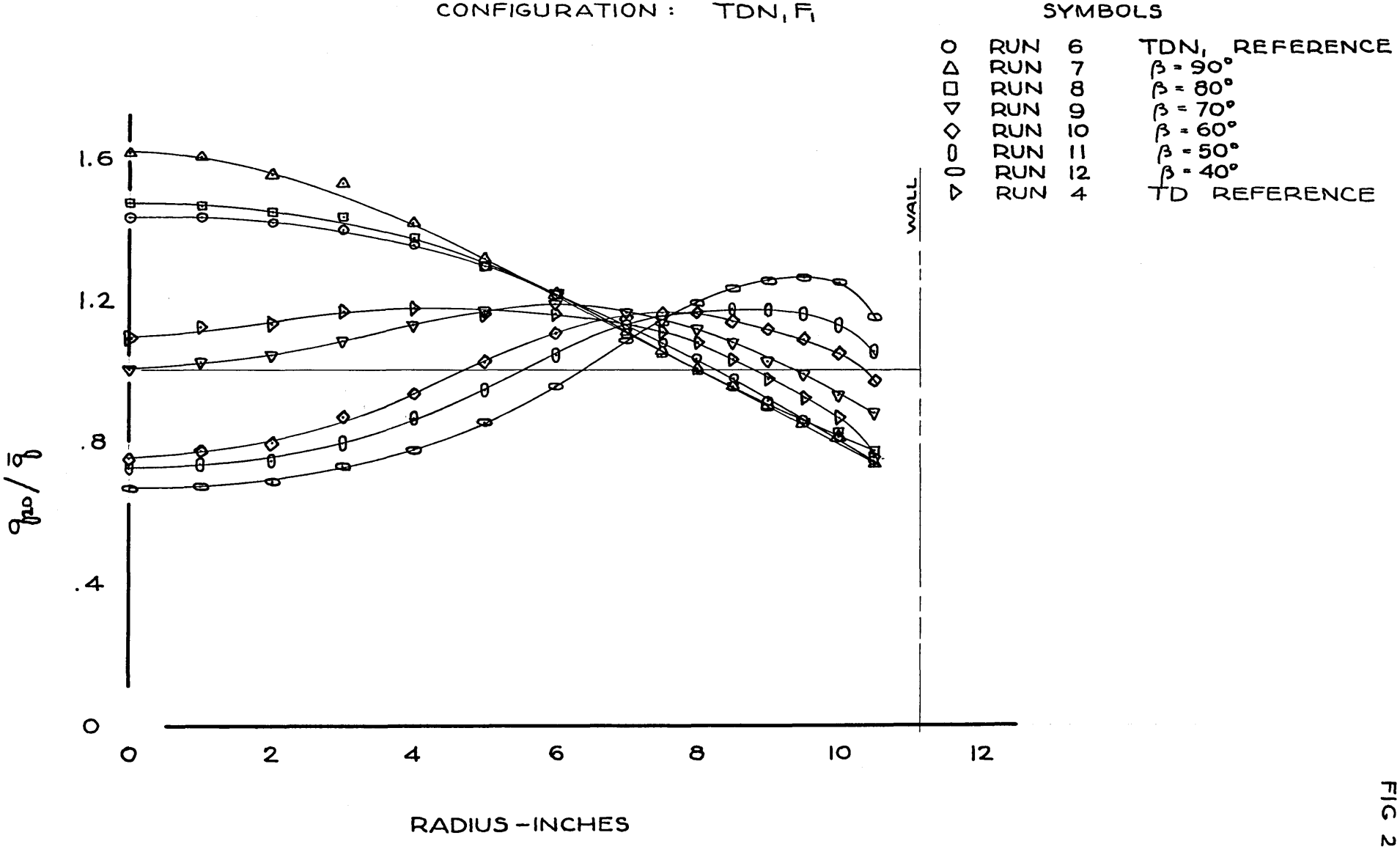

FIG 2

AVERAGE VELOCITY DISTRIBUTION AT END OF TAILPIPE

CONFIGURATION : TDN, F_3

SYMBOLS

○	RUN	14	$\beta = 50°$
△	RUN	15	$\beta = 40°$
□	RUN	16	$\beta = 34°$

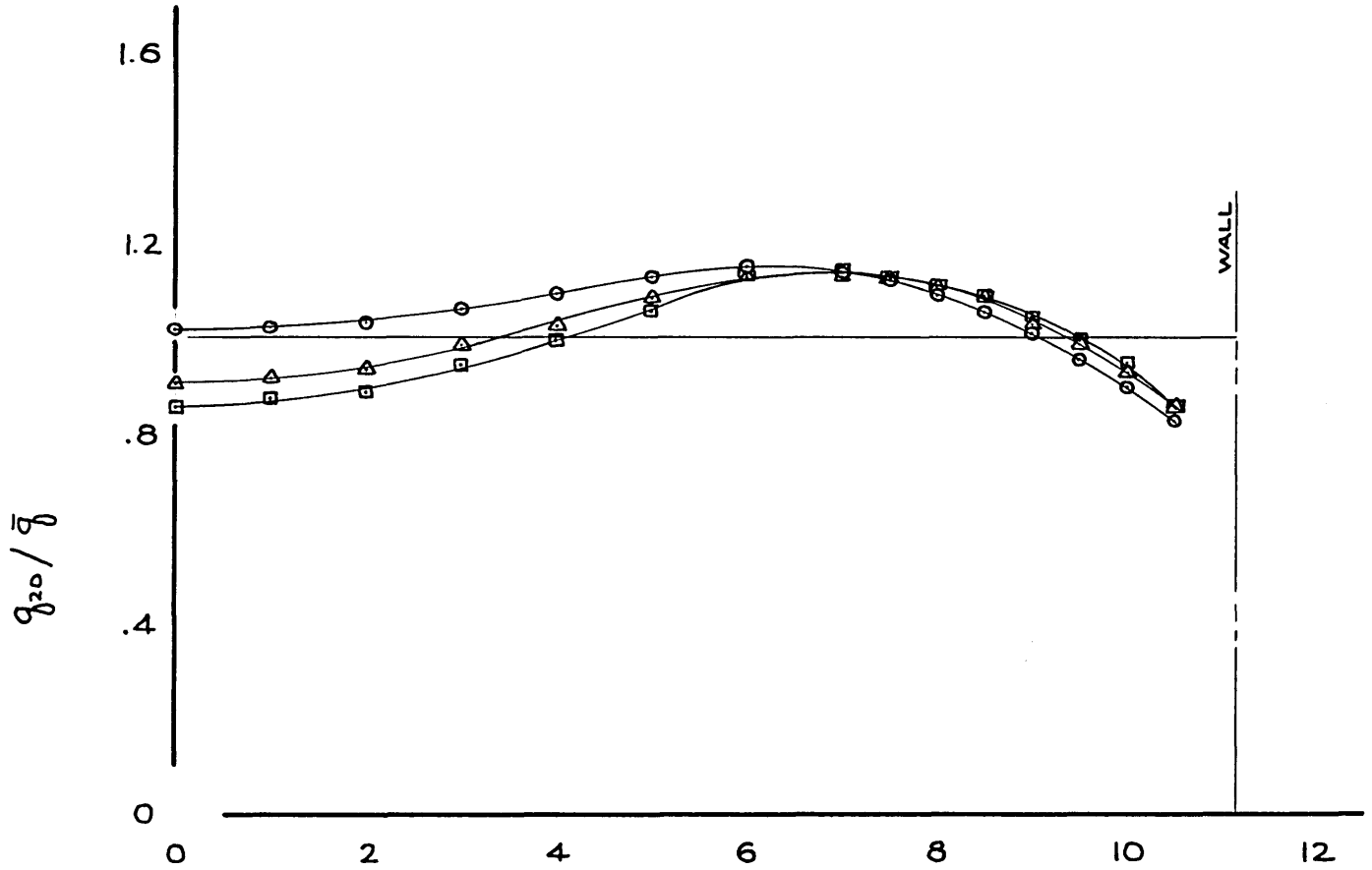

FIG 3

AVERAGE VELOCITY DISTRIBUTION AT END OF TAILPIPE

CONFIGURATION : TDN, F_5

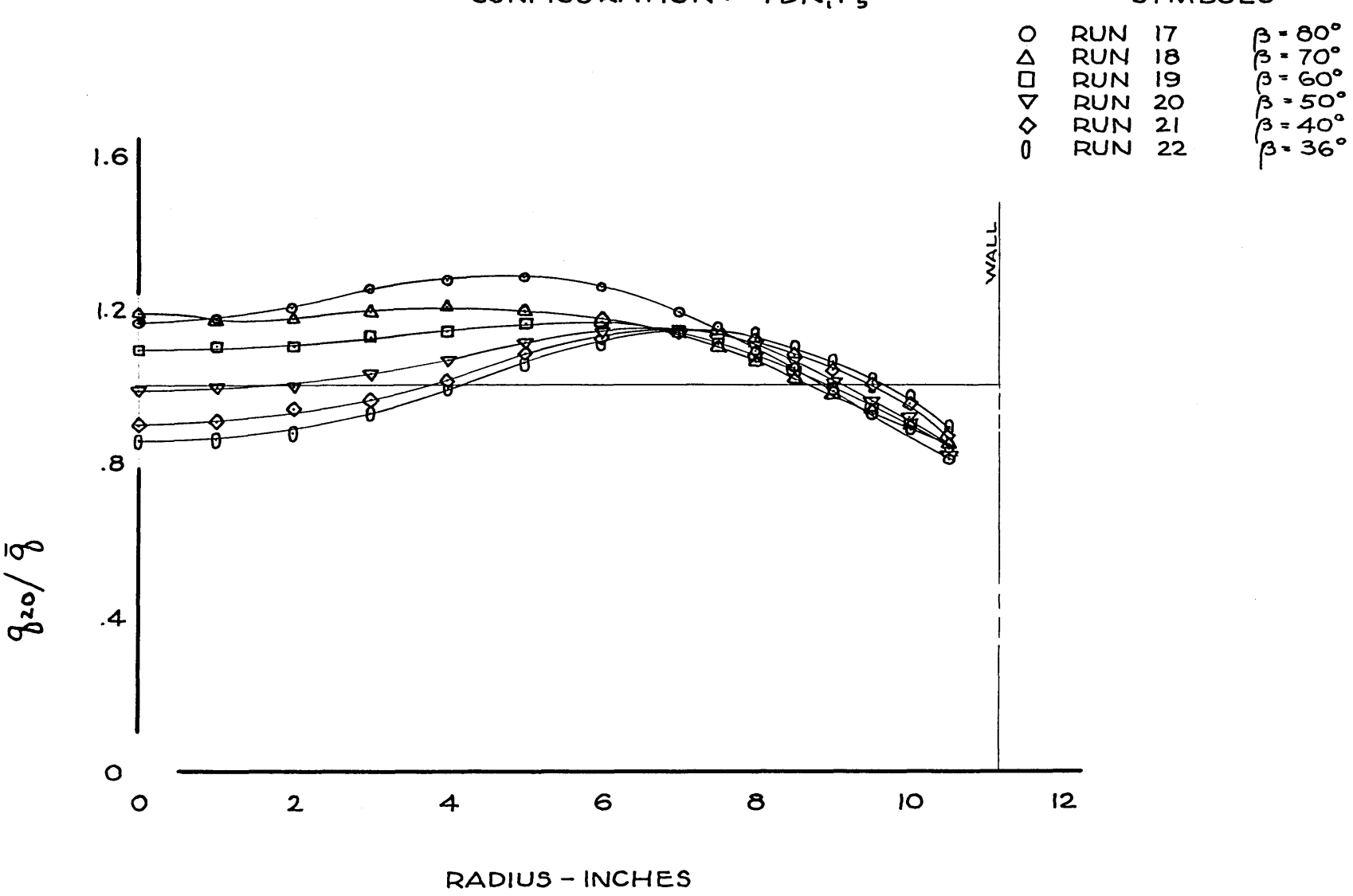

FIG. 4

AVERAGE VELOCITY DISTRIBUTION AT END OF TAILPIPE

CONFIGURATION : $TDN_1N_2F_2$

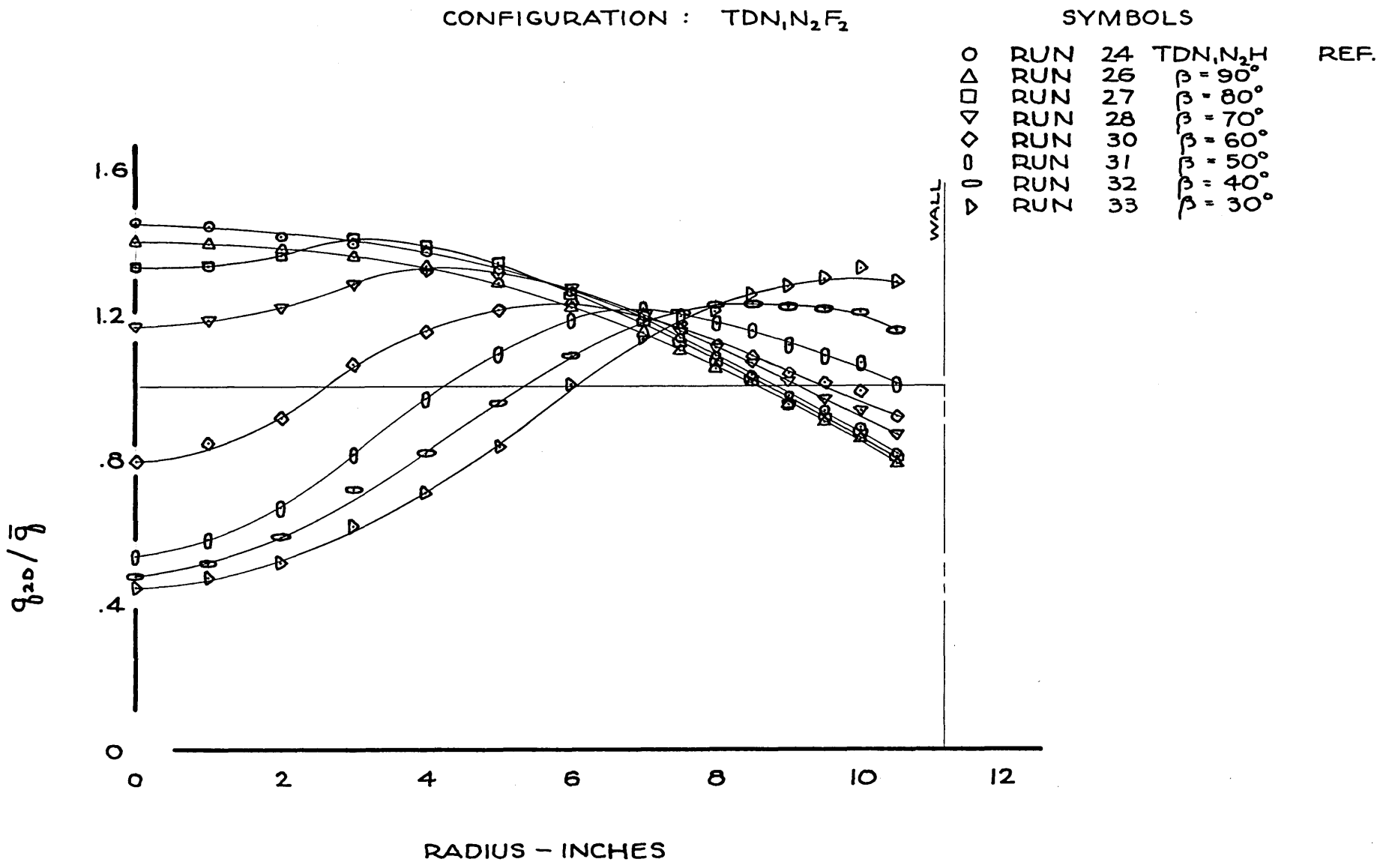

FIG. 5

AVERAGE VELOCITY DISTRIBUTION AT END OF TAILPIPE

CONFIGURATION : $TDN_1N_2F_4$

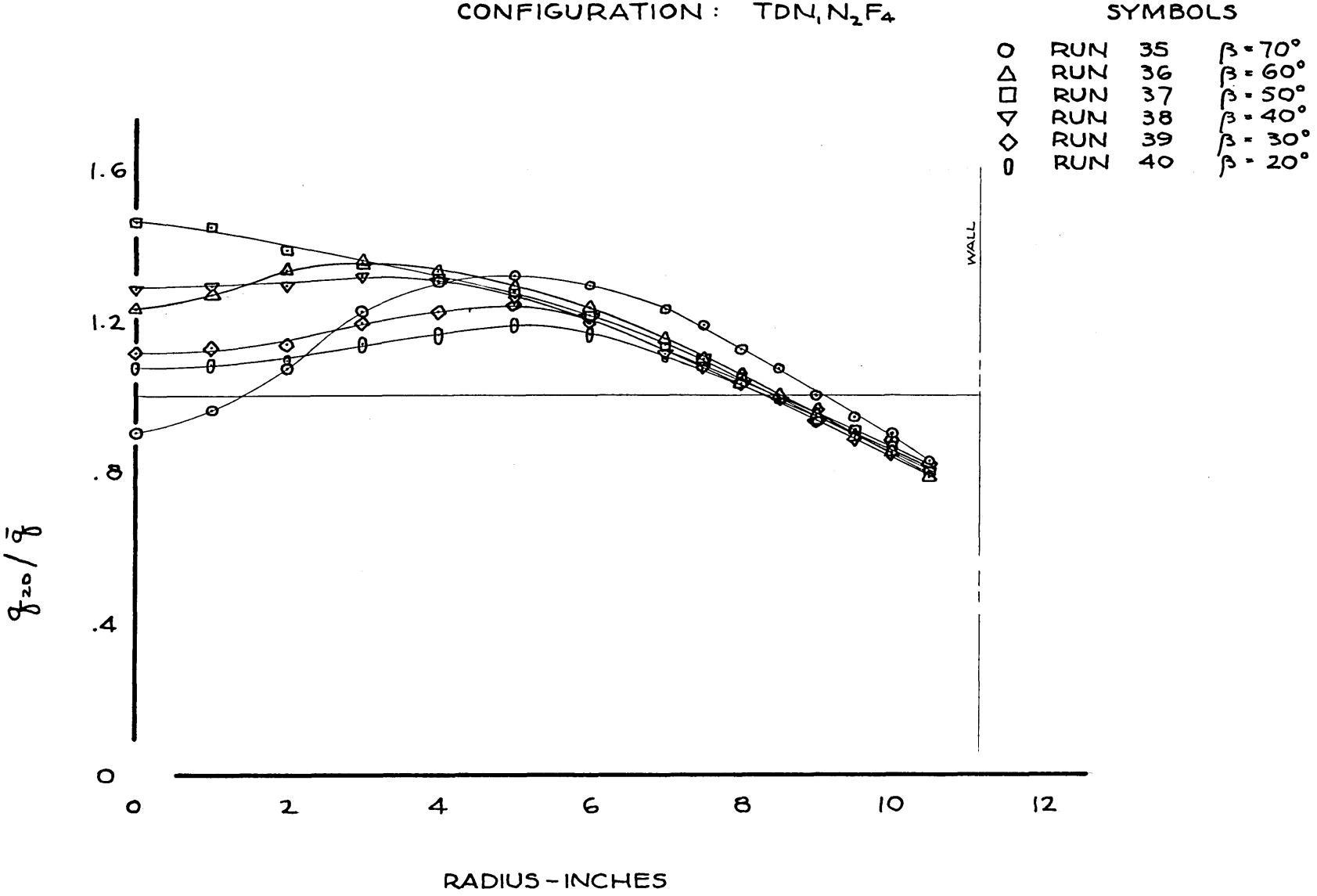

FIG. 6

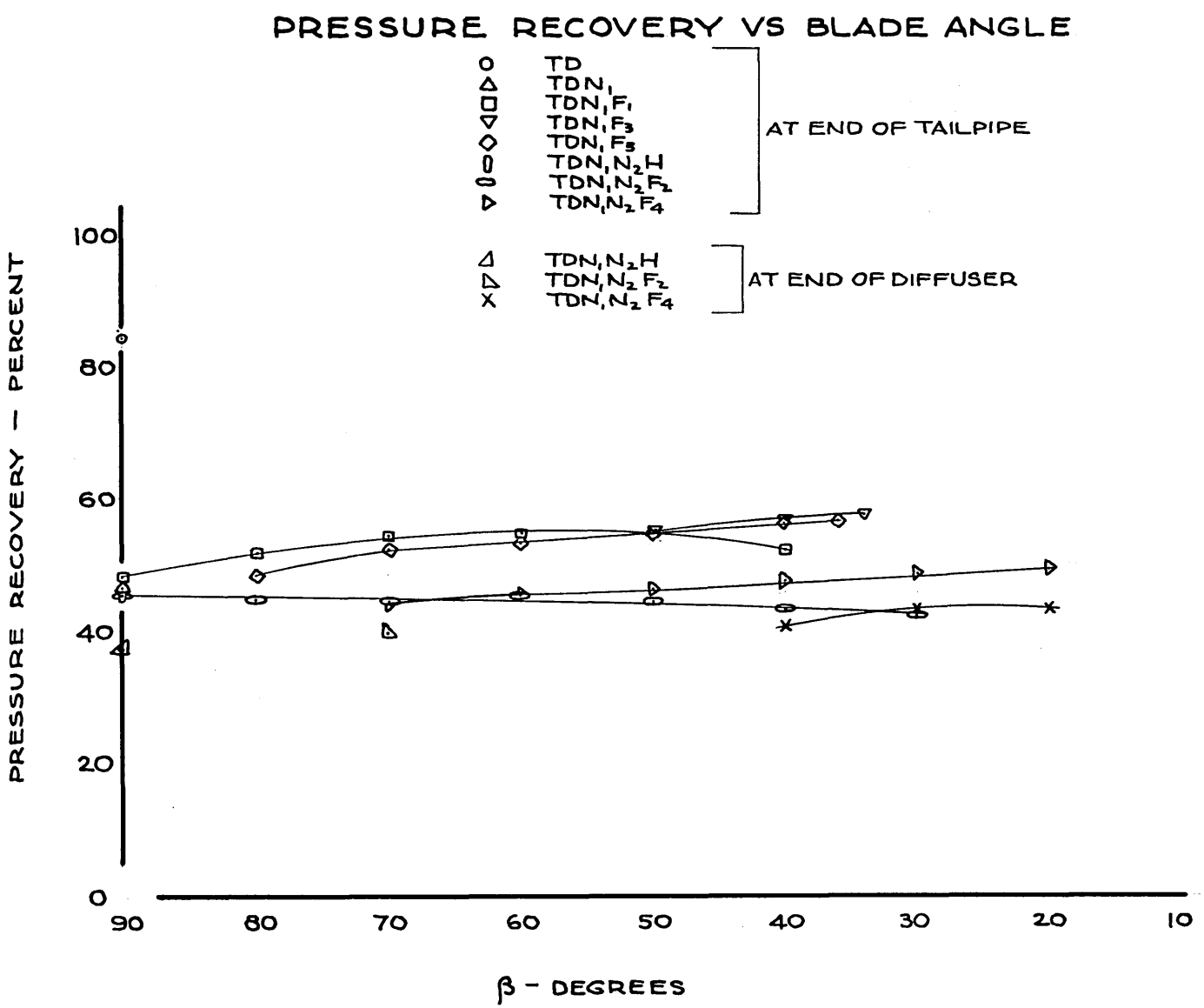
PRESSURE RECOVERY VS BLADE ANGLE
TD
TDN, F1
TDN, F3
TDN, F5
TDN, N2H
TDN, N2F2
TDN, N2F4
AT END OF TAILPIPE
TDN, N2H
TDN, N2F2
TDN, N2F4
AT END OF DIFFUSER
PRESSURE RECOVERY - PERCENT
100
80
60
40
20
0
90
80
70
60
50
40
30
20
10
β - DEGREES

FIG. 7

WINDMILL BLADE ANGLE VS RADIUS

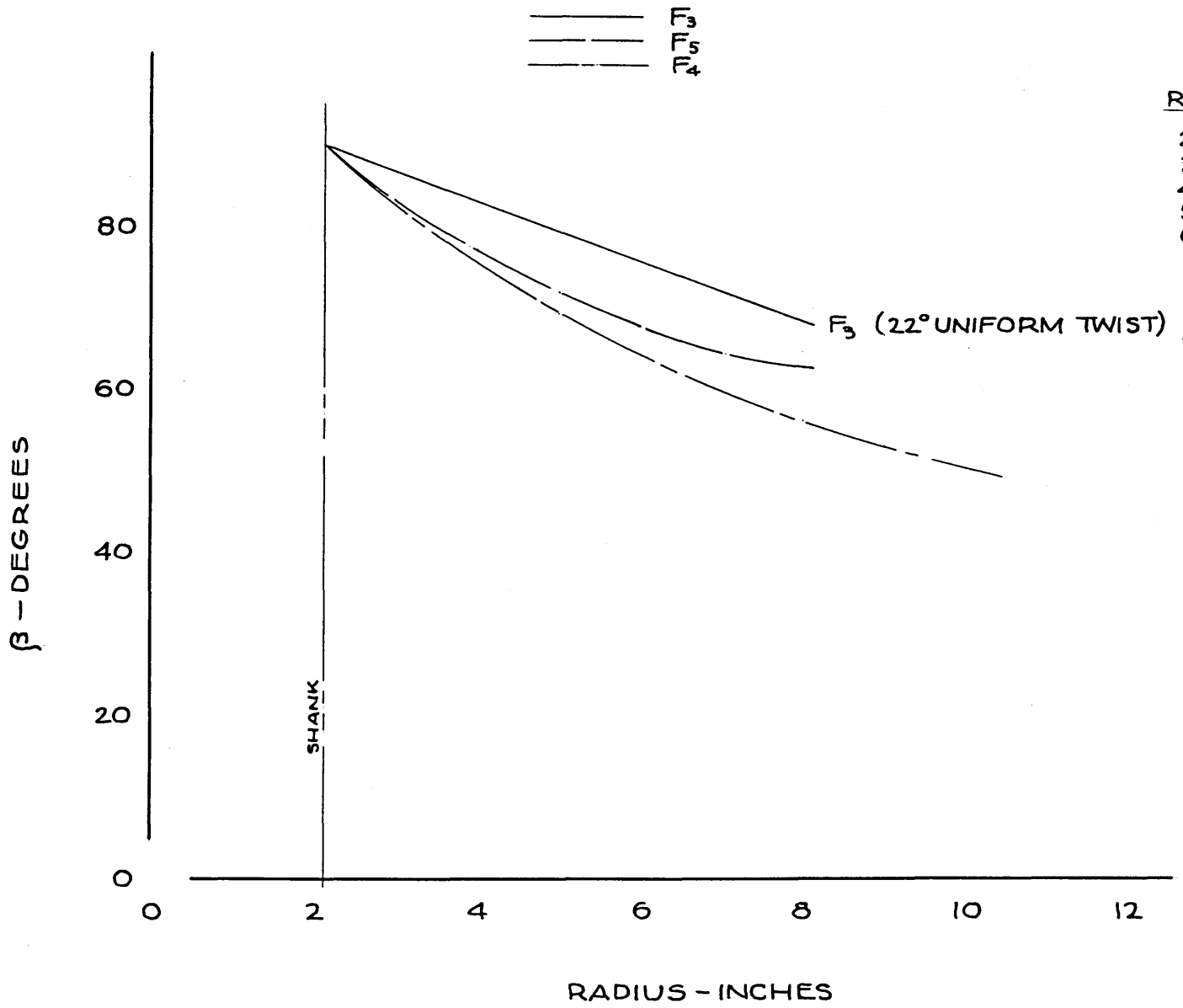

RADIUS	β-DEGREES F_5	F_4
2.125	90.0	90.0
3.0	83.3	82.9
4.0	77.2	75.6
5.0	72.0	69.4
6.0	67.8	64.2
7.0	64.5	59.8
8.0	62.8	56.1
9.0		53.1
10.0		50.3

FIG. 8

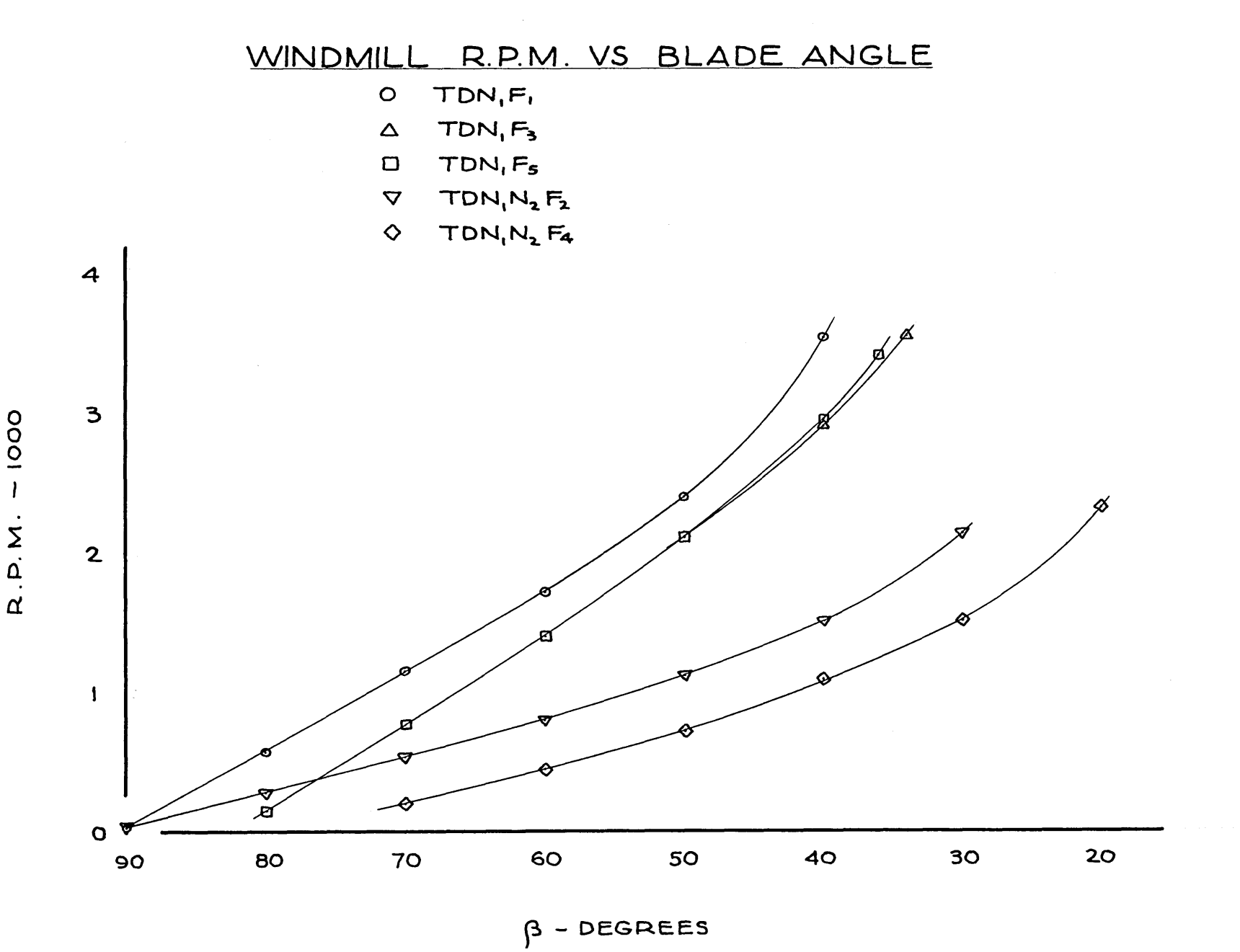
WINDMILL R.P.M. VS BLADE ANGLE
TDN, F1
TDN, F3
TDN, F5
TDN, N2 F2
TDN, N2 F4
R.P.M. - 1000
0
1
2
3
4
90
80
70
60
50
40
30
20
β - DEGREES

FIG. 9

DIRECTION INDICATOR MEASUREMENTS

CONFIGURATION : TDN_1F_1 & TDN_1

RUN 13

MAXIMUM ANGULAR DEFLECTION VS BLADE ANGLE

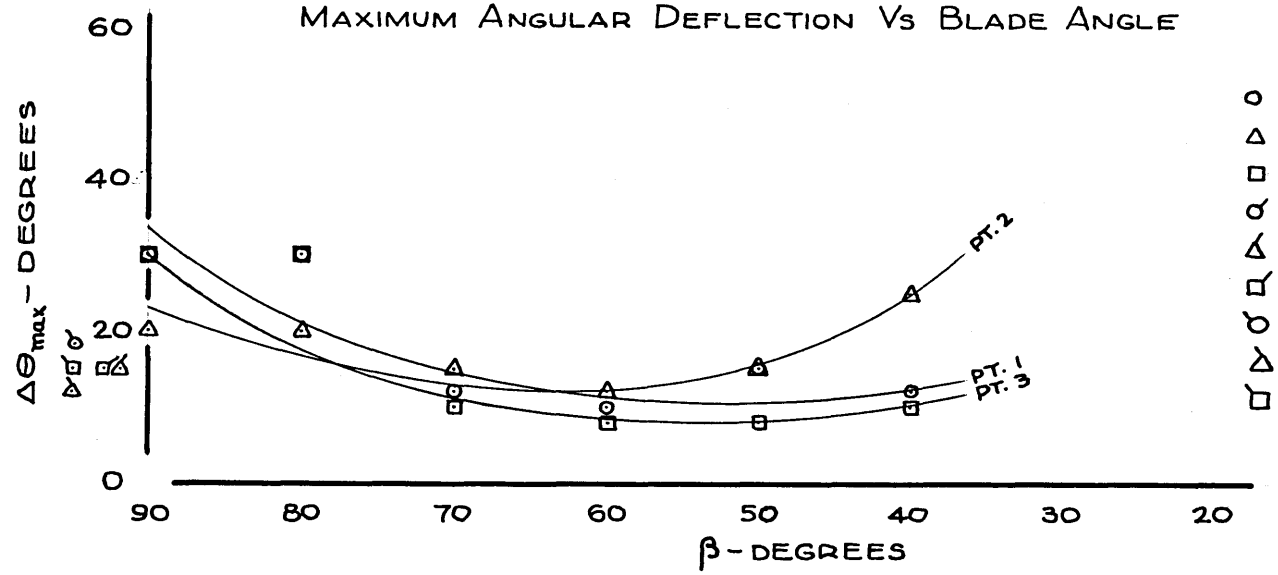

SYMBOLS

o	TDN_1F_1	PT. 1	
Δ	TDN_1F_1	PT. 2	℄
□	TDN_1F_1	PT. 3	
ơ	TDN_1	PT. 1	
Δ	TDN_1	PT. 2	℄
□	TDN_1	PT. 3	
o	TD	PT. 1	
Δ	TD	PT. 2	℄
□	TD	PT. 3	

AVERAGE ANGULAR DEFLECTION VS BLADE ANGLE

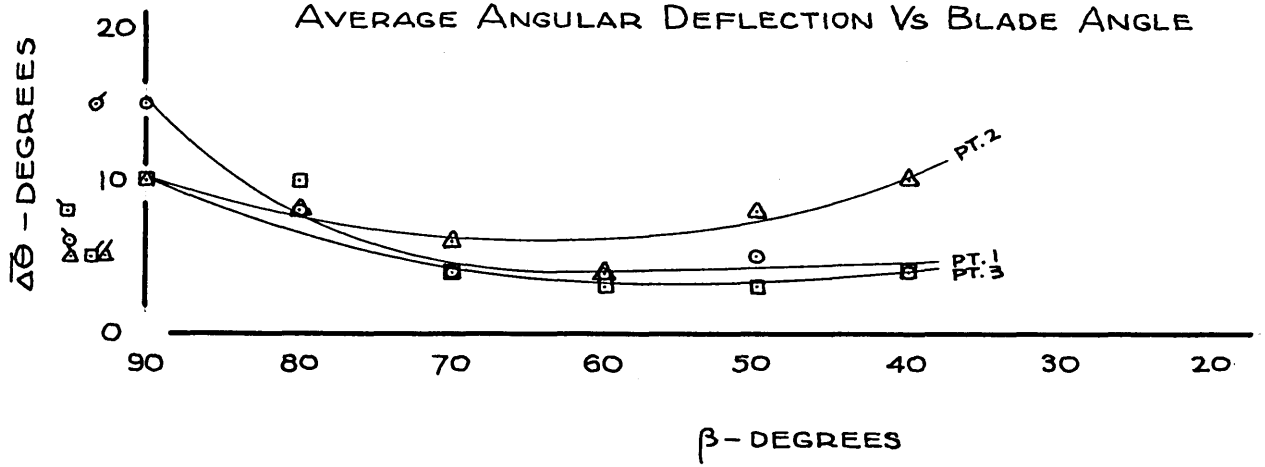

FIG. 10

DIRECTION INDICATOR MEASUREMENTS

CONFIGURATION : TDN, F_5 , TDN, F_5S , & TDN, S

RUN 23

MAXIMUM ANGULAR DEFLECTION VS BLADE ANGLE

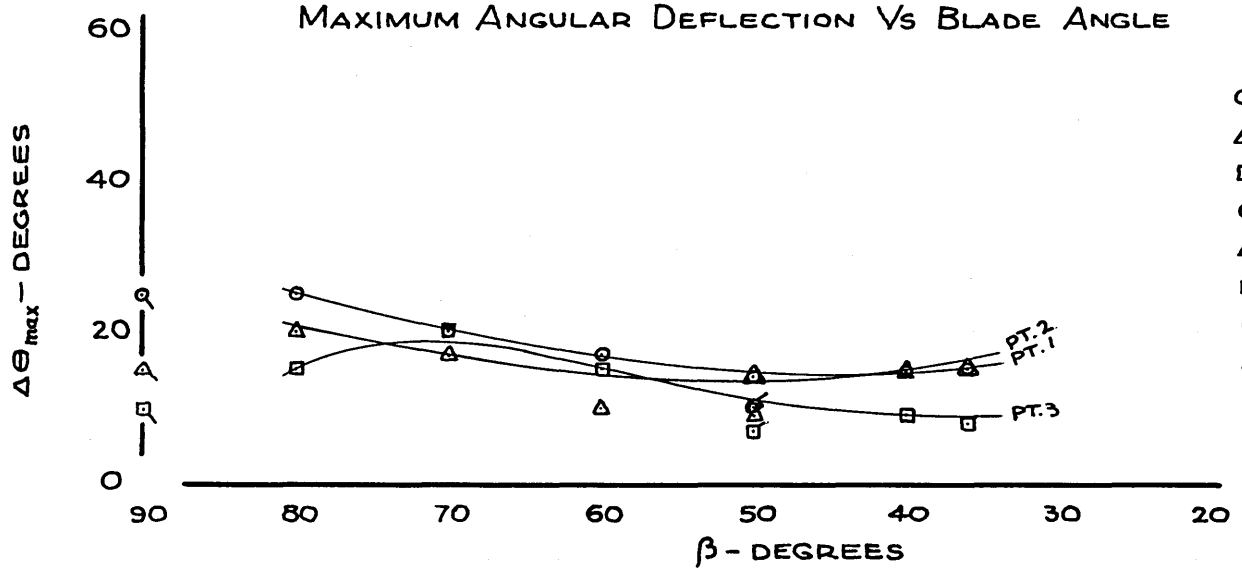

SYMBOLS

o	TDN, F_5	PT. 1	
Δ	TDN, F_5	PT. 2	&
□	TDN, F_5	PT. 3	
ơ	TDN, F_5S	PT. 1	
Δ	TDN, F_5S	PT. 2	&
□	TDN, F_5S	PT. 3	
Q	TDN, S	PT. 1	
Δ	TDN, S	PT. 2	&
□	TDN, S	PT. 3	

AVERAGE ANGULAR DEFLECTION VS BLADE ANGLE

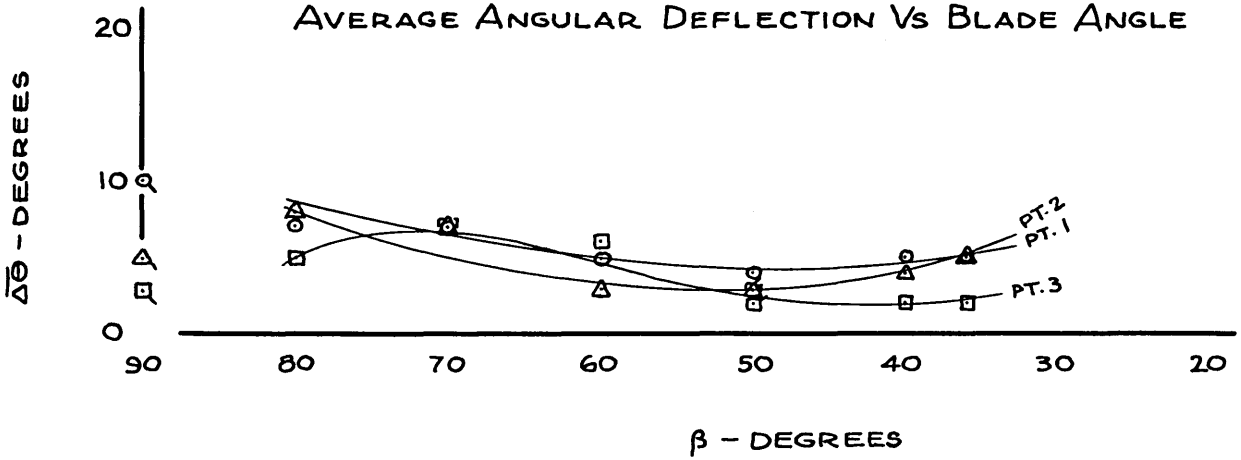

FIG. 11

DIRECTION INDICATOR MEASUREMENTS

CONFIGURATION : $TDN_1N_2F_2$ & TDN_1N_2H

RUN 34

MAXIMUM ANGULAR DEFLECTION VS BLADE ANGLE

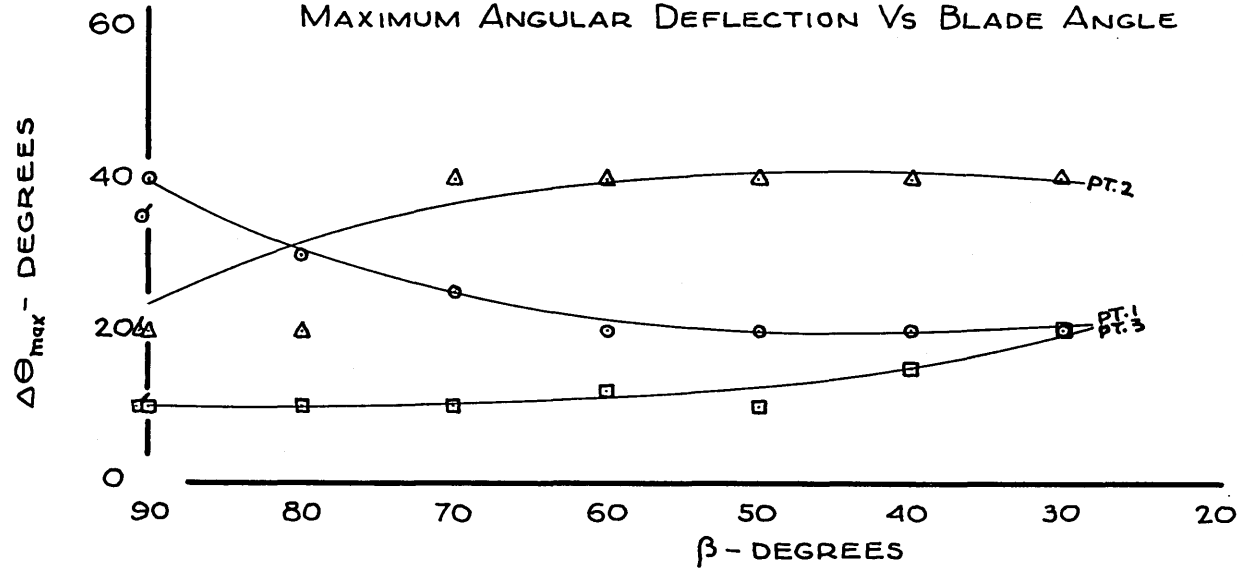

SYMBOLS

- ○ $TDN_1N_2F_2$ PT. 1
- △ $TDN_1N_2F_2$ PT. 2 ℄
- □ $TDN_1N_2F_2$ PT. 3
- ○ TDN_1N_2H PT. 1
- △ TDN_1N_2H PT. 2 ℄
- □ TDN_1N_2H PT. 3

AVERAGE ANGULAR DEFLECTION VS BLADE ANGLE

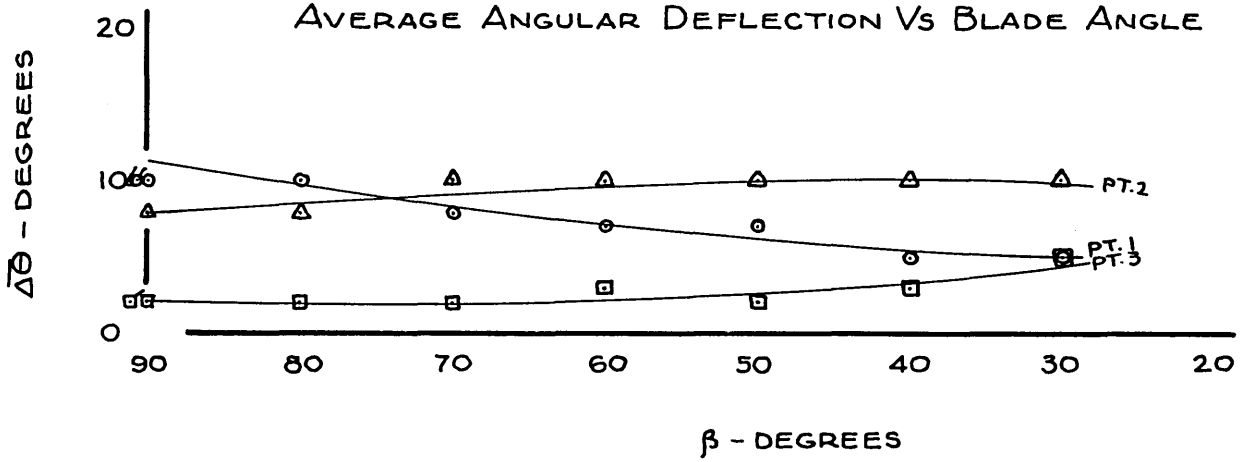

FIG. 12

DIRECTION INDICATOR MEASUREMENTS

CONFIGURATION : $TDN_1N_2F_4$

RUN 42

MAXIMUM ANGULAR DEFLECTION VS BLADE ANGLE

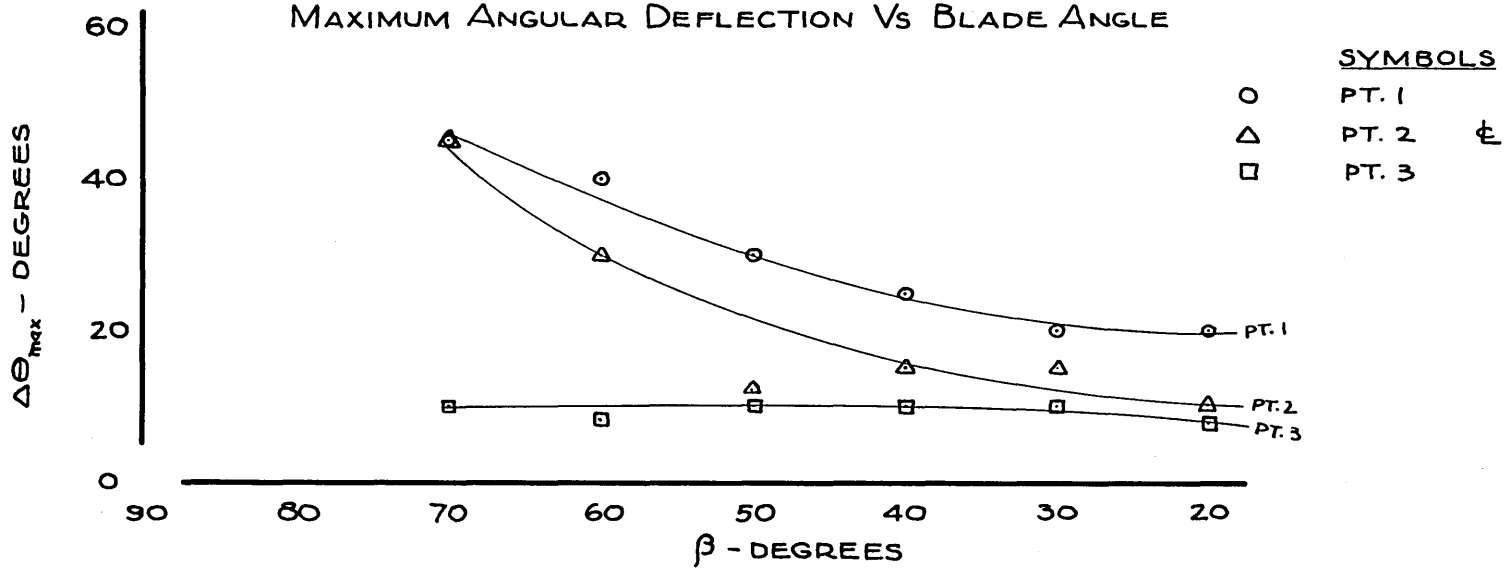

AVERAGE ANGULAR DEFLECTION VS BLADE ANGLE

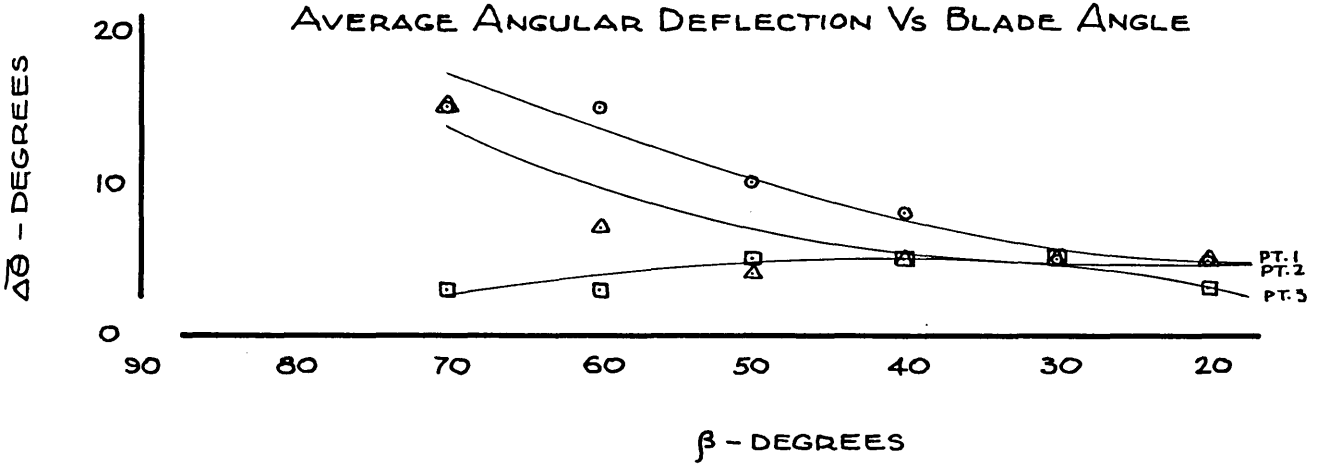

FIG. 13

Explanation of Tuft Study Diagram

The diagrams on the following pages represent what the observer would see looking upstream into the tailpipe thus,

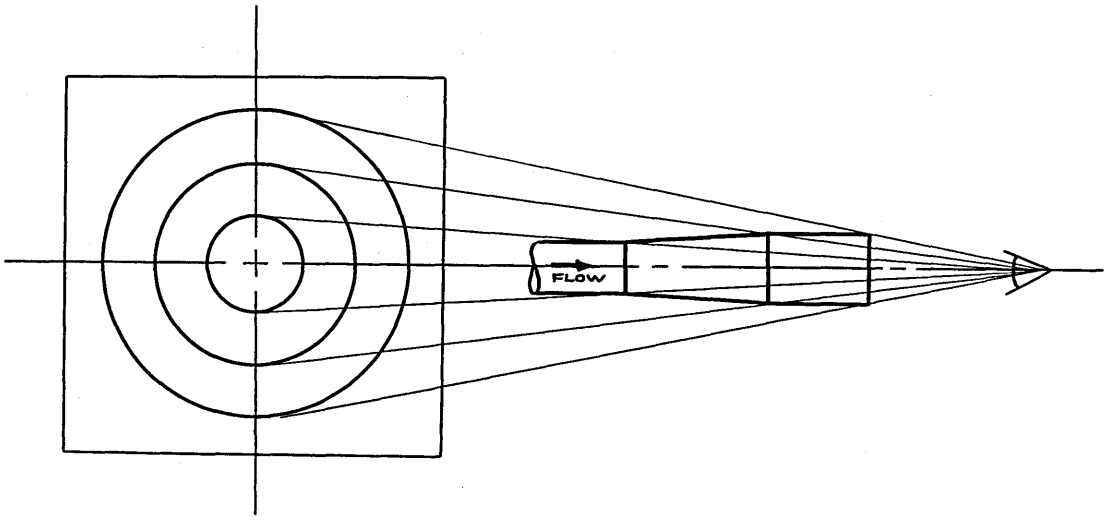

The area between the outside and middle circle represents the tailpipe wall, and the area enclosed between the middle and inside circles represents the diffuser wall. The type of flow is represented by cross hatching as follows,

Smooth flow 

Rough flow, unseparated 

Separated 

FIG. 14

TUFT STUDIES CONFIGURATION: NOTED

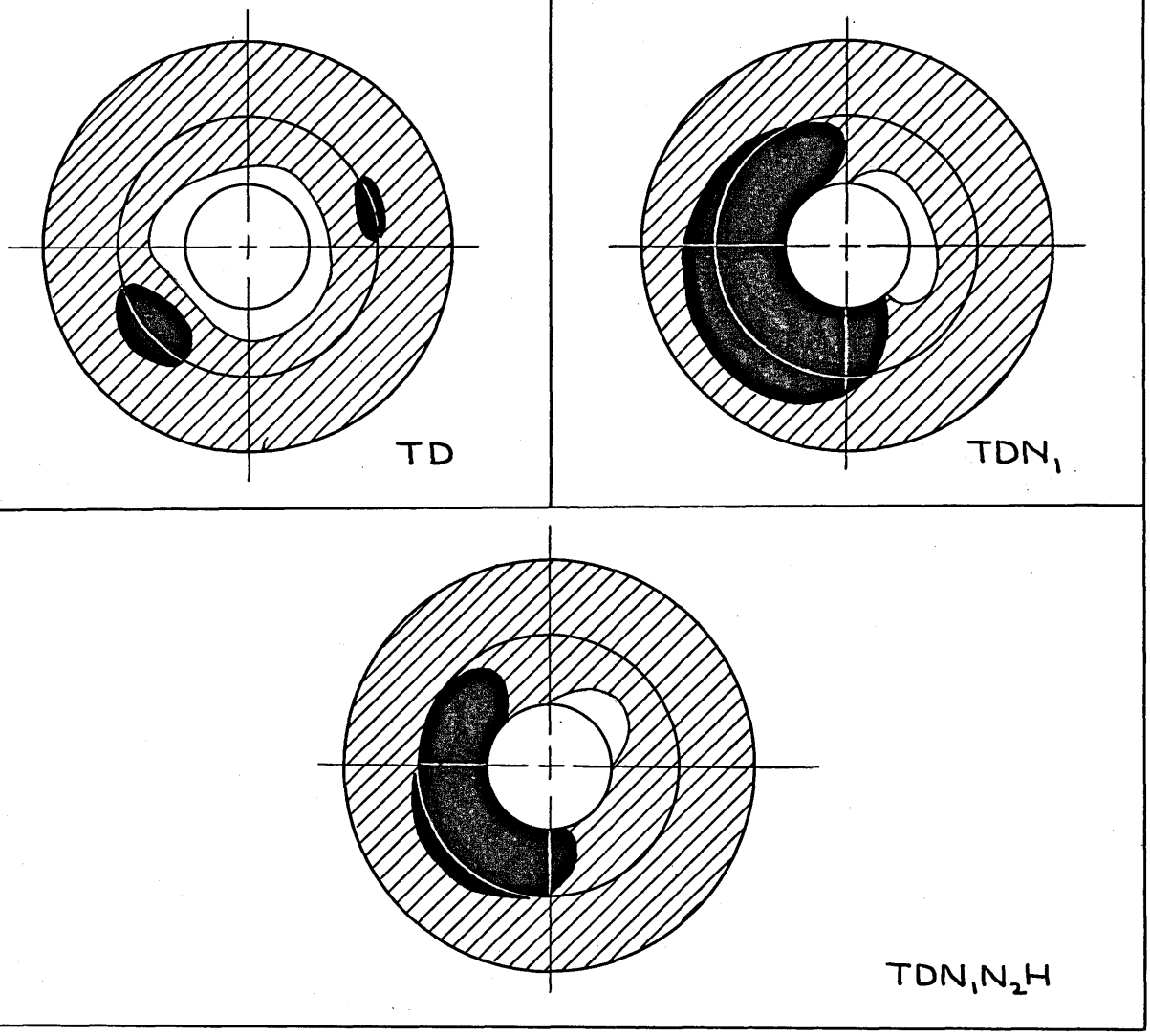

FIG. 15

TUFT STUDIES CONFIGURATION: TDN_1F_1

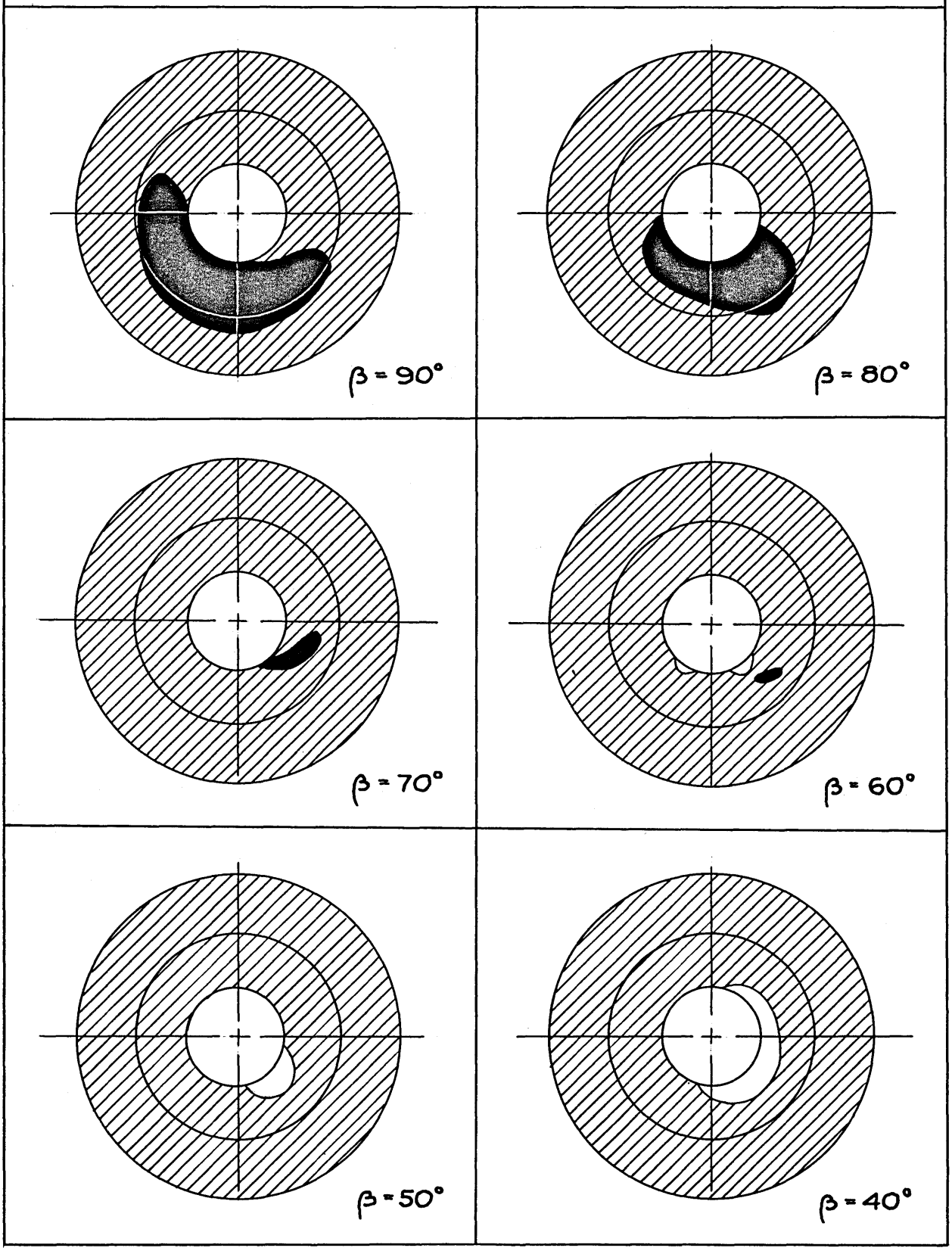

FIG. 16

TUFT STUDIES CONFIGURATION: TDN, F_5

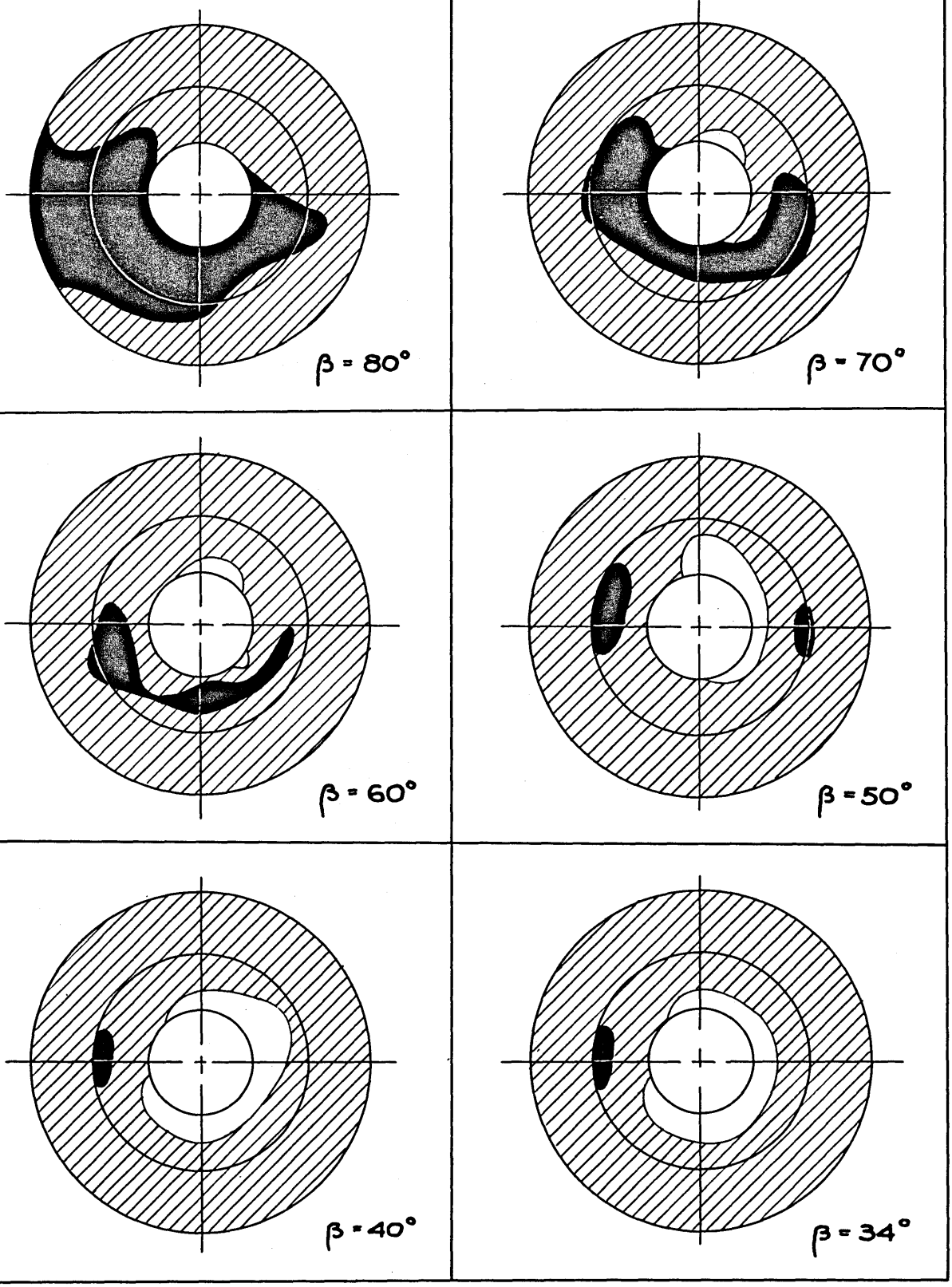

FIG. 17

TUFT STUDIES CONFIGURATION: $TDN_1N_2F_2$

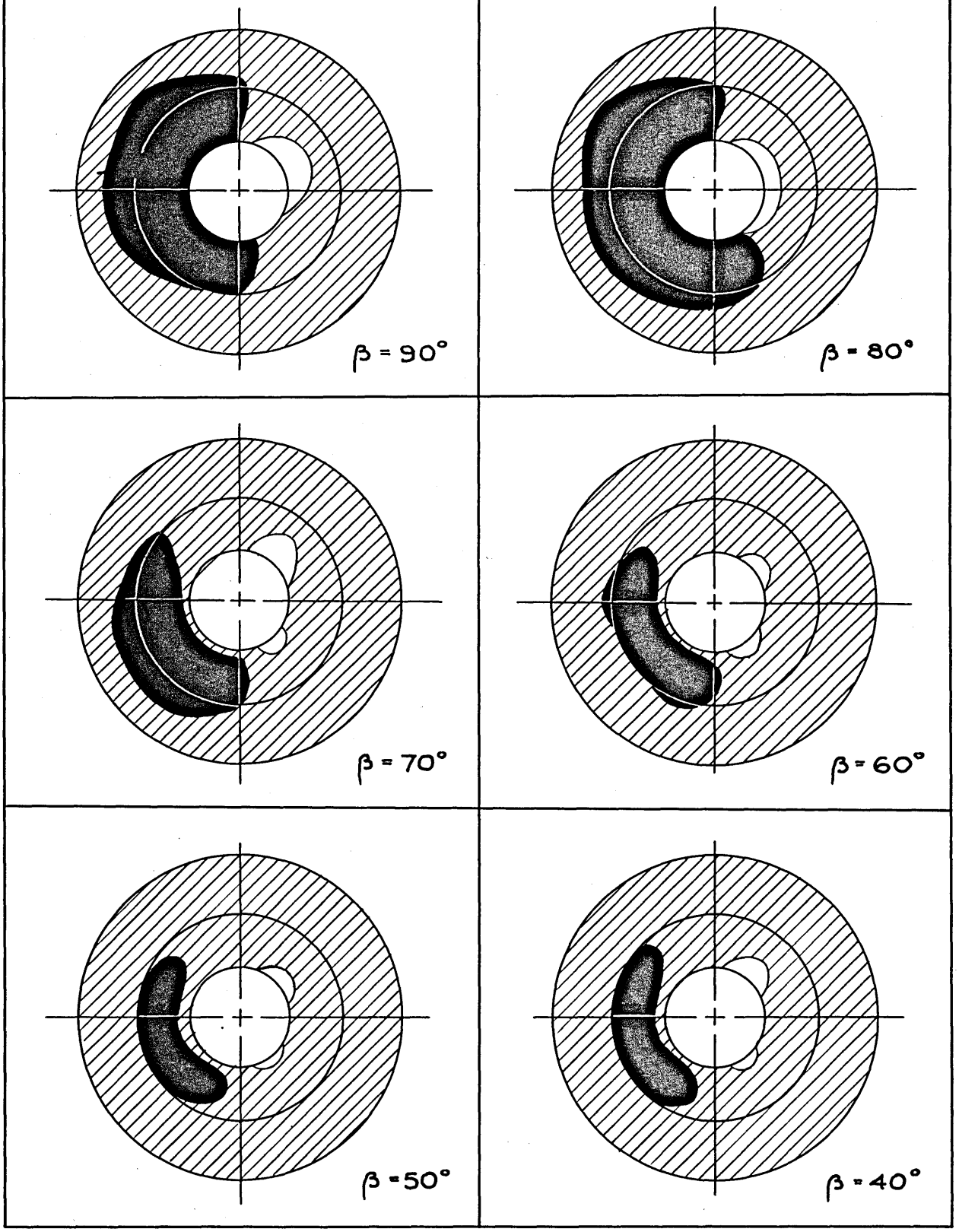

FIG. 18

TUFT STUDIES CONFIGURATION: $TDN_1N_2F_2$

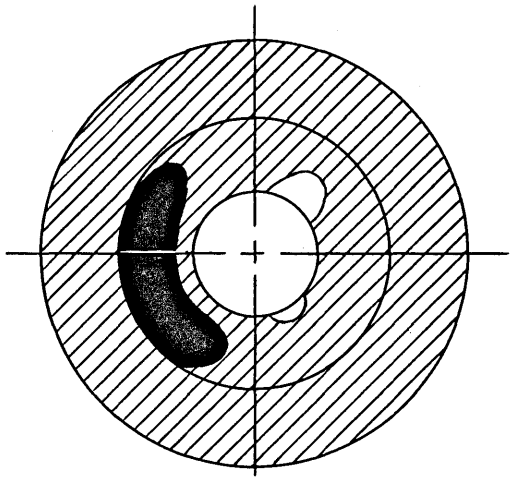

$\beta = 30°$

FIG. 19

TUFT STUDIES CONFIGURATION: $TDN_1N_2F_4$

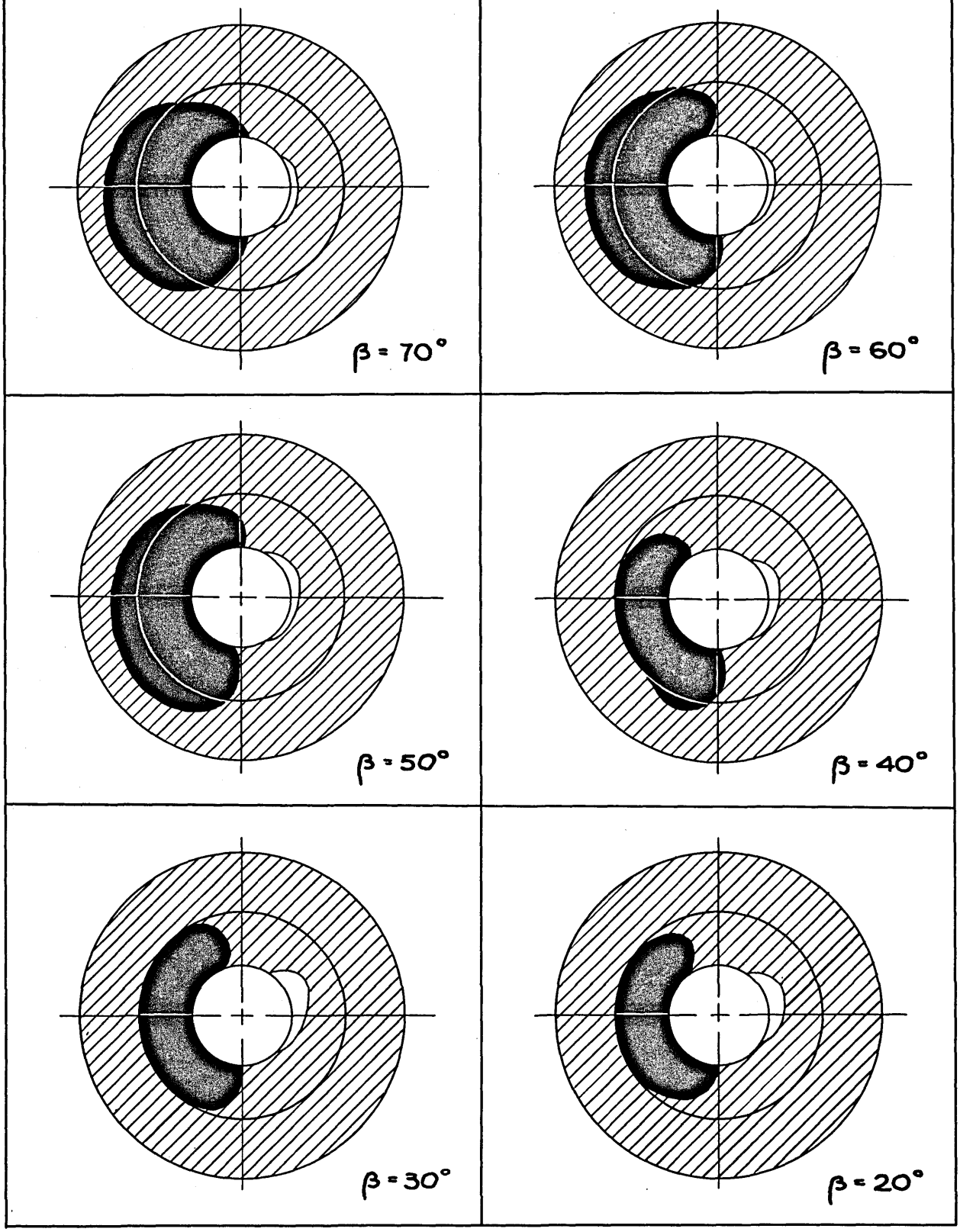

VII CONCLUSIONS

A. General Remarks

Detailed conclusions to be drawn from this investigation are as follows,

(1) The presence of a large nacelle near the diffuser inlet increases turbulence and energy losses greatly, and induces earlier flow separation on the diffuser wall.

(2) The velocity distribution at the tailpipe exit is poor both with and without the upstream nacelle installed.

(3) The use of a windmill mounted on the rear of the upstream nacelle does not greatly improve the velocity distribution at the tailpipe exit, but does decrease turbulence, reduces energy losses, and decreases the area of flow separation.

(4) A windmill mounted near the diffuser outlet reduces the amount of flow separation in the diffuser only slightly, reduces energy losses only slightly, but reduces turbulence appreciably and promotes a good velocity distribution at the tailpipe exit.

(5) The blade of the windmill should have sufficient twist to prevent blade stalling at either root or tip, although it is doubtful if tip stalling will normally occur.

(6) A damping screen appreciably reduced turbulence for the few conditions tested.

B. Recommendations for Further Study

The windmill mounted at the diffuser exit showed the most promising results. It is capable of giving a fairly uniform velocity distribution, while at the same time reducing the level of turbulence.

To reduce the turbulence still further the use of damping screens is suggested. Since the pressure drop across a screen is considerable, any reduction of energy losses elsewhere

is desireable. The best way to do this is to remove the forward nacelle, but since considerations other than aerodynamic enter into this decision in the case of the WBWT no further discussion is merited here. A windmill mounted on the forward nacelle could be used, since its favorable effect on energy losses has been demonstrated.

The next step should be to design and test an improved wind direction indicator. The indicator should preferably incorporate the following characteristics,

1. Single vane type
2. Damping ratio approximately 0.7, independent of air velocity
3. High natural frequency at all air velocities
4. Responsive only to change in direction of air velocity.

The single vane type will have no undesireable instability at large deflections and can be made small enough to give an accurate local value of wind direction. A damping ratio of 0.7 and a high natural frequency are needed for good frequency response characteristics. For the instrument to have the same characteristics under all flow conditions the damping ratio and natural frequency should be independent of air velocity. All these requirements can be achieved by incorporating non-aerodynamic springs and dampers, but by doing this the instrument becomes more sensitive to changes in air speed, an undesireable feature. Some compromise will have to be made, but further study of this problem is needed. A method of recording the indicator movement which has no influence on the behavior of the instrument, such as a type of optical measurement, would be most satisfactory.

With an accurate wind direction indicator the reduction of turbulence with such combinations of windmills and damping screens as has been suggested above should be investigated.

VIII REFERENCES

1. Peters, H.: Conversion of Energy in Cross-Sectional Diffusers under Different Conditions of Inflow. T.M. No. 737, N.A.C.A., 1934.

2. Patterson, G.N.: Modern Diffuser Design. Aircraft Engineering, vol. X, No. 115, Sept. 1938, pp. 267-273.

3. Collar, A.R.: The Use of a Freely Rotating Windmill to Improve the Flow in a Wind Tunnel. R. & M. No. 1866 British A.R.C., 1939.

4. Den Hartog, J.P.: Mechanical Vibrations. Mc Graw-Hill Book Co., Inc., 1940, pp. 221-228.

5. Summers, R.A.: An Investigation of the Effect of Honeycomb on Large-Scale Disturbances in Wind Tunnels. Massachusetts Institute of Technology. Thesis for masters degree in aero. engr., 1946.

6. Dryden, H.L. and Schubauer, G.B.: The Use of Damping Screens for the Reduction of Wind Tunnel Turbulence. Jour. Aero. Sc., vol. 14, No. 4, April 1947, pp. 221-228.

7. Schwartz, I.A.: Investigation of an Annular Diffuser-Fan Combination Handling Rotating Flow. R.M. No. L9B28, N.A.C.A. 25 April 1949.

IX APPENDIX

A. Nomenclature

A	cross sectional area of duct	ft^2
C_L	lift coefficient	—
c	damping constant	ft lb sec rad^{-1}
D	duct diameter	ft
h	total pressure head	inches of water
I	moment of inertia	slug ft^2
k	spring constant	ft lb rad^{-1}
l	centerline distance from axis of rotation to quarter chord of surface	ft
n_n	undamped natural frequency	cycles sec^{-1}
p	static pressure head	inches of water
q	local dynamic pressure head ($\frac{1}{2}\rho U^2$)	inches of water
q_2	weighted dynamic pressure head at any given radius	inches of water
$\overline{q}$	mean dynamic pressure head at any particular station	inches of water
r	radial distance from duct centerline	ft
S	projected surface area	ft^2
T	torque	ft lb
U	local free stream velocity	ft sec^{-1}
α	angle of attack	rad
ζ	damping ratio	---
θ	angular position	rad
$\overline{\Delta\theta}$	time mean angular deflection	rad
$\Delta\theta_{max}$	maximum angular deflection	rad
μ	coefficient of viscosity	lb sec ft^{-2}
ρ	density	slug ft^{-3}

Subscripts

1,2,3 ... station location (see fig. 66)

i uncorrected for instrument error

Configuration symbols		Ref. Fig.
T	Tunnel only, up to but not including diffuser	66
D	diffuser and tailpipe	66
N_1	nacelle (mock up of WBWT prop. and motor fairing)	67
N_2	aft windmill nacelle	68
F_1	small windmill, untwisted blades	8, 69, 71
F_3	small windmill, linearly twisted	8, 69, 71
F_5	small windmill, variably twisted blades	8, 69, 71
F_2	large windmill, untwisted blades	8, 70, 71
F_4	large windmill, constant pitch	8, 70, 71
H	windmill hub only	71
S	damping screen at end of tailpipe 18 mesh, .010 inch dia.	

B. Pitot Tube Calibration

The pitot tube used in Runs 1-3 was calibrated in Run 43 in the M.I.T. Student Wind Tunnel against the 'standard' pitot tube used by the Wright Brothers Wind Tunnel. The procedure was to make two runs over the same speed range; first with the standard pitot tube mounted in the test section, then with the uncalibrated pitot tube and mount in the test section with the static pressure orifices in the same location as for the standard pitot tube. Total and static pressure heads were read from a vertical manometer when the tunnel speed had been stabilized at the correct value. The correction is computed as $(q-q_i)$ and plotted vs q_i in fig. 20. The data is tabulated below.

RUN 43 7/1/49

heads - inches H_2O

	STANDARD PITOT TUBE			PITOT TUBE RIG			
E.A.S. M.P.H.	h	p	q	h_i	p_i	q_i	$(q-q_i)$
20	.16	.00	.16	—	—	—	—
30	.46	.00	.46	.49	.02	.47	-.01
40	.82	.00	.82	.83	.04	.79	.03
50	1.28	.00	1.28	1.28	.05	1.23	.05
60	1.81	.00	1.81	1.81	.06	1.76	.05
70	2.48	.00	2.48	2.48	.09	2.39	.09
80	3.21	.00	3.21	3.21	.12	3.09	.12
90	4.09	.02	4.07	4.08	.16	3.92	.15
100	4.98	.02	4.96	4.99	.19	4.80	.16

PITOT TUBE CALIBRATION

RUN 43 M.I.T. STUDENT TUNNEL

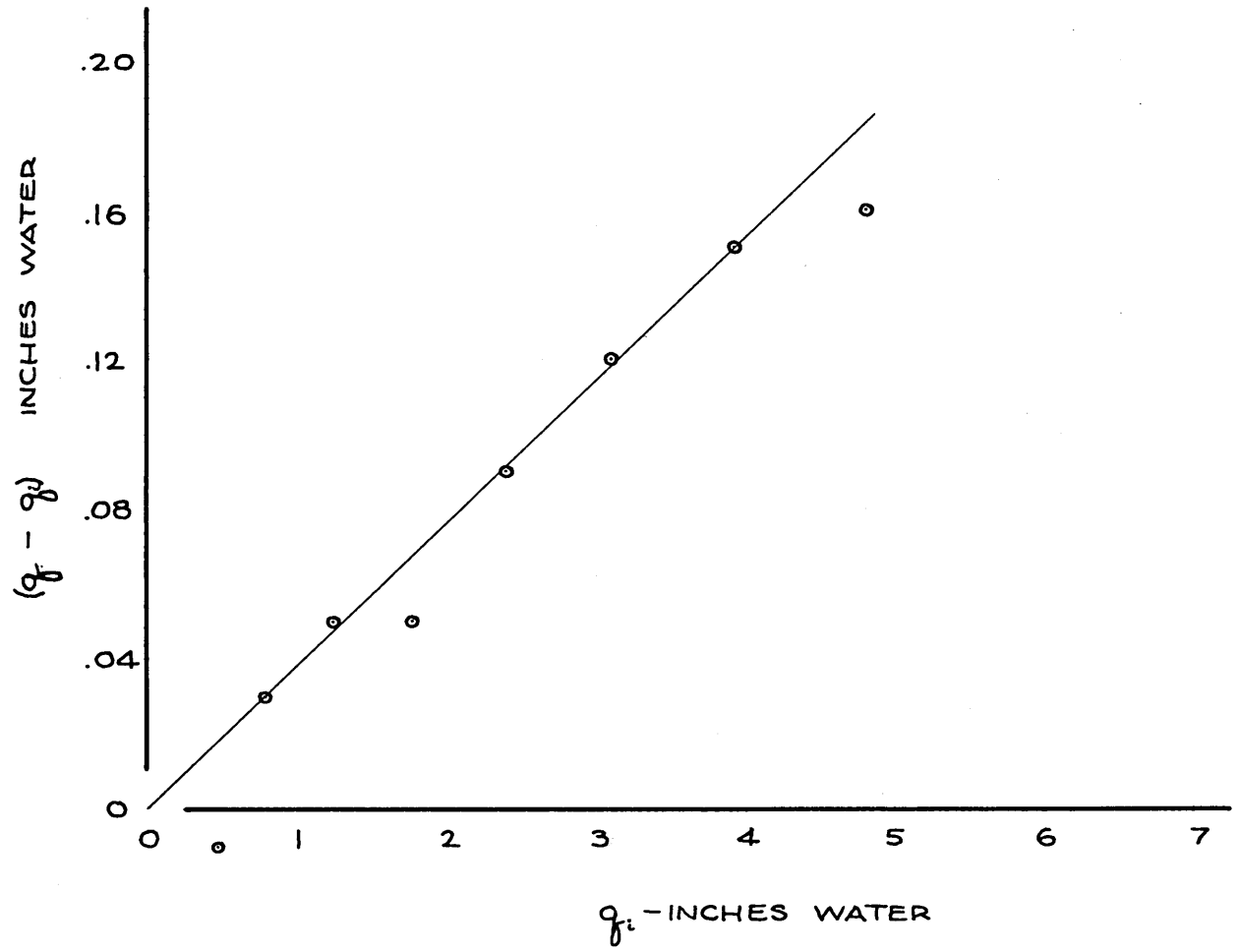

FIG. 20

C. Direction Indicator Characteristics

The dynamic response characteristics of the wind direction indicator can be best described by the parameters

1. Damping ratio, ζ

2. Undamped natural frequency, n_n

Considering the indicator to be a body with a single degree of freedom the equation of motion for the condition of a uniform air stream is,

$$I\ddot{\theta} + c\dot{\theta} + k\theta = 0 \tag{2}$$

where θ is the angular deflection from the equilibrium position, and all derivatives are taken with respect to time. As shown in ref. 4, the expressions for ζ and n_n are,

$$\zeta = \frac{c}{2\sqrt{kI}} \tag{3}$$

and

$$n_n = \frac{1}{2\pi\sqrt{\frac{k}{I}}} \tag{4}$$

the coefficient c is calculated for each component from the expression

$$c = \frac{dT}{d\dot{\theta}} = qS\frac{dC_L}{d\alpha}\frac{l^2}{U} \tag{5}$$

and the coefficient k is given by

$$k = \frac{dT}{d\theta} = qS\frac{dC_L}{d\alpha}l \tag{6}$$

where T is torque in ft. lb. and l is the distance measured along the centerline of the indicator from the axis a-a to the quarter chord line of the surface considered. The moment of inertia I is

based on a density of .310 lb/cu-inch for all components, thus giving some allowance for the soldered connections. The dimensions are taken from fig. 73 and the computed values of all coefficients are listed in the following table for an air speed of 100 M.P.H.

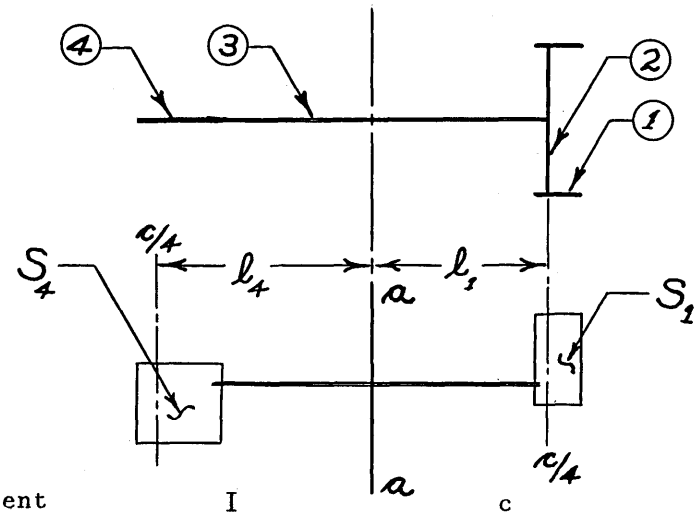

Component	I	c	k
1	2.208×10^{-8}	1.448×10^{-6}	4.045×10^{-3}
2	2.360×10^{-8}	---	---
3	$.566 \times 10^{-8}$	---	---
4	1.595×10^{-8}	1.156×10^{-6}	-2.961×10^{-3}

$I = 6.729 \times 10^{-8}$ slug ft.^{2}

$c = 2.604 \times 10^{-6}$ ft lb sec rad^{-1}

$k = 1.084 \times 10^{-3}$ ft lb rad^{-1}

Hence,

$\zeta = 0.15$

$n_n = 20$ cycles per second

The aerodynamic forces on components 2 and 3, as well as mutual interference effects between all components has been neglected in this simple analysis. The low damping ratio causes amplification of the input signal near the natural frequency so that quantitative results obtained from the indicator are not accurate. However the variation of output as the configuration is altered allows a qualitative estimate of the change in intensity of turbulence.

D. Pressure Recovery

H. Peters, ref. 1, gives an analysis of diffuser efficiency in which it is shown that the commonly used expression

$$\eta = \frac{p_2 - p_1}{q_1\left[1-\left(\frac{A_1}{A_2}\right)^2\right]} \tag{7}$$

is in error when the velocity distribution at the inlet and exit are not uniform. The correct equation is shown to be,

$$\eta_{TOT} = \frac{p_2 - p_1}{\bar{q}_1\left[X-Y\left(\frac{A_1}{A_2}\right)^2\right]} \tag{8}$$

where subscripts 1 and 2 refer respectively to the diffuser inlet and outlet, and

$$\bar{q} = \tfrac{1}{2}\rho\left[\frac{\int U dA}{A}\right]^2$$

The constants X and Y are necessarily qreater than 1 and reflect the deviation from a uniform distribution. By applying this equation to the diffuser - tailpipe combination to find the efficiency of energy conversion between station 2 and 4 we have

$$\eta_{TOT} = \frac{p_4 - p_2}{\bar{q}_2\left[X-Y\left(\frac{A_2}{A_4}\right)^2\right]} \tag{9}$$

From an inspection of fig. 1 it appears that the constant X will not differ greatly from 1.00 due to the nearly uniform velocity distribution. Since $\left(\frac{A_2}{A_4}\right)^2$ is approximately $\frac{1}{5}$, the error introduced by taking Y = 1.00 will not be great. For a preliminary investigation the assumption that X = Y = 1.00 is considered

justifiable in view of the simplification of an otherwise lengthy computation. To avoid misinterpretation we define this modified efficiency as,

$$\text{Pressure Recovery} = \frac{p_4 - p_2}{\bar{q}_2\left[1-\left(\frac{A_2}{A_4}\right)^2\right]} = \frac{p_4 - p_2}{\bar{q}_2 - \bar{q}_4} \tag{10}$$

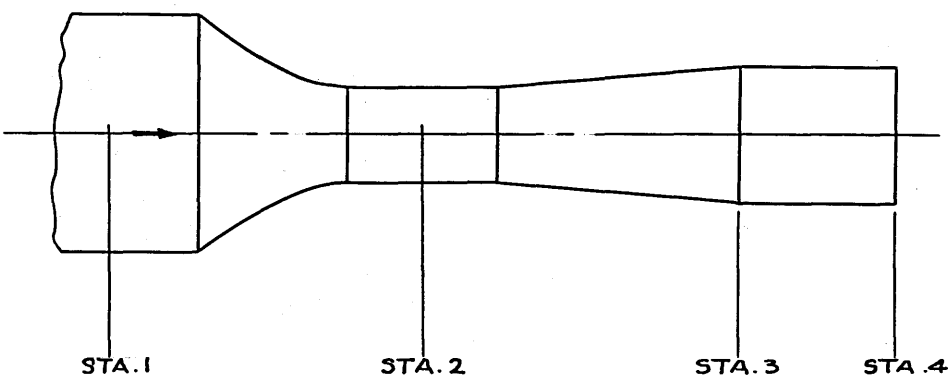

To calculate pressure recovery it is necessary to find $\bar{q}_2$ and $\bar{q}_4$. Since we have assumed X = 1.00, Bernoulli's equation gives,

$$p_1 + q_1 = p_2 + \bar{q}_2 \tag{11}$$

from continuity

$$U_1 A_1 = U_2 A_2 \tag{12}$$

from which we find

$$\bar{q}_2 = \frac{p_1 - p_2}{\left[1-\left(\frac{A_2}{A_1}\right)^2\right]} \tag{13}$$

But, A_2 = 177 sq in

A_1 = 1910 sq in

A_4 = 391 sq in

hence $\bar{q}_2 = 1.009\ (p_1 - p_2)$

$$\text{similarly, } \bar{q}_4 = \bar{q}_2 \left(\frac{A_2}{A_4}\right)^2 = .205\ \bar{q}_2 = .207(p_1 - p_2) \tag{14}$$

so that,

$$\text{Pressure Recovery} = \frac{1.249(p_4 - p_2)}{(p_1 - p_2)} \tag{15}$$

Pressure Recovery Data

At Station 4

Run	Pressure Recovery - %	Run	Pressure Recovery - %
4	84.2	21	56.4
6	46.5	22	56.6
7	48.0	24	45.7
8	51.9	26	45.6
9	54.5	27	44.9
10	55.0	28	44.2
11	54.8	30	45.1
12	52.2	31	44.4
14	55.0	32	43.1
15	56.8	33	42.0
16	57.6	35	44.0
17	48.4	36	45.5
18	52.1	37	46.2
19	53.1	38	47.7
20	54.8	39	48.5
		40	49.3

At Station 3

Run	Pressure Recovery - %
25	37.4
29	39.4
38	40.8
39.	43.1
41	43.3

WEIGHTED q DISTRIBUTION DATA

QUANTITY	RADIUS-IN.	RUN 4	RUN 6	RUN 7	RUN 8	RUN 9	RUN 10	RUN 11	RUN 12
$q_{2D}/\bar{q}$	0	1.092	1.434	1.611	1.475	1.000	.752	.722	.666
	1	1.122	1.433	1.603	1.468	1.022	.773	.736	.672
	2	1.130	1.418	1.553	1.450	1.043	.798	.747	.685
	3	1.169	1.399	1.528	1.435	1.085	.870	.796	.728
	4	1.175	1.358	1.419	1.378	1.128	.937	.861	.777
	5	1.160	1.298	1.316	1.298	1.168	1.024	.947	.857
	6	1.161	1.215	1.210	1.212	1.182	1.109	1.042	.957
	7	1.130	1.130	1.110	1.103	1.165	1.151	1.126	1.081
	7.5	1.105	1.079	1.057	1.052	1.143	1.165	1.152	1.140
	8.0	1.076	1.032	1.009	1.003	1.119	1.162	1.168	1.190
	8.5	1.030	.978	.957	.956	1.080	1.140	1.178	1.232
	9.0	.975	.910	.900	.907	1.029	1.119	1.178	1.250
	9.5	.920	.860	.847	.858	.988	1.089	1.160	1.260
	10.0	.861	.810	.812	.828	.928	1.049	1.127	1.250
	10.5	.750	.744	.738	.773	.880	.969	1.052	1.150
	-	2.18	3.59	3.55	3.44	3.35	3.33	3.27	3.35
	-	-4.37	-2.12	-2.21	-2.43	-2.58	-2.60	-2.54	-2.43
	-	.05	.01	.01	.01	.01	.01	.01	-.01

WEIGHTED q DISTRIBUTION DATA

QUANTITY	RADIUS-IN.	RUN 14	RUN 15	RUN 16	RUN 17	RUN 18	RUN 19	RUN 20	RUN 21
$q_{2D}/\bar{q}$	0	1.020	.900	.856	1.165	1.188	1.093	.987	.899
	1	1.022	.914	.872	1.177	1.175	1.103	.995	.902
	2	1.032	.936	.885	1.203	1.175	1.103	.999	.940
	3	1.064	.986	.943	1.256	1.196	1.130	1.032	.965
	4	1.098	1.025	.995	1.278	1.209	1.145	1.068	1.015
	5	1.130	1.085	1.060	1.286	1.196	1.162	1.116	1.082
	6	1.153	1.130	1.134	1.260	1.174	1.170	1.142	1.122
	7	1.140	1.132	1.140	1.195	1.140	1.145	1.140	1.140
	7.5	1.122	1.123	1.129	1.156	1.100	1.110	1.125	1.137
	8.0	1.090	1.105	1.112	1.094	1.062	1.078	1.102	1.116
	8.5	1.058	1.082	1.090	1.048	1.019	1.042	1.058	1.075
	9.0	1.009	1.025	1.042	.987	.978	.992	1.008	1.040
	9.5	.952	.984	.993	.926	.936	.941	.957	1.005
	10.0	.896	.922	.942	.882	.890	.900	.916	.950
	10.5	.822	.850	.851	.807	.847	.832	.817	.857
p_1	-	3.36	3.31	3.31	3.38	3.30	3.28	3.25	3.22
p_2	-	-2.60	-2.70	-2.77	-2.19	-2.37	-2.42	-2.50	-2.61
p_4	-	.03	.04	.04	-.03	.00	.01	.02	.03

WEIGHTED q DISTRIBUTION DATA

QUANTITY	RADIUS-IN.	RUN 22	RUN 24	RUN 26	RUN 27	RUN 28	RUN 30	RUN 31	RUN 32
$q_{2D}/\bar{q}$	0	.855	1.455	1.400	1.333	1.165	.797	.532	.478
	1	.860	1.442	1.394	1.338	1.184	.847	.580	.513
	2	.877	1.418	1.380	1.361	1.220	.917	.666	.585
	3	.928	1.394	1.360	1.406	1.282	1.065	.819	.713
	4	.995	1.373	1.335	1.388	1.325	1.155	.966	.815
	5	1.060	1.325	1.283	1.343	1.311	1.214	1.090	.955
	6	1.118	1.263	1.218	1.258	1.269	1.225	1.186	1.086
	7	1.139	1.196	1.150	1.180	1.194	1.183	1.214	1.177
	7.5	1.142	1.133	1.100	1.128	1.152	1.155	1.196	1.202
	8.0	1.132	1.088	1.050	1.070	1.108	1.115	1.175	1.220
	8.5	1.095	1.030	1.010	1.015	1.068	1.083	1.151	1.229
	9.0	1.060	.975	.949	.955	1.011	1.037	1.117	1.220
	9.5	1.004	.931	.900	.915	.966	1.010	1.083	1.213
	10.0	.964	.888	.852	.875	.933	.983	1.065	1.205
	10.5	.888	.812	.982	.802	.866	.917	1.009	1.158
p_1	-	3.19	3.52	3.52	3.52	3.50	3.51	3.52	3.52
p_2	-	-2.62	-2.16	-2.07	-2.04	-2.03	-2.02	-1.98	-1.93
p_4	-	.02	-.08	-.03	-.04	-.08	-.02	-.02	-.04

WEIGHTED q DISTRIBUTION DATA

QUANTITY	RADIUS-IN.	RUN 33	RUN 35	RUN 36	RUN 37	RUN 38	RUN 39	RUN 40
$q_{2D}/\bar{q}$	0	.448	.903	1.230	1.463	1.281	1.113	1.078
	1	.477	.965	1.269	1.450	1.290	1.130	1.085
	2	.513	1.074	1.335	1.387	1.294	1.140	1.094
	3	.612	1.227	1.360	1.357	1.320	1.199	1.140
	4	.707	1.301	1.331	1.320	1.312	1.225	1.165
	5	.835	1.320	1.291	1.280	1.265	1.245	1.191
	6	1.008	1.291	1.236	1.215	1.215	1.195	1.165
	7	1.135	1.231	1.156	1.141	1.111	1.136	1.119
	7.5	1.170	1.190	1.100	1.099	1.074	1.089	1.080
	8.0	1.204	1.125	1.034	1.053	1.032	1.051	1.038
	8.5	1.258	1.076	1.005	.995	.990	1.006	.998
	9.0	1.275	1.001	.951	.935	.935	.960	.957
	9.5	1.299	.942	.890	.908	.886	.917	.907
	10.0	1.328	.900	.853	.865	.844	.883	.866
	10.5	1.285	.822	.786	.794	.783	.822	.813
p_1	-	3.54	3.42	3.41	3.40	3.30	3.36	3.34
p_2	-	-1.90	-1.91	-1.96	-2.00	-1.99	-2.10	-2.12
p_4	-	-.07	-.03	.00	-.01	.03	.02	.04

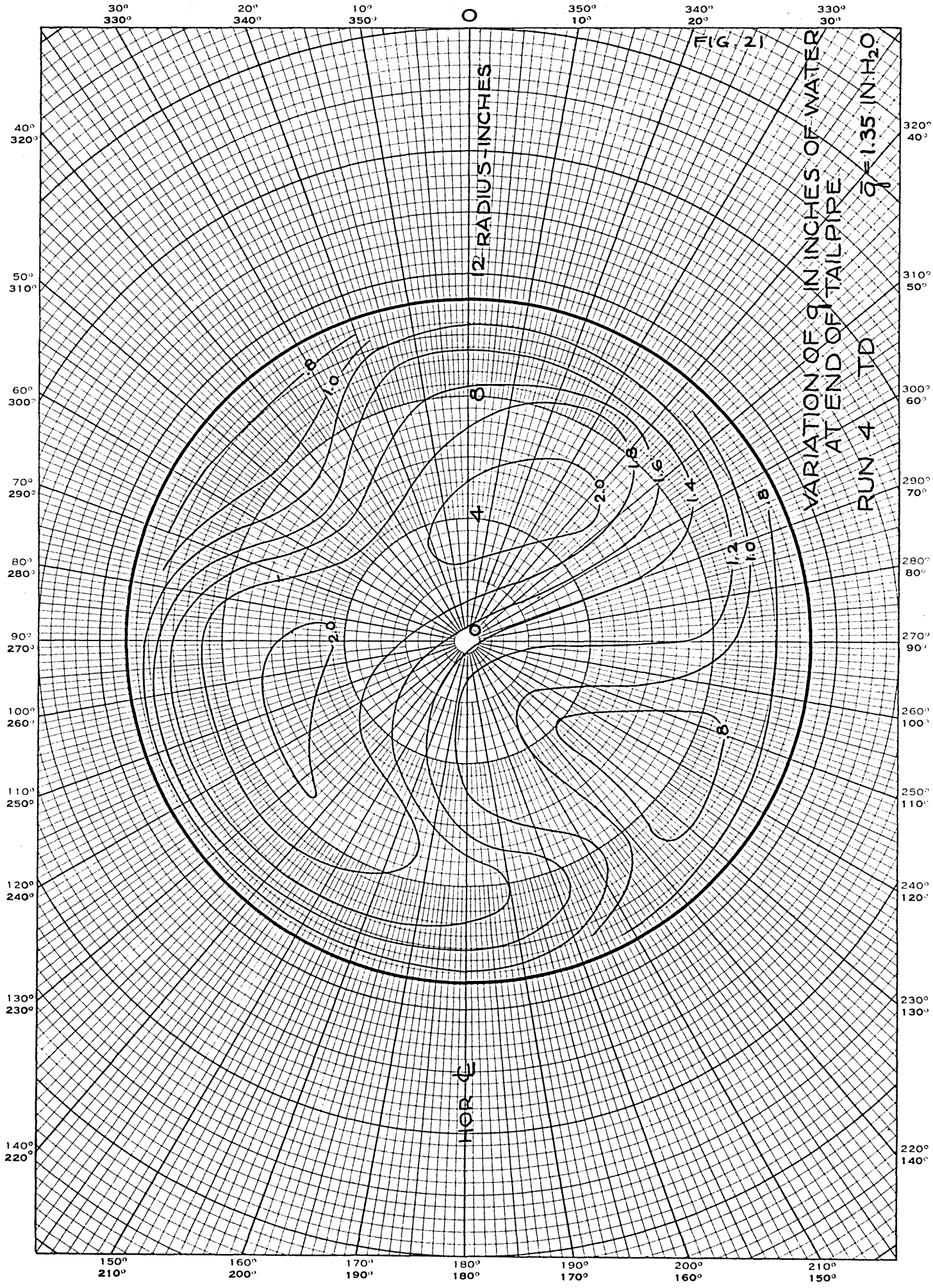
FIG. 21
VARIATION OF q IN INCHES OF WATER AT END OF TAILPIPE
RUN 4 TD
$\bar{q}$ = 1.35 IN. H_2O
RADIUS-INCHES
HORIZ
0
4
8
1.0
1.2
1.4
1.6
1.8
2.0
30° 330°
20° 340°
10° 350°
0°
350° 10°
340° 20°
330° 30°
40° 320°
50° 310°
60° 300°
70° 290°
80° 280°
90° 270°
100° 260°
110° 250°
120° 240°
130° 230°
140° 220°
150° 210°
160° 200°
170° 190°
180°
190° 170°
200° 160°
210° 150°

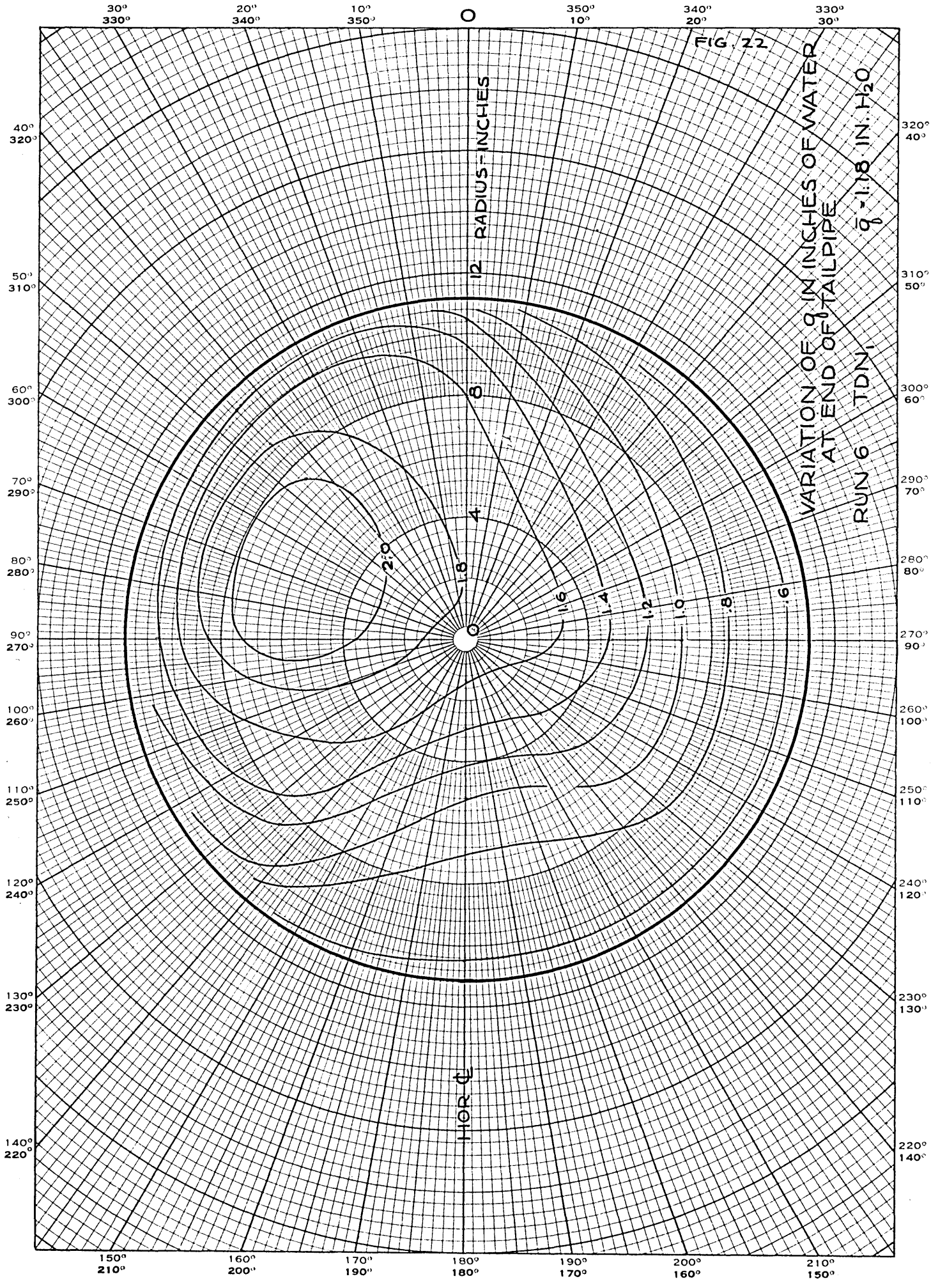
FIG. 22
VARIATION OF q IN INCHES OF WATER AT END OF TAILPIPE
RUN 6 TDN
q = 1.18 IN. H2O
12 RADIUS-INCHES
8
4
0
2.0
1.8
1.6
1.4
1.2
1.0
.8
.6
HOR. dL
0°
30° 330°
20° 340°
10° 350°
350° 10°
340° 20°
330° 30°
40° 320°
50° 310°
60° 300°
70° 290°
80° 280°
90° 270°
100° 260°
110° 250°
120° 240°
130° 230°
140° 220°
150° 210°
160° 200°
170° 190°
180° 180°
190° 170°
200° 160°
210° 150°
320° 40°
310° 50°
300° 60°
290° 70°
280° 80°
270° 90°
260° 100°
250° 110°
240° 120°
230° 130°
220° 140°

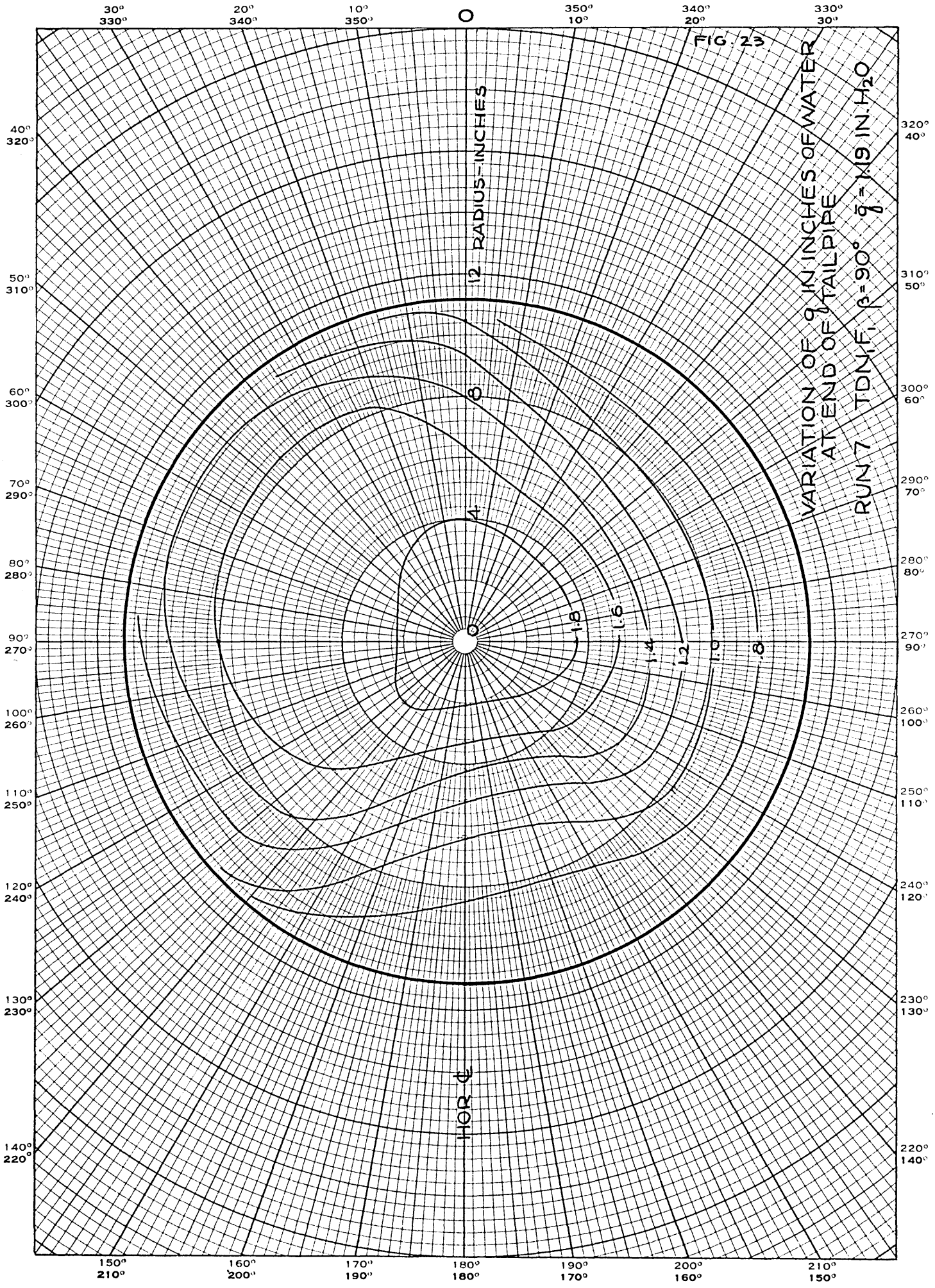
FIG. 23
VARIATION OF q IN INCHES OF WATER AT END OF TAILPIPE
RUN 7 TDN.F. β=90° q̄ = 1.19 IN. H2O
12 RADIUS-INCHES
8
4
0
1.8
1.6
1.4
1.2
1.0
.8
HOR ℄
0°
30° 330°
20° 340°
10° 350°
350° 10°
340° 20°
330° 30°
40° 320°
50° 310°
60° 300°
70° 290°
80° 280°
90° 270°
100° 260°
110° 250°
120° 240°
130° 230°
140° 220°
150° 210°
160° 200°
170° 190°
180° 180°
190° 170°
200° 160°
210° 150°
320° 40°
310° 50°
300° 60°
290° 70°
280° 80°
270° 90°
260° 100°
250° 110°
240° 120°
230° 130°
220° 140°

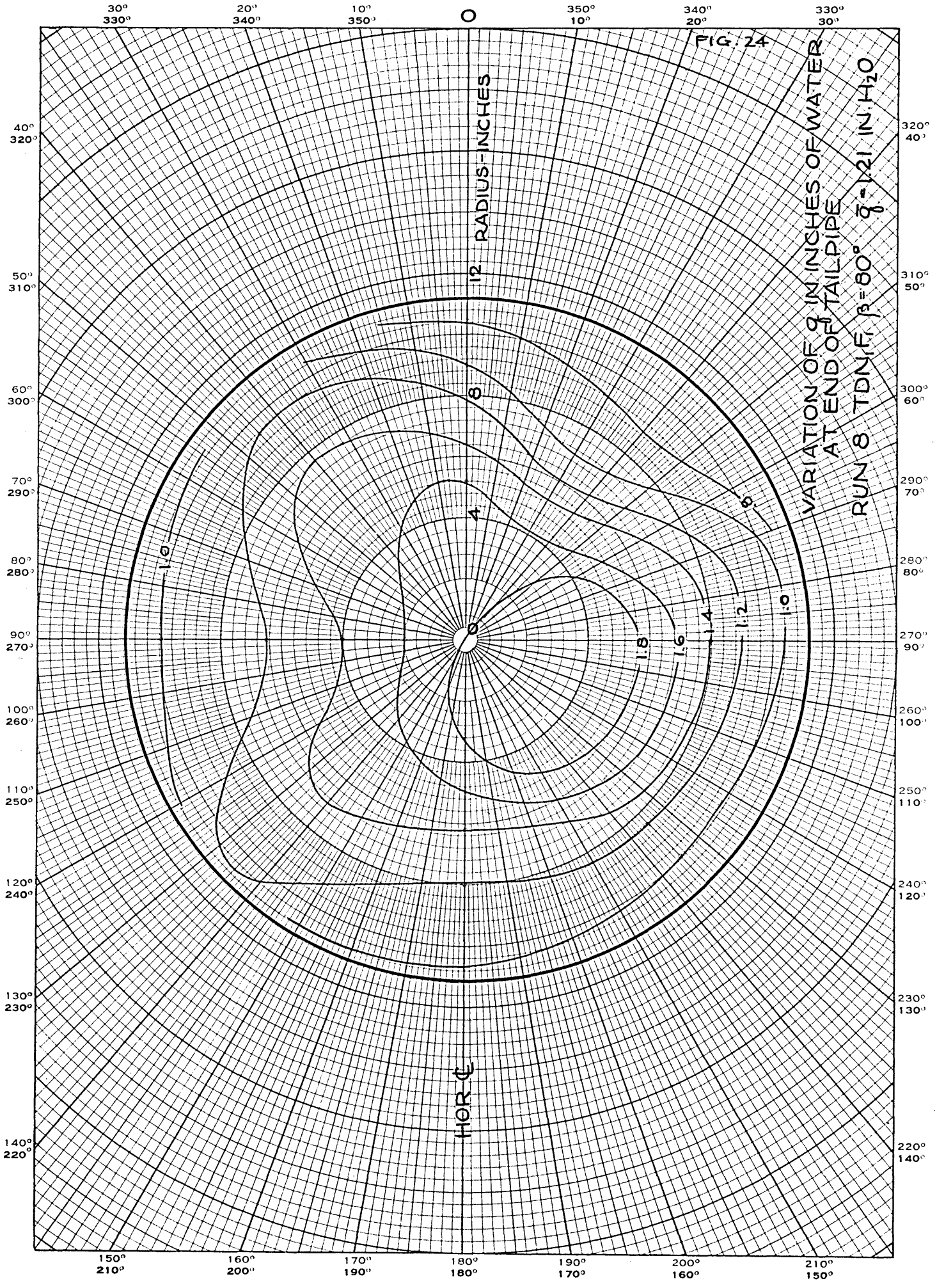
FIG. 24
VARIATION OF q IN INCHES OF WATER AT END OF TAILPIPE
RUN 8 TDN/F, β=80° q̄=1.21 IN. H2O
RADIUS-INCHES
12
8
4
0
1.0
1.2
1.4
1.6
1.8
HOR ℄
0° 360°
10° 350°
20° 340°
30° 330°
40° 320°
50° 310°
60° 300°
70° 290°
80° 280°
90° 270°
100° 260°
110° 250°
120° 240°
130° 230°
140° 220°
150° 210°
160° 200°
170° 190°
180°
190° 170°
200° 160°
210° 150°

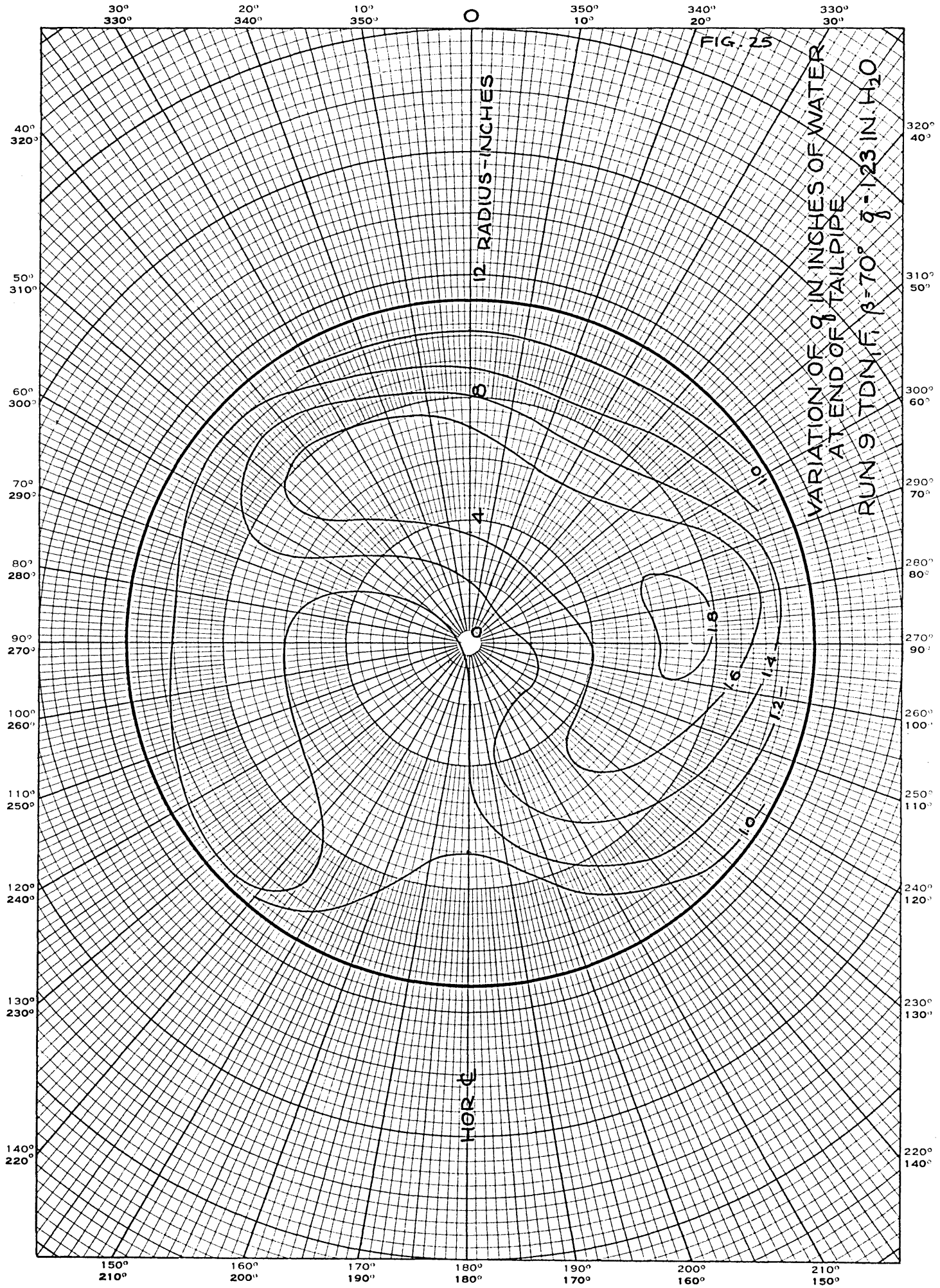
FIG. 25
VARIATION OF q IN INCHES OF WATER AT END OF TAILPIPE
RUN 9 TDN, F, β 70° q = 1.23 IN. H2O
12 RADIUS-INCHES
8
4
0
1.0
1.2
1.4
1.6
1.8
HOR ℄
0°
30° 330°
20° 340°
10° 350°
350° 10°
340° 20°
330° 30°
40° 320°
50° 310°
60° 300°
70° 290°
80° 280°
90° 270°
100° 260°
110° 250°
120° 240°
130° 230°
140° 220°
150° 210°
160° 200°
170° 190°
180° 180°
190° 170°
200° 160°
210° 150°
320° 40°
310° 50°
300° 60°
290° 70°
280° 80°
270° 90°
260° 100°
250° 110°
240° 120°
230° 130°
220° 140°

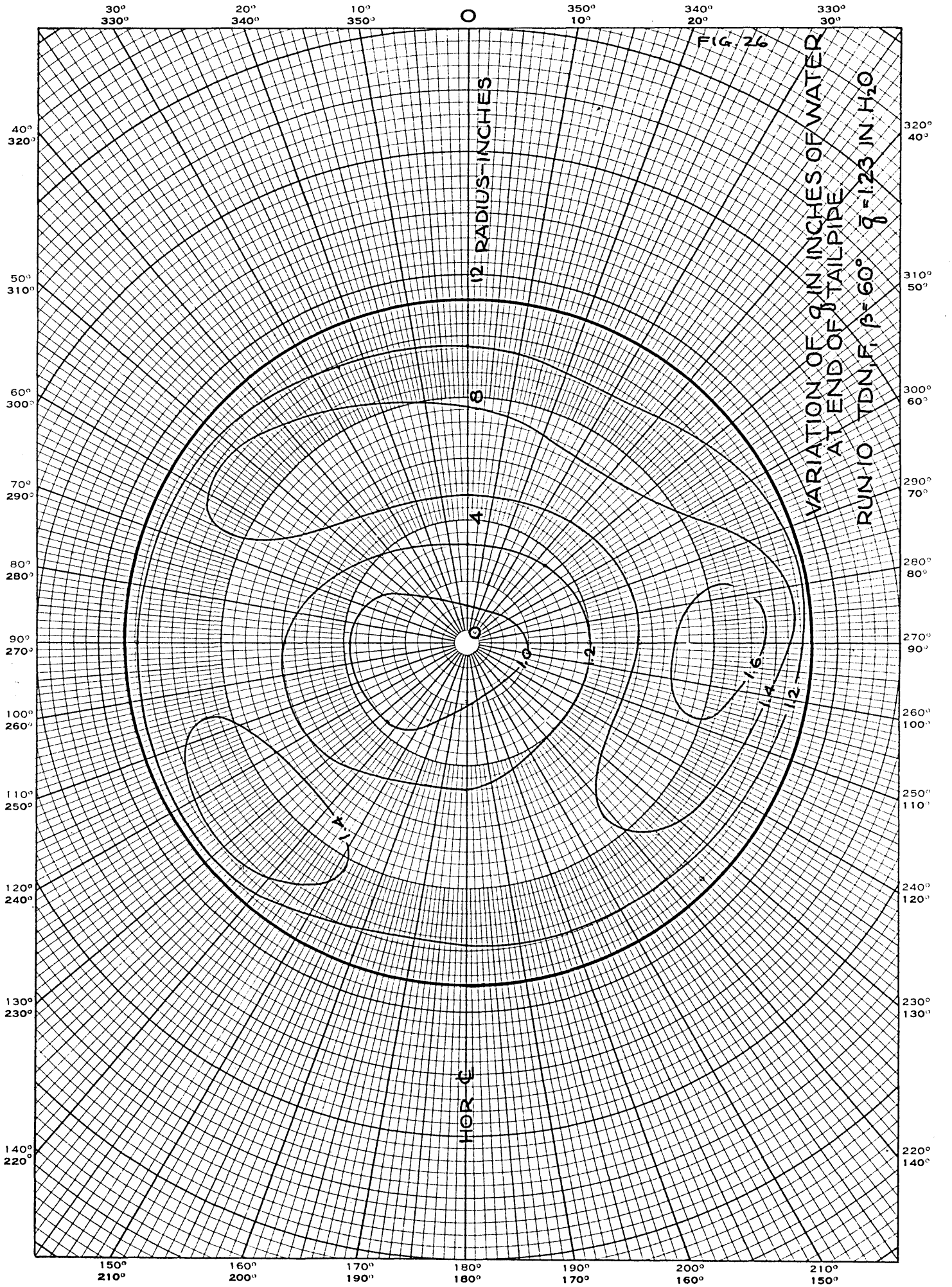
FIG. 26
VARIATION OF q IN INCHES OF WATER AT END OF TAILPIPE
RUN 10 TDN, F, β = 60° q = 1.23 IN. H2O
12 RADIUS-INCHES
8
4
0
1.0
1.2
1.4
1.6
1.12
1.4
HORIZ
0°
30° 330°
20° 340°
10° 350°
350° 10°
340° 20°
330° 30°
40° 320°
50° 310°
60° 300°
70° 290°
80° 280°
90° 270°
100° 260°
110° 250°
120° 240°
130° 230°
140° 220°
150° 210°
160° 200°
170° 190°
180° 180°
190° 170°
200° 160°
210° 150°
220° 140°
230° 130°
240° 120°
250° 110°
260° 100°
270° 90°
280° 80°
290° 70°
300° 60°
310° 50°
320° 40°

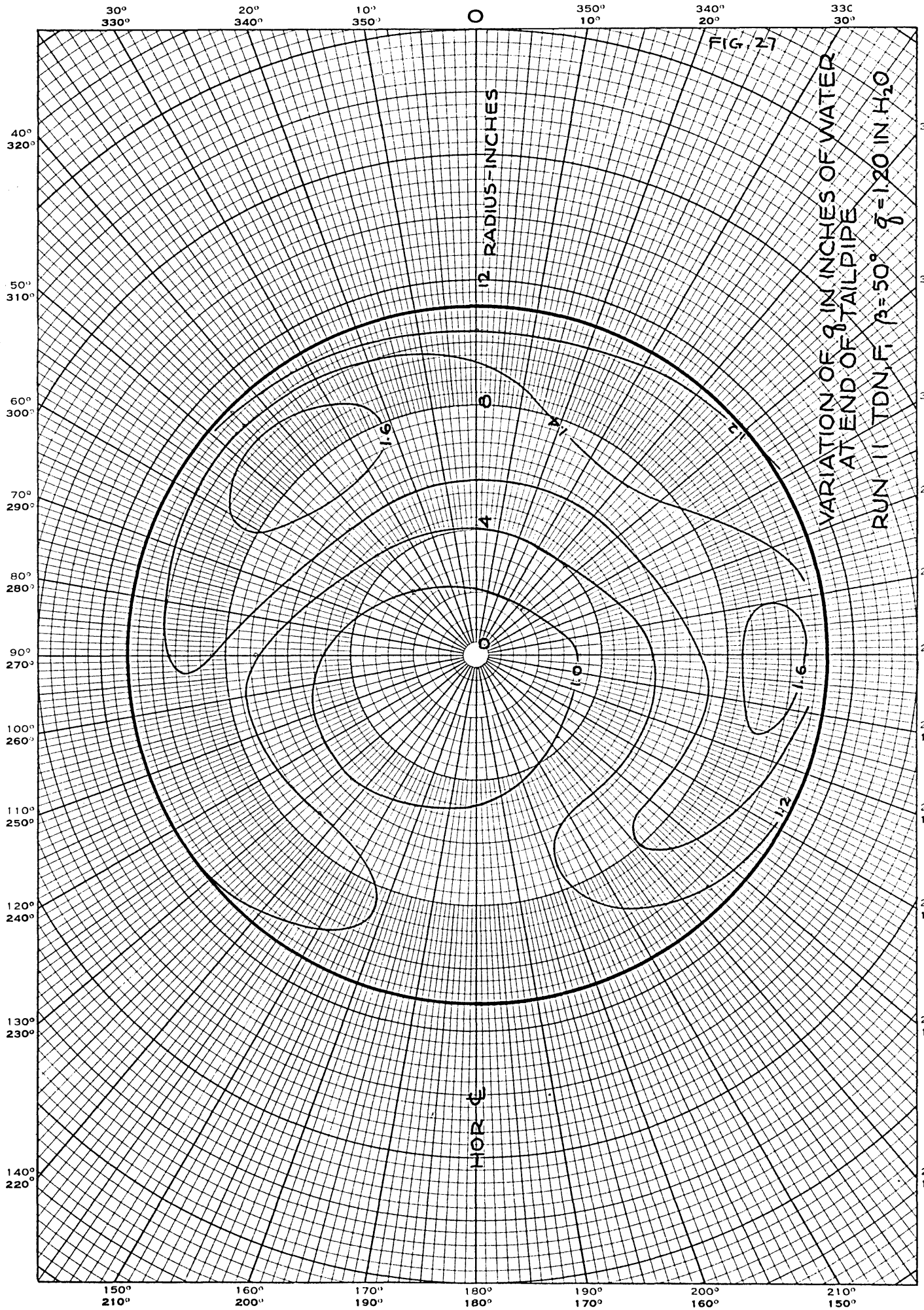
FIG. 27
VARIATION OF q IN INCHES OF WATER AT END OF TAILPIPE
RUN 11 TDN, F, β=50° q̄ = 1.20 IN. H2O
12 RADIUS-INCHES
8
4
0
1.6
1.1
2
1.0
1.6
1.2
HORIZ
0°
30° 330°
20° 340°
10° 350°
350° 10°
340° 20°
330° 30°
40° 320°
50° 310°
60° 300°
70° 290°
80° 280°
90° 270°
100° 260°
110° 250°
120° 240°
130° 230°
140° 220°
150° 210°
160° 200°
170° 190°
180° 180°
190° 170°
200° 160°
210° 150°
320° 40°
310° 50°
300° 60°
290° 70°
280° 80°
270° 90°
260° 100°
250° 110°
240° 120°
230° 130°
220° 140°

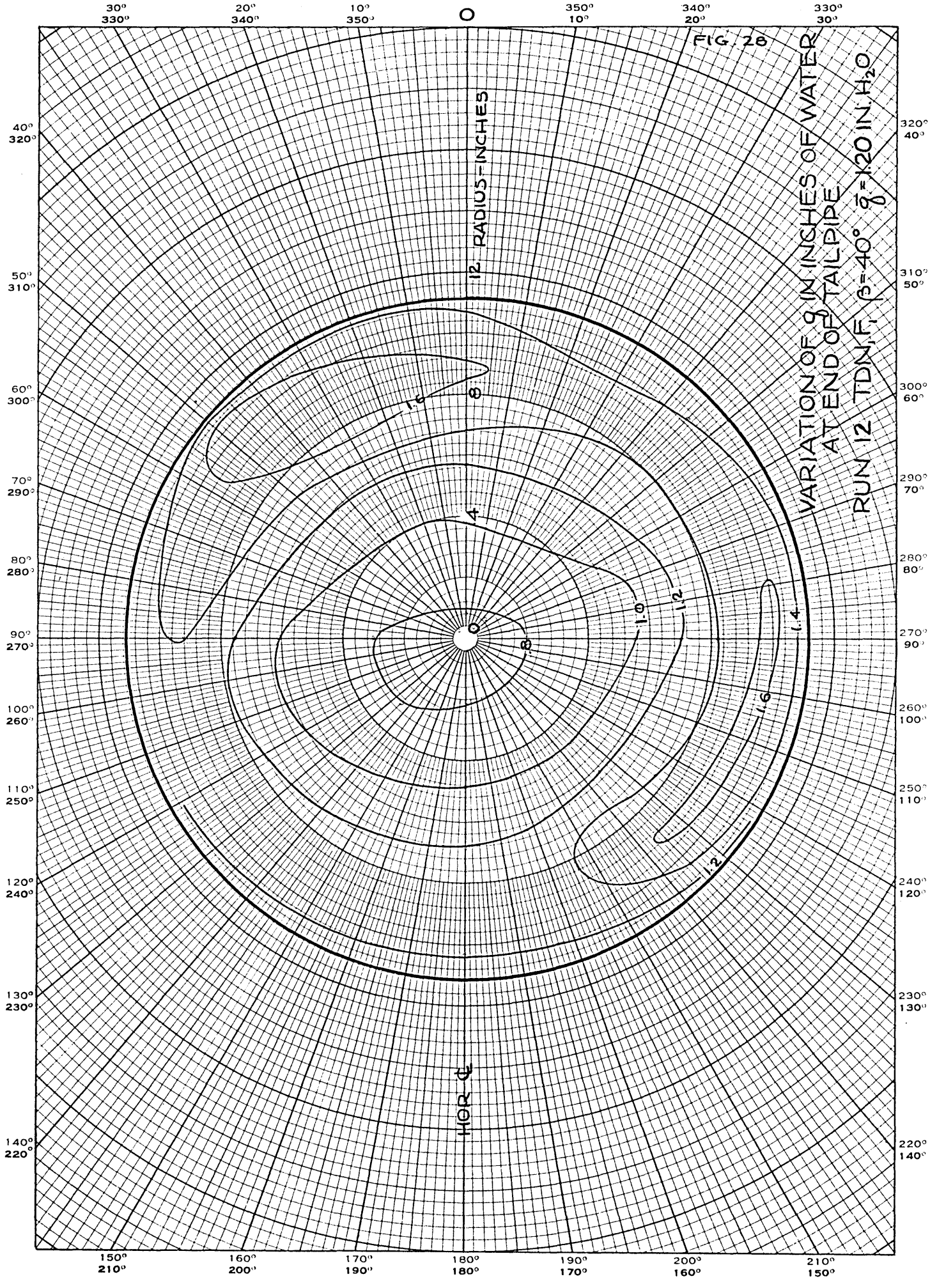
FIG. 28
VARIATION OF q IN INCHES OF WATER AT END OF TAIL PIPE
RUN 12 TDN. F. β=40° q=1.20 IN. H2O
12 RADIUS-INCHES
8
4
0
1.6
1.0
1.2
1.4
1.6
1.2
HOR. ℄
O
30° 330°
20° 340°
10° 350°
350° 10°
340° 20°
330° 30°
40° 320°
50° 310°
60° 300°
70° 290°
80° 280°
90° 270°
100° 260°
110° 250°
120° 240°
130° 230°
140° 220°
320° 40°
310° 50°
300° 60°
290° 70°
280° 80°
270° 90°
260° 100°
250° 110°
240° 120°
230° 130°
220° 140°
150° 210°
160° 200°
170° 190°
180° 180°
190° 170°
200° 160°
210° 150°

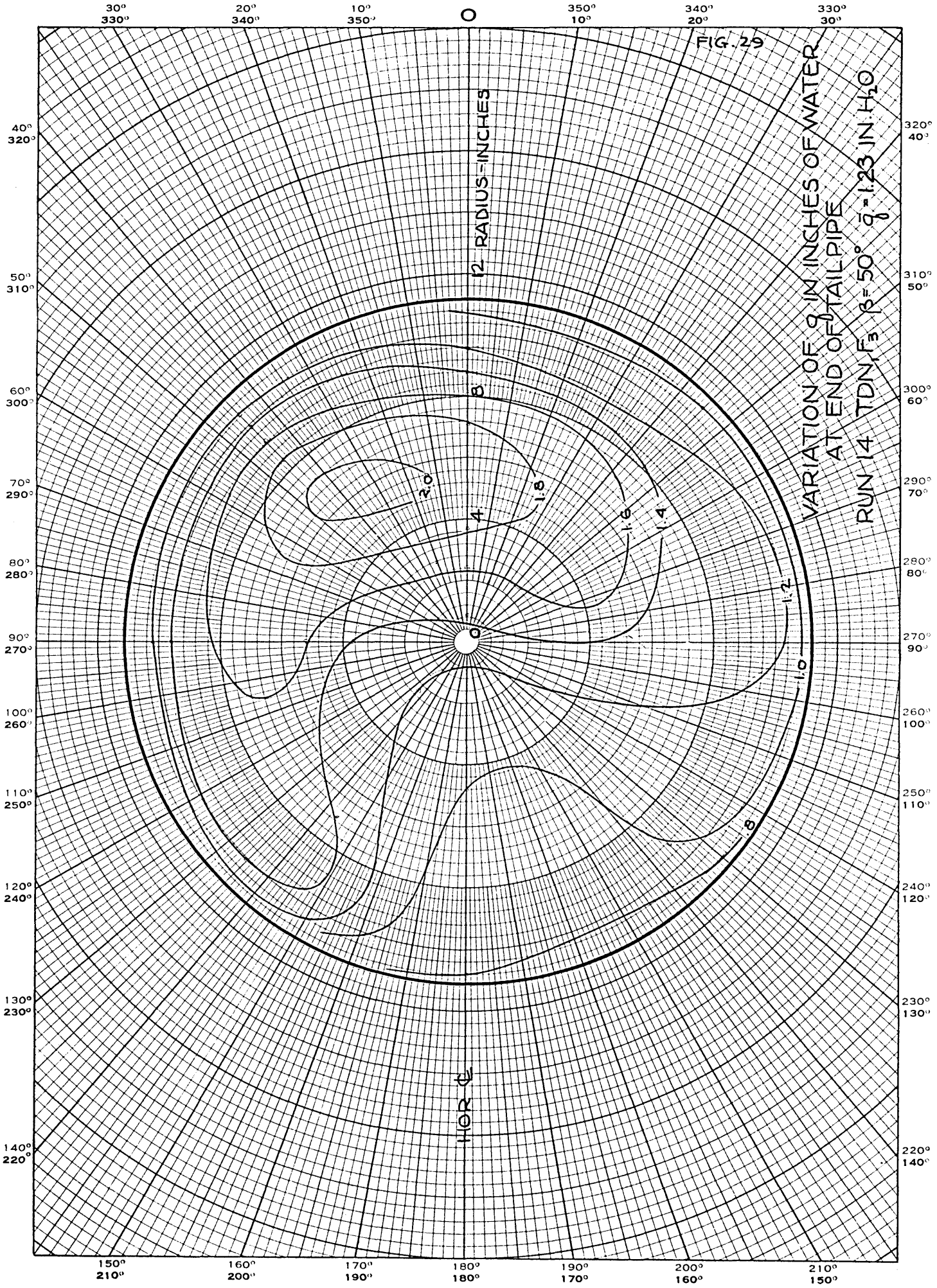
FIG. 29
VARIATION OF q IN INCHES OF WATER AT END OF TAIL PIPE
RUN 14 TDN, F3 β = 50° q = 1.23 IN. H2O
12 RADIUS-INCHES
8
4
0
2.0
1.8
1.6
1.4
1.2
1.0
.8
HOR ℄
0° 360°
10° 350°
20° 340°
30° 330°
40° 320°
50° 310°
60° 300°
70° 290°
80° 280°
90° 270°
100° 260°
110° 250°
120° 240°
130° 230°
140° 220°
150° 210°
160° 200°
170° 190°
180°
190° 170°
200° 160°
210° 150°
220° 140°
230° 130°
240° 120°
250° 110°
260° 100°
270° 90°
280° 80°
290° 70°
300° 60°
310° 50°
320° 40°
330° 30°
340° 20°
350° 10°

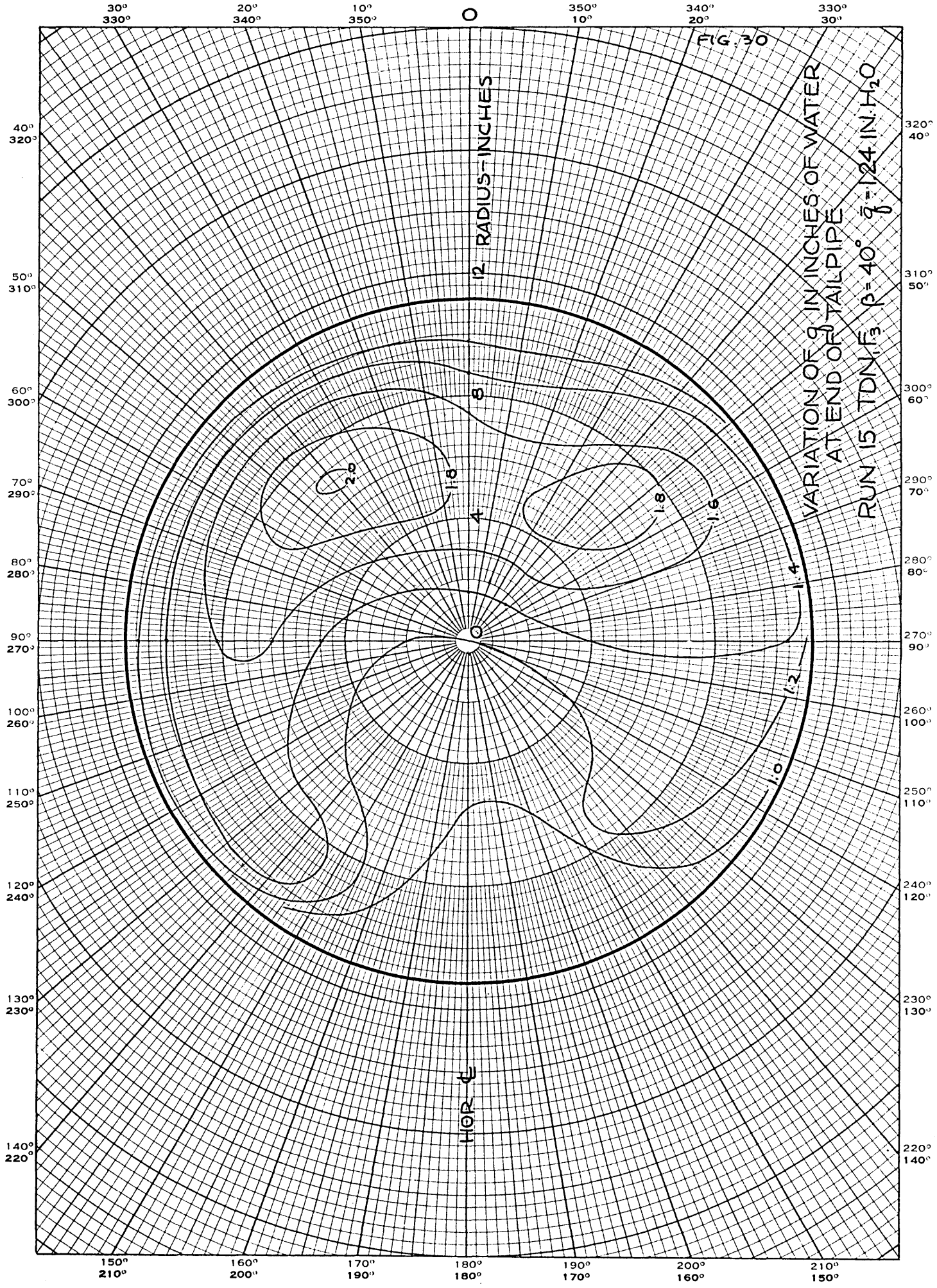
FIG. 30
VARIATION OF q IN INCHES OF WATER AT END OF TAILPIPE
RUN 15 TDN-F3 β = 40° q = 1.24 IN. H2O
RADIUS-INCHES
12
8
4
0
2.0
1.8
1.8
1.6
1.4
1.2
1.0
HOR. ℄
0°
30° 330°
20° 340°
10° 350°
350° 10°
340° 20°
330° 30°
40° 320°
50° 310°
60° 300°
70° 290°
80° 280°
90° 270°
100° 260°
110° 250°
120° 240°
130° 230°
140° 220°
150° 210°
160° 200°
170° 190°
180° 180°
190° 170°
200° 160°
210° 150°
320° 40°
310° 50°
300° 60°
290° 70°
280° 80°
270° 90°
260° 100°
250° 110°
240° 120°
230° 130°
220° 140°

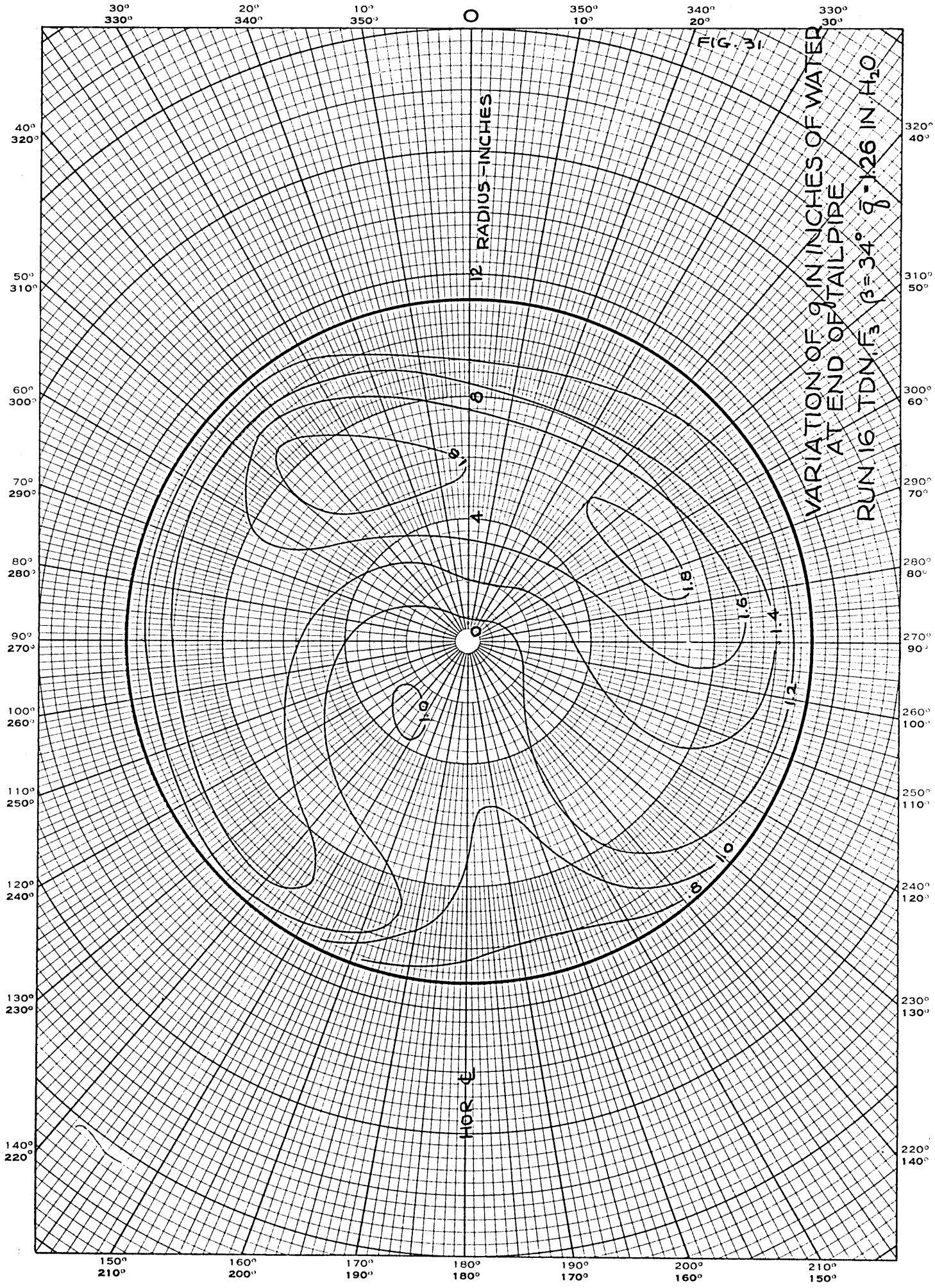
FIG. 31
VARIATION OF q IN INCHES OF WATER AT END OF TAILPIPE
RUN 16 TDN, F3 β=34° q̄=.26 IN. H2O
12 RADIUS-INCHES
8
4
0
HOR ℄
.8
1.0
1.2
1.4
1.6
1.8
2.0
2.2
30° 330°
20° 340°
10° 350°
0
350° 10°
340° 20°
330° 30°
40° 320°
50° 310°
60° 300°
70° 290°
80° 280°
90° 270°
100° 260°
110° 250°
120° 240°
130° 230°
140° 220°
320° 40°
310° 50°
300° 60°
290° 70°
280° 80°
270° 90°
260° 100°
250° 110°
240° 120°
230° 130°
220° 140°
150° 210°
160° 200°
170° 190°
180° 180°
190° 170°
200° 160°
210° 150°

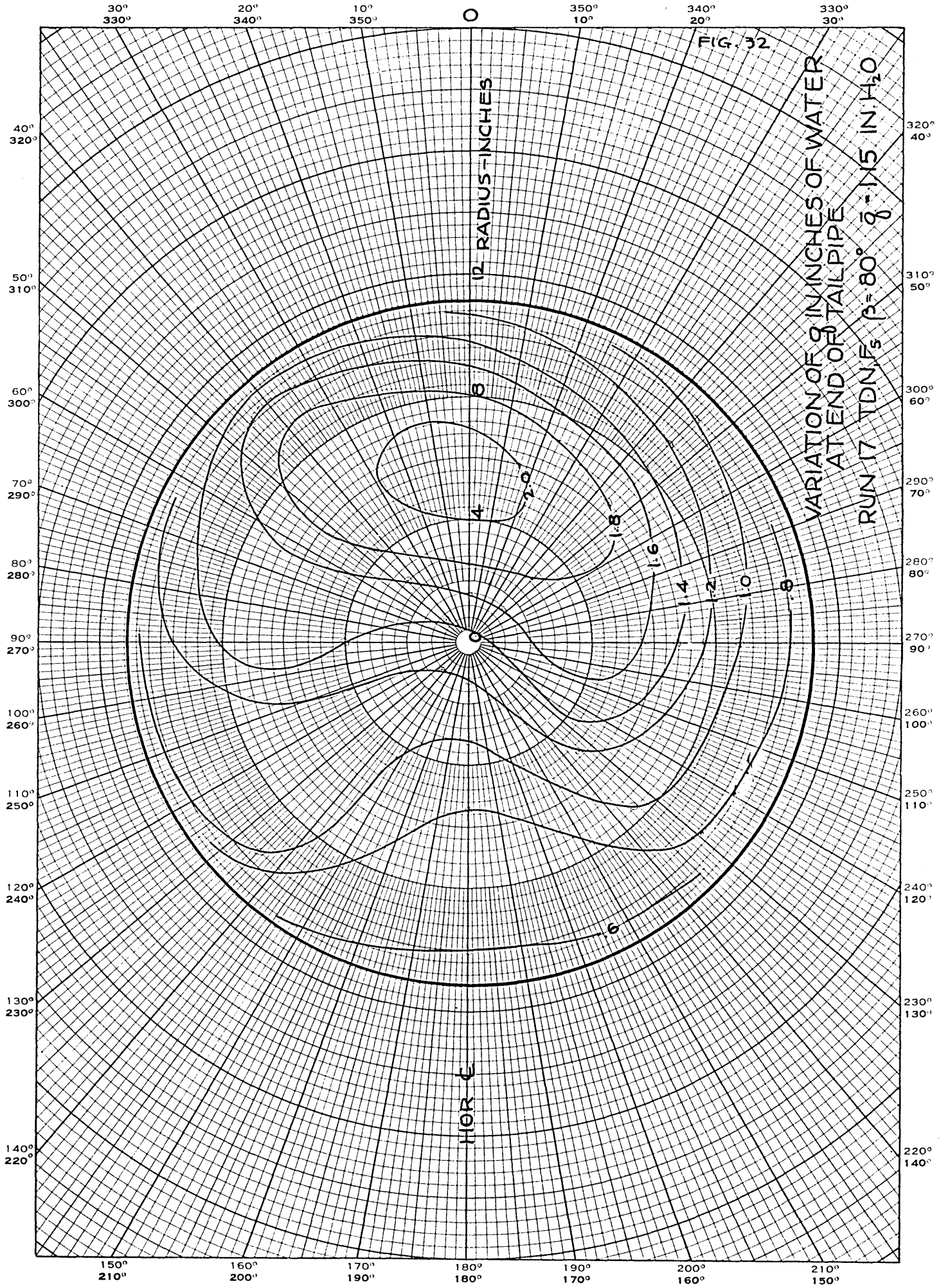
FIG. 32
VARIATION OF q IN INCHES OF WATER AT END OF TAIL PIPE
RUN 17 TDN, F_s $\beta = 80°$ $\bar{q} = 1.15$ IN. H_2O
12 RADIUS-INCHES
8
4
0
2.0
1.8
1.6
1.4
1.2
1.0
.8
6
HOR. ℄
0°
30° 330°
20° 340°
10° 350°
350° 10°
340° 20°
330° 30°
40° 320°
50° 310°
60° 300°
70° 290°
80° 280°
90° 270°
100° 260°
110° 250°
120° 240°
130° 230°
140° 220°
150° 210°
160° 200°
170° 190°
180° 180°
190° 170°
200° 160°
210° 150°
220° 140°
230° 130°
240° 120°
250° 110°
260° 100°
270° 90°
280° 80°
290° 70°
300° 60°
310° 50°
320° 40°

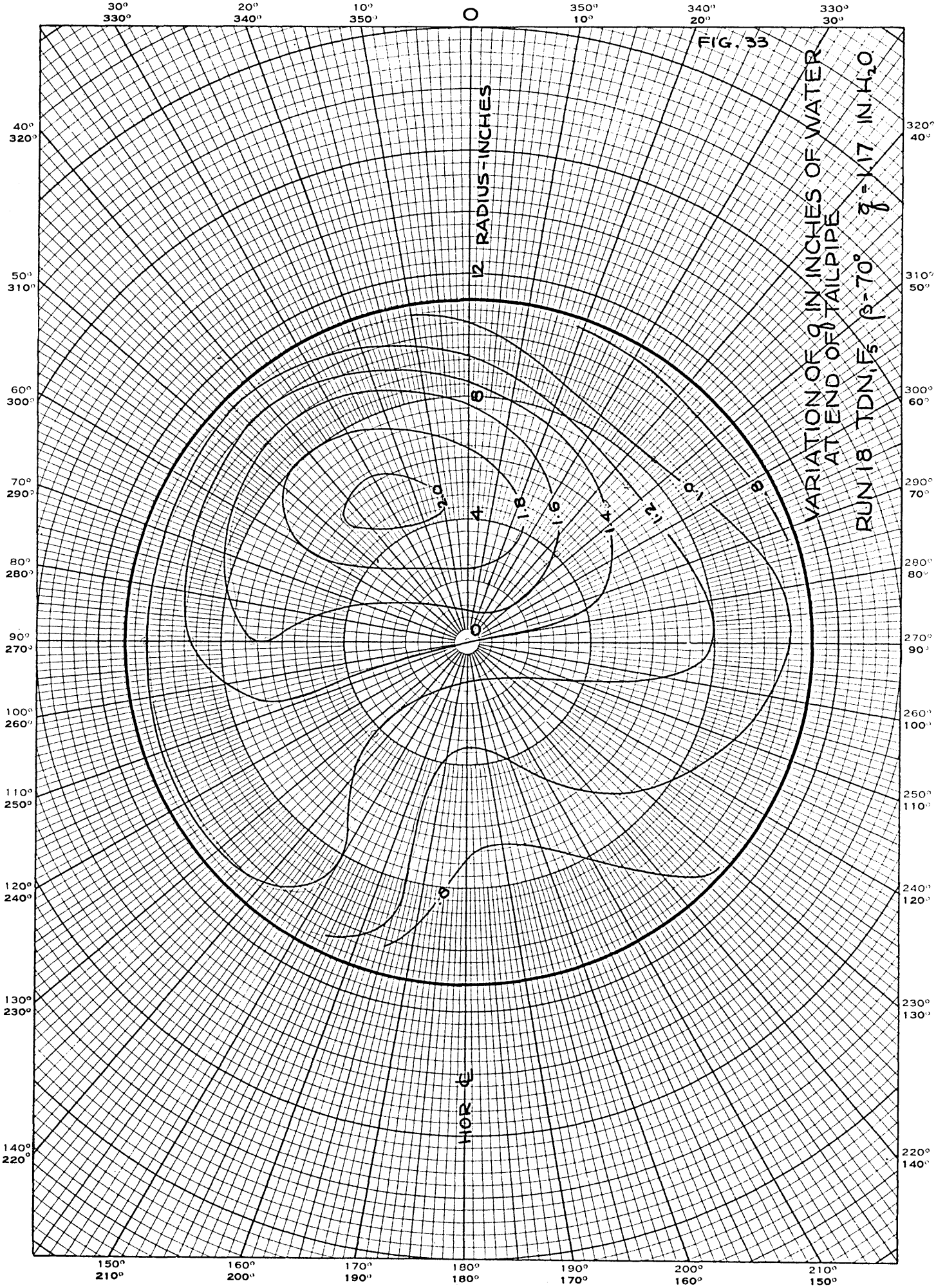
FIG. 33
VARIATION OF q IN INCHES OF WATER AT END OF TAILPIPE
RUN 18 TDN, F_s β=70° ζ=.17 IN. H_2O
12 RADIUS-INCHES
HOR ℄
0
30° 330°
20° 340°
10° 350°
350° 10°
340° 20°
330° 30°
40° 320°
50° 310°
60° 300°
70° 290°
80° 280°
90° 270°
100° 260°
110° 250°
120° 240°
130° 230°
140° 220°
320° 40°
310° 50°
300° 60°
290° 70°
280° 80°
270° 90°
260° 100°
250° 110°
240° 120°
230° 130°
220° 140°
150° 210°
160° 200°
170° 190°
180° 180°
190° 170°
200° 160°
210° 150°
.8
.4
2.0
1.8
1.6
1.4
1.2
.1
.8
.6
.4
.2
.0

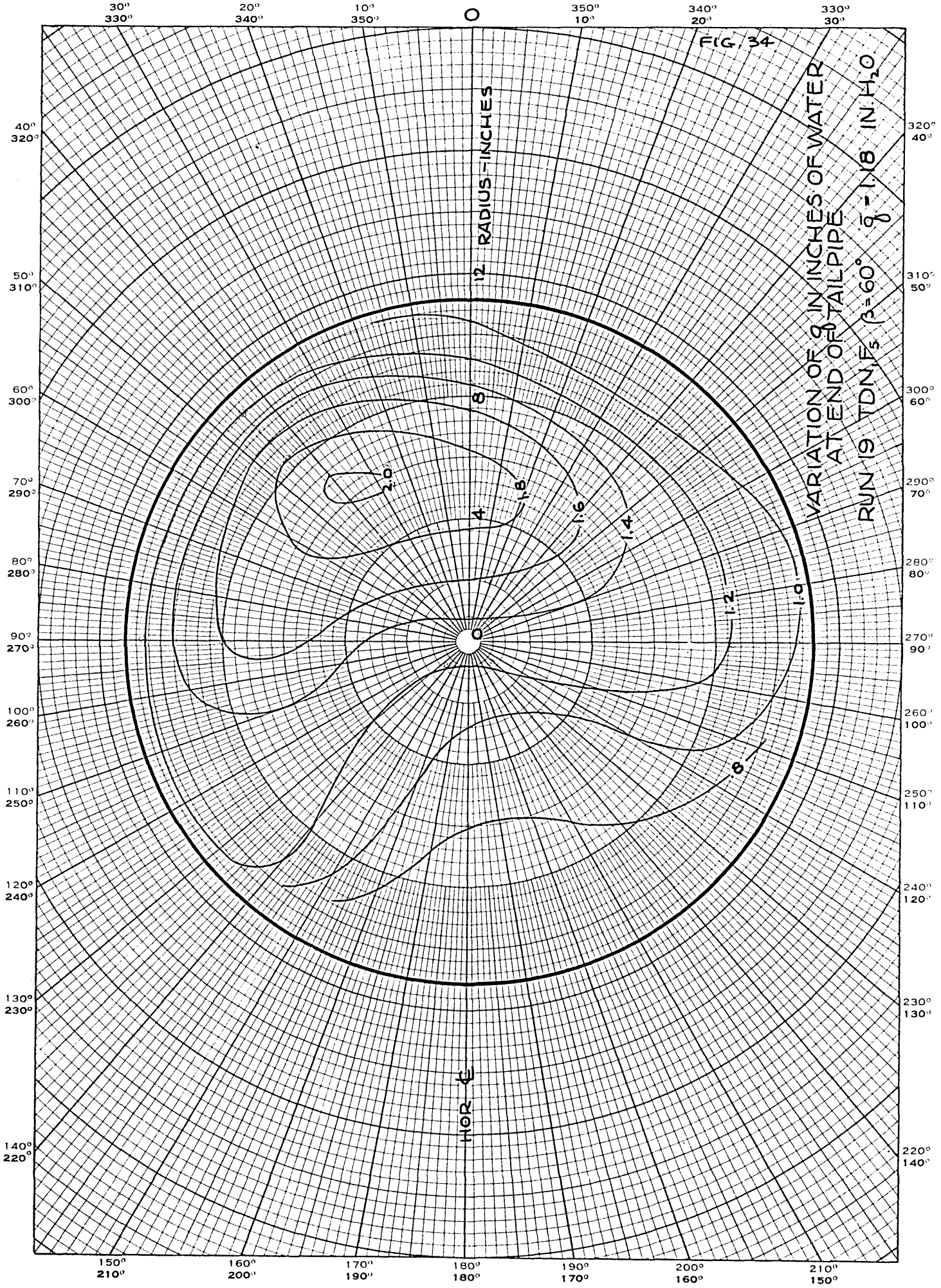
FIG. 34
VARIATION OF q IN INCHES OF WATER AT END OF TAILPIPE
RUN 19 TDN, Fs β=60° q̄ = 1.18 IN. H2O
RADIUS-INCHES
12
8
4
0
2.0
1.8
1.6
1.4
1.2
1.0
.8
HOR. ℄
0°
30° 330°
20° 340°
10° 350°
350° 10°
340° 20°
330° 30°
40° 320°
50° 310°
60° 300°
70° 290°
80° 280°
90° 270°
100° 260°
110° 250°
120° 240°
130° 230°
140° 220°
150° 210°
160° 200°
170° 190°
180° 180°
190° 170°
200° 160°
210° 150°
220° 140°
230° 130°
240° 120°
250° 110°
260° 100°
270° 90°
280° 80°
290° 70°
300° 60°
310° 50°
320° 40°

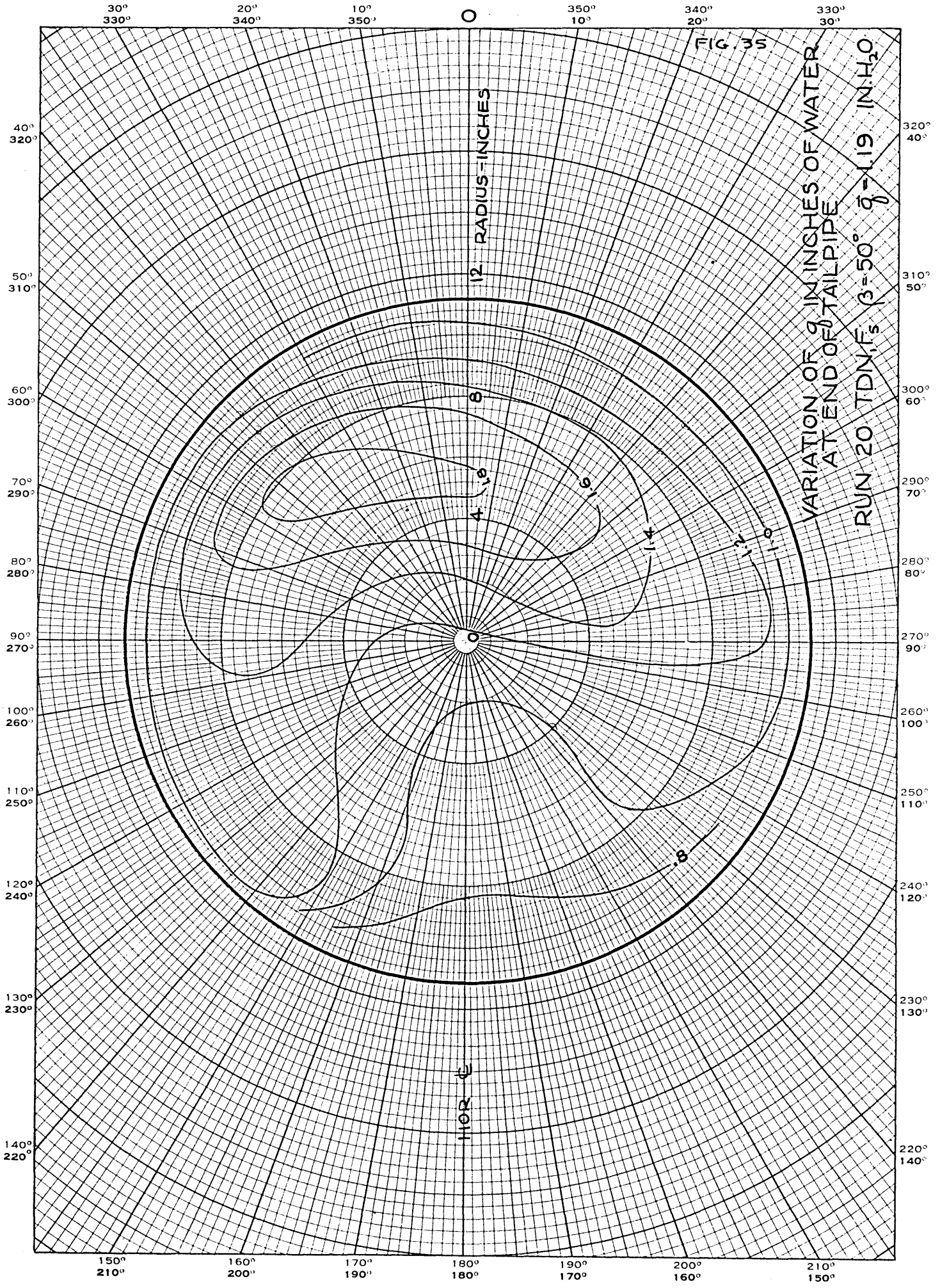
FIG. 35
VARIATION OF q IN INCHES OF WATER AT END OF TAILPIPE
RUN 20 TDN, F_s $\beta = 50°$ $\bar{q} = 1.19$ IN. H_2O
RADIUS - INCHES
HOR. ℄
0
4
8
12
.8
1.4
1.9
2.1
1.0
30° 330°
20° 340°
10° 350°
0°
350° 10°
340° 20°
330° 30°
40° 320°
50° 310°
60° 300°
70° 290°
80° 280°
90° 270°
100° 260°
110° 250°
120° 240°
130° 230°
140° 220°
150° 210°
160° 200°
170° 190°
180°
190° 170°
200° 160°
210° 150°

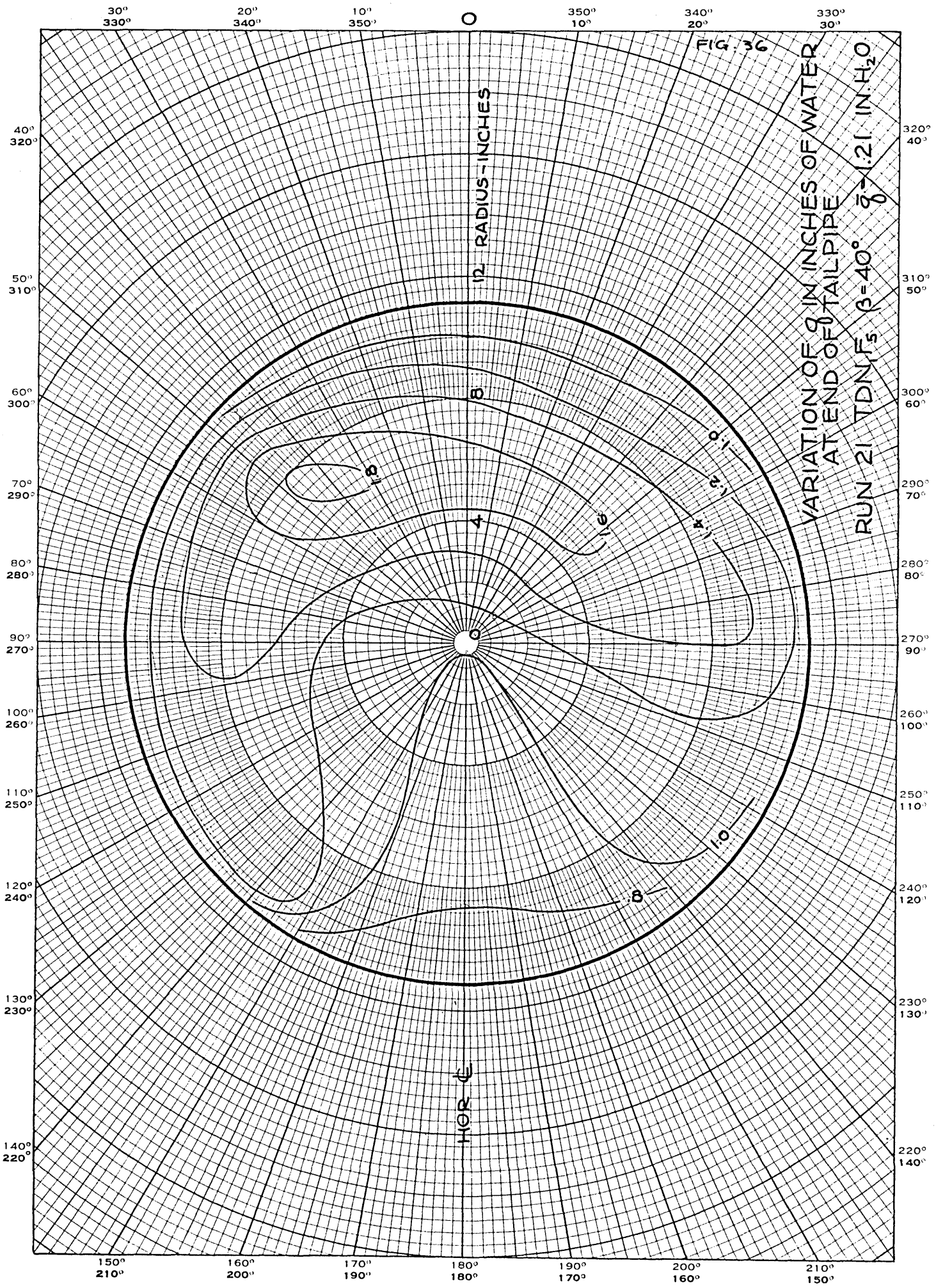
FIG. 36
VARIATION OF q IN INCHES OF WATER AT END OF TAILPIPE
RUN 21 TDN F5 β=40° q̄=1.21 IN. H2O
12 RADIUS-INCHES
8
4
0
HOR ℄
.8
1.0
1.2
1.4
1.6
1.8
0°
10°
20°
30°
40°
50°
60°
70°
80°
90°
100°
110°
120°
130°
140°
150°
160°
170°
180°
190°
200°
210°
220°
230°
240°
250°
260°
270°
280°
290°
300°
310°
320°
330°
340°
350°

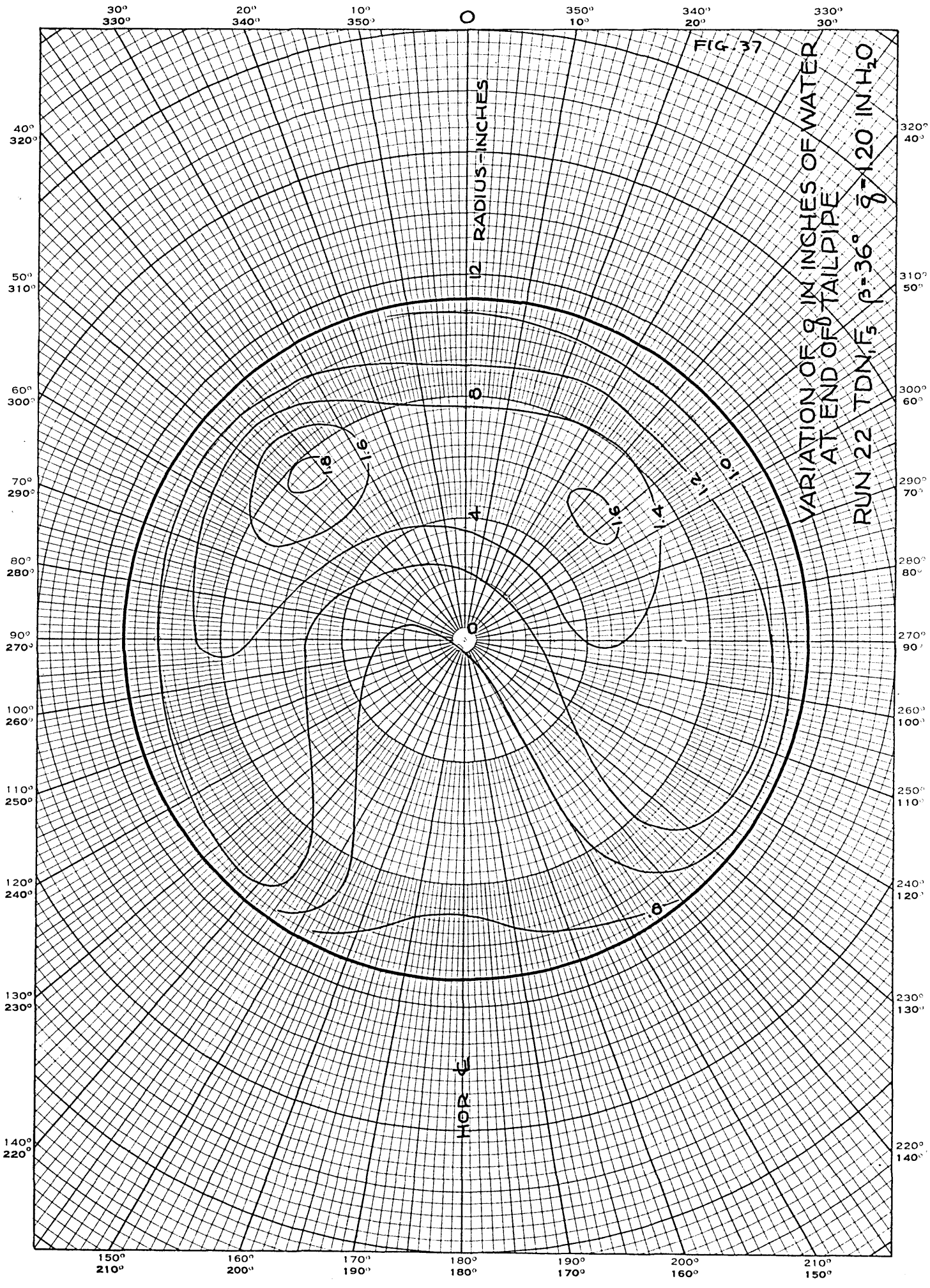
FIG. 37
VARIATION OF q IN INCHES OF WATER AT END OF TAILPIPE
RUN 22 TDN. F5 β=36° q̄=120 IN. H2O
RADIUS-INCHES
12
8
4
0
1.8
1.6
1.6
1.4
1.2
1.0
.8
HOR. ℄
0°
30° 330°
20° 340°
10° 350°
350° 10°
340° 20°
330° 30°
40° 320°
50° 310°
60° 300°
70° 290°
80° 280°
90° 270°
100° 260°
110° 250°
120° 240°
130° 230°
140° 220°
150° 210°
160° 200°
170° 190°
180° 180°
190° 170°
200° 160°
210° 150°
220° 140°
230° 130°
240° 120°
250° 110°
260° 100°
270° 90°
280° 80°
290° 70°
300° 60°
310° 50°
320° 40°

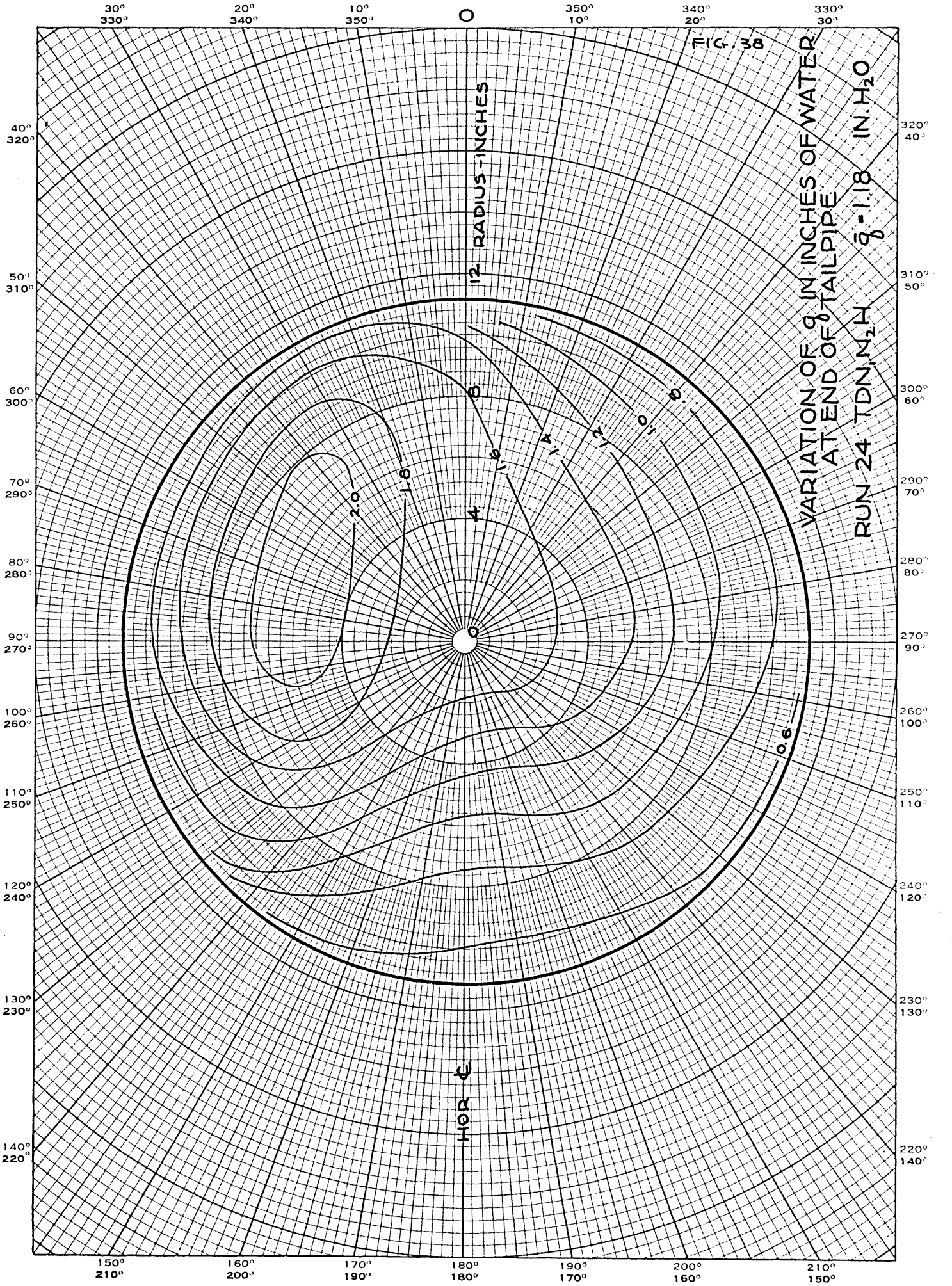
FIG. 38
VARIATION OF q IN INCHES OF WATER AT END OF TAILPIPE
RUN 24 TDN, N_2H_4
$\bar{q}_b$ = 1.18 IN. H_2O
12 RADIUS-INCHES
8
4
0
2.0
1.8
1.6
1.4
1.2
1.0
0.8
0.6
HOR. ℄
0° 360°
10° 350°
20° 340°
30° 330°
40° 320°
50° 310°
60° 300°
70° 290°
80° 280°
90° 270°
100° 260°
110° 250°
120° 240°
130° 230°
140° 220°
150° 210°
160° 200°
170° 190°
180°
190° 170°
200° 160°
210° 150°
220° 140°
230° 130°
240° 120°
250° 110°
260° 100°
270° 90°
280° 80°
290° 70°
300° 60°
310° 50°
320° 40°
330° 30°
340° 20°
350° 10°

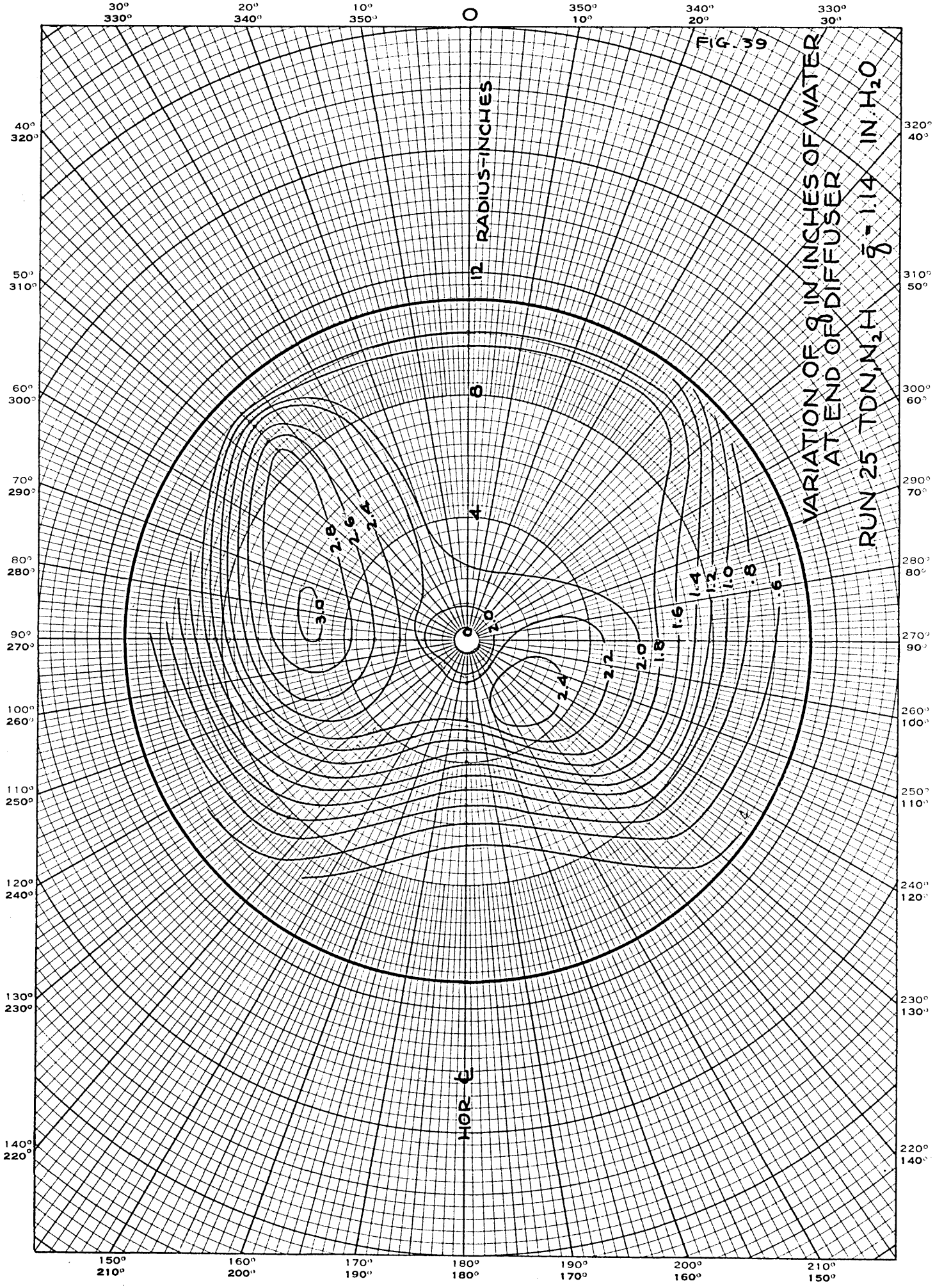
FIG. 39
VARIATION OF q IN INCHES OF WATER AT END OF DIFFUSER
RUN 25 TDN,N2H4 q̄ = 1.14 IN. H2O
12 RADIUS-INCHES
8
4
0
HOR. ℄
30° 330°
20° 340°
10° 350°
0
350° 10°
340° 20°
330° 30°
40° 320°
50° 310°
60° 300°
70° 290°
80° 280°
90° 270°
100° 260°
110° 250°
120° 240°
130° 230°
140° 220°
320° 40°
310° 50°
300° 60°
290° 70°
280° 80°
270° 90°
260° 100°
250° 110°
240° 120°
230° 130°
220° 140°
150° 210°
160° 200°
170° 190°
180° 180°
190° 170°
200° 160°
210° 150°
3.0
2.8
2.6
2.4
2.4
2.2
2.0
1.8
1.6
1.4
1.2
1.0
.8
.6
2.0

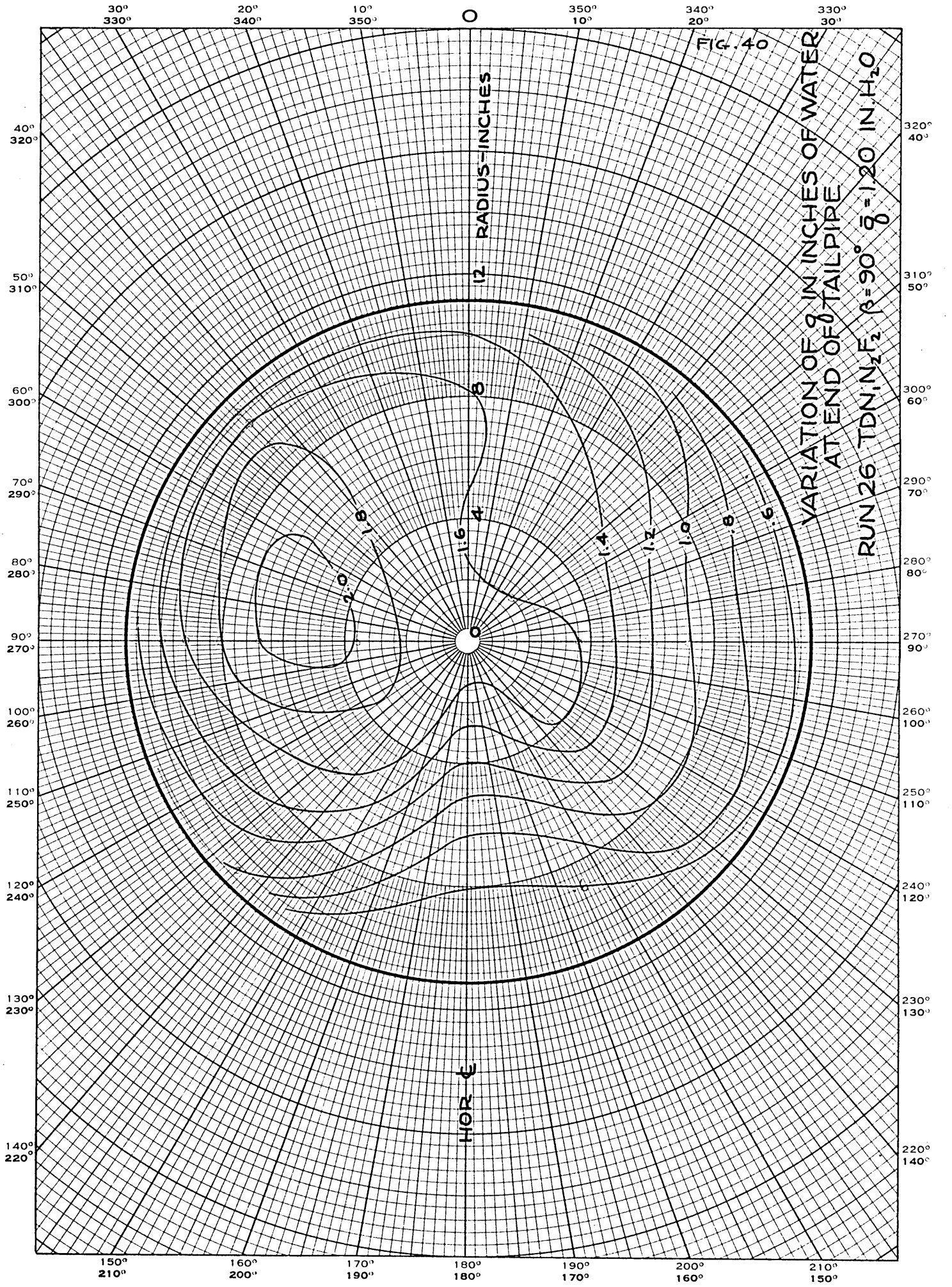
FIG. 40
VARIATION OF δ IN INCHES OF WATER AT END OF TAILPIPE
RUN 26 TDN, N2F2 (β=90° δ=1.20 IN. H2O
RADIUS-INCHES
12
8
4
0
HOR. ℄
0°
10°
20°
30°
40°
50°
60°
70°
80°
90°
100°
110°
120°
130°
140°
150°
160°
170°
180°
190°
200°
210°
220°
230°
240°
250°
260°
270°
280°
290°
300°
310°
320°
330°
340°
350°
.6
.8
1.0
1.2
1.4
1.6
1.8
2.0

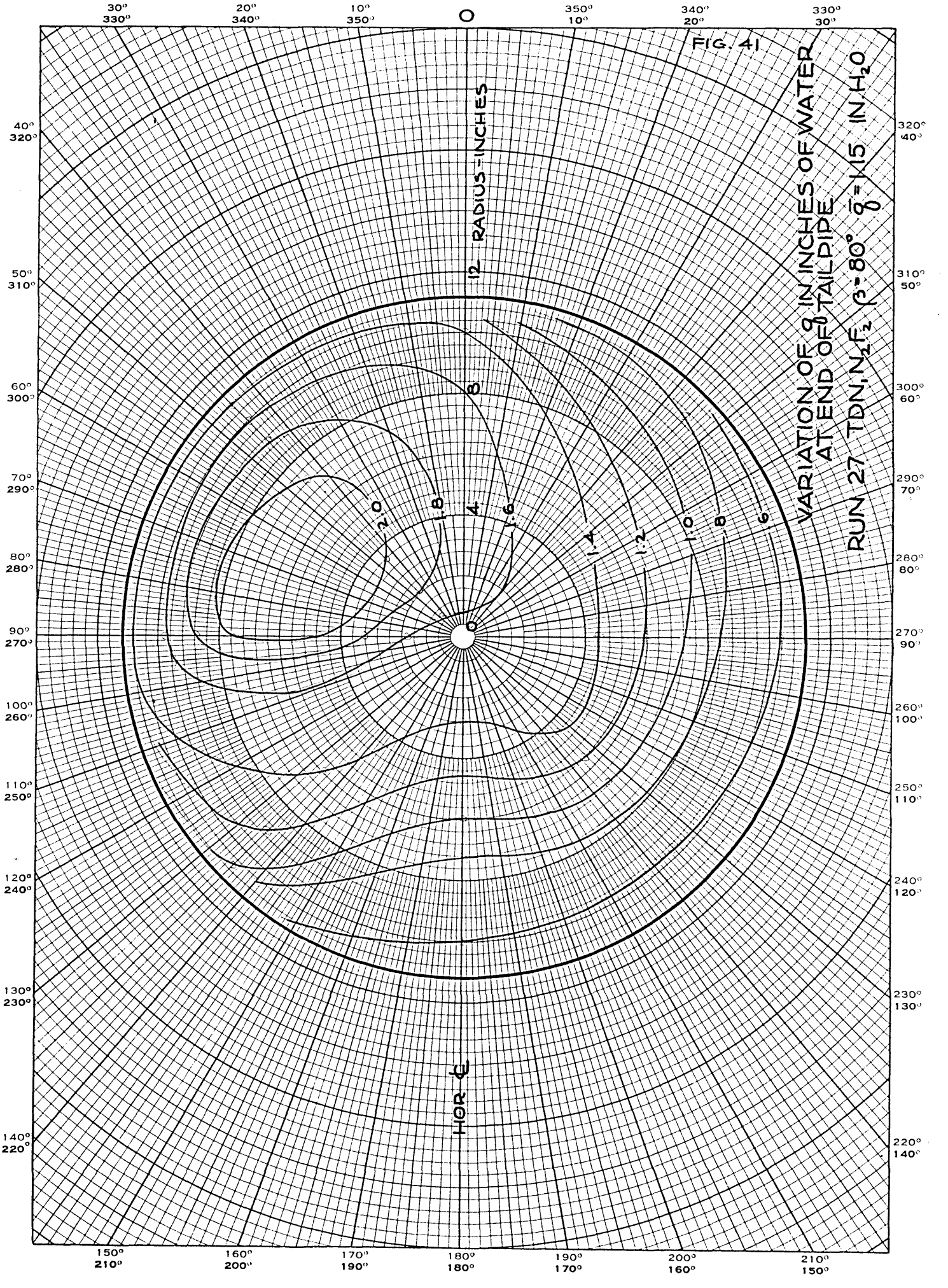
FIG. 41
VARIATION OF q IN INCHES OF WATER AT END OF TAILPIPE
RUN 27 TDN, N_2F_2 $\beta = 80°$ $\bar{q} = 1.15$ IN. H_2O
12 RADIUS-INCHES
HOR ℄
0
30° 330°
20° 340°
10° 350°
350° 10°
340° 20°
330° 30°
40° 320°
50° 310°
60° 300°
70° 290°
80° 280°
90° 270°
100° 260°
110° 250°
120° 240°
130° 230°
140° 220°
320° 40°
310° 50°
300° 60°
290° 70°
280° 80°
270° 90°
260° 100°
250° 110°
240° 120°
230° 130°
220° 140°
150° 210°
160° 200°
170° 190°
180° 180°
190° 170°
200° 160°
210° 150°
.2
.4
.6
.8
1.0
1.2
1.4
1.6
1.8
2.0
4
8

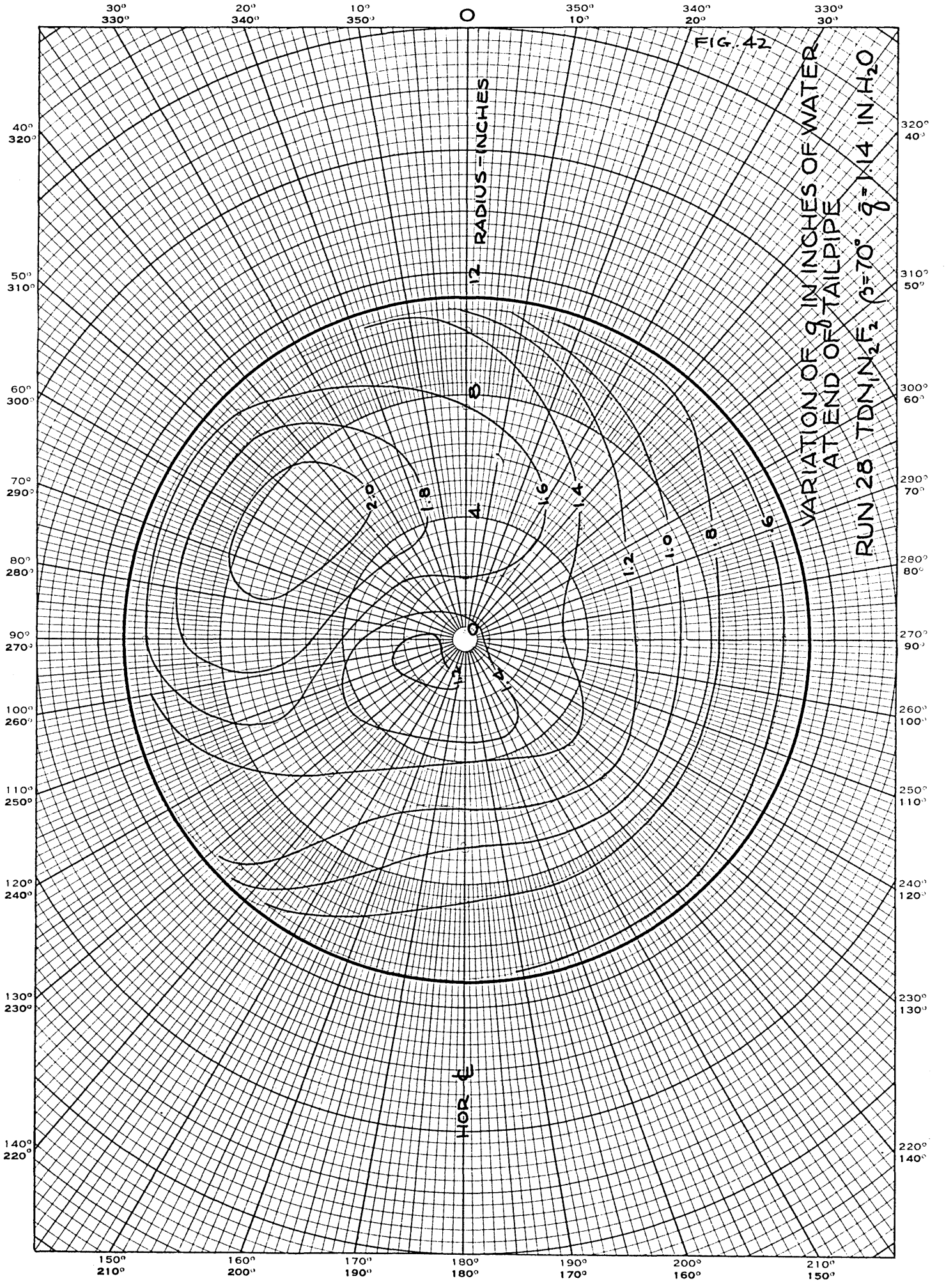
FIG. 42
VARIATION OF q IN INCHES OF WATER AT END OF TAILPIPE
RUN 28 TDN, N_2, F_2 $\beta=70°$ $\bar{q}=1.14$ IN. H_2O
RADIUS - INCHES
HORIZ
0
12
8
4
2.0
1.8
1.6
1.4
1.2
1.0
.8
.6
.4
.2
30° 330°
20° 340°
10° 350°
0
350° 10°
340° 20°
330° 30°
40° 320°
50° 310°
60° 300°
70° 290°
80° 280°
90° 270°
100° 260°
110° 250°
120° 240°
130° 230°
140° 220°
320° 40°
310° 50°
300° 60°
290° 70°
280° 80°
270° 90°
260° 100°
250° 110°
240° 120°
230° 130°
220° 140°
150° 210°
160° 200°
170° 190°
180° 180°
190° 170°
200° 160°
210° 150°

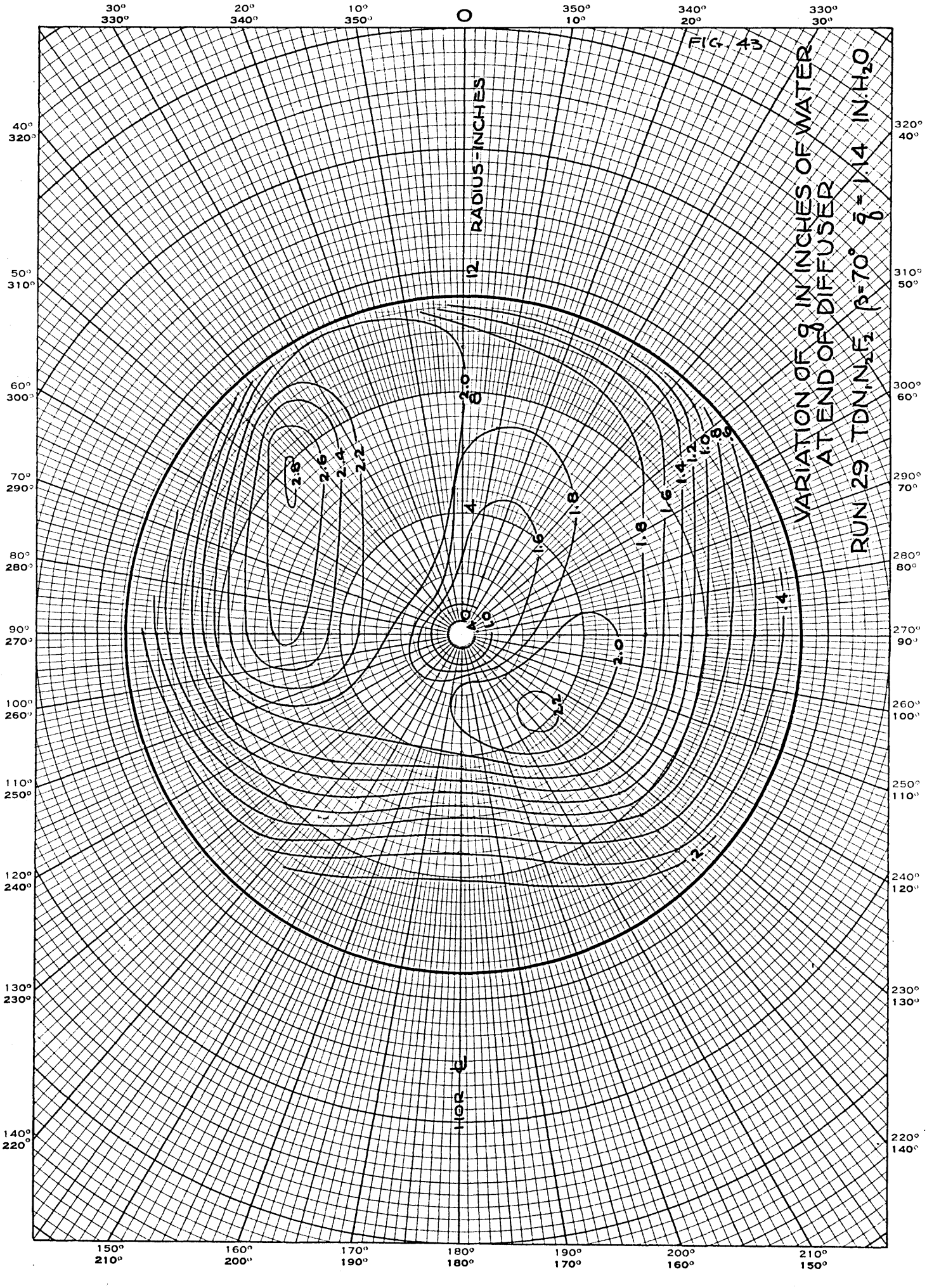
FIG. 43
VARIATION OF q IN INCHES OF WATER AT END OF DIFFUSER
RUN 29 TDN, N2F2 β=70° q̄=1.14 IN. H2O
RADIUS-INCHES
HOR. ℄
0
12
8
4
30° 330°
20° 340°
10° 350°
350° 10°
340° 20°
330° 30°
40° 320°
50° 310°
60° 300°
70° 290°
80° 280°
90° 270°
100° 260°
110° 250°
120° 240°
130° 230°
140° 220°
320° 40°
310° 50°
300° 60°
290° 70°
280° 80°
270° 90°
260° 100°
250° 110°
240° 120°
230° 130°
220° 140°
150° 210°
160° 200°
170° 190°
180° 180°
190° 170°
200° 160°
210° 150°
2.8
2.6
2.4
2.2
2.0
1.8
1.6
1.4
1.2
1.0
.8
.6
.4
.2

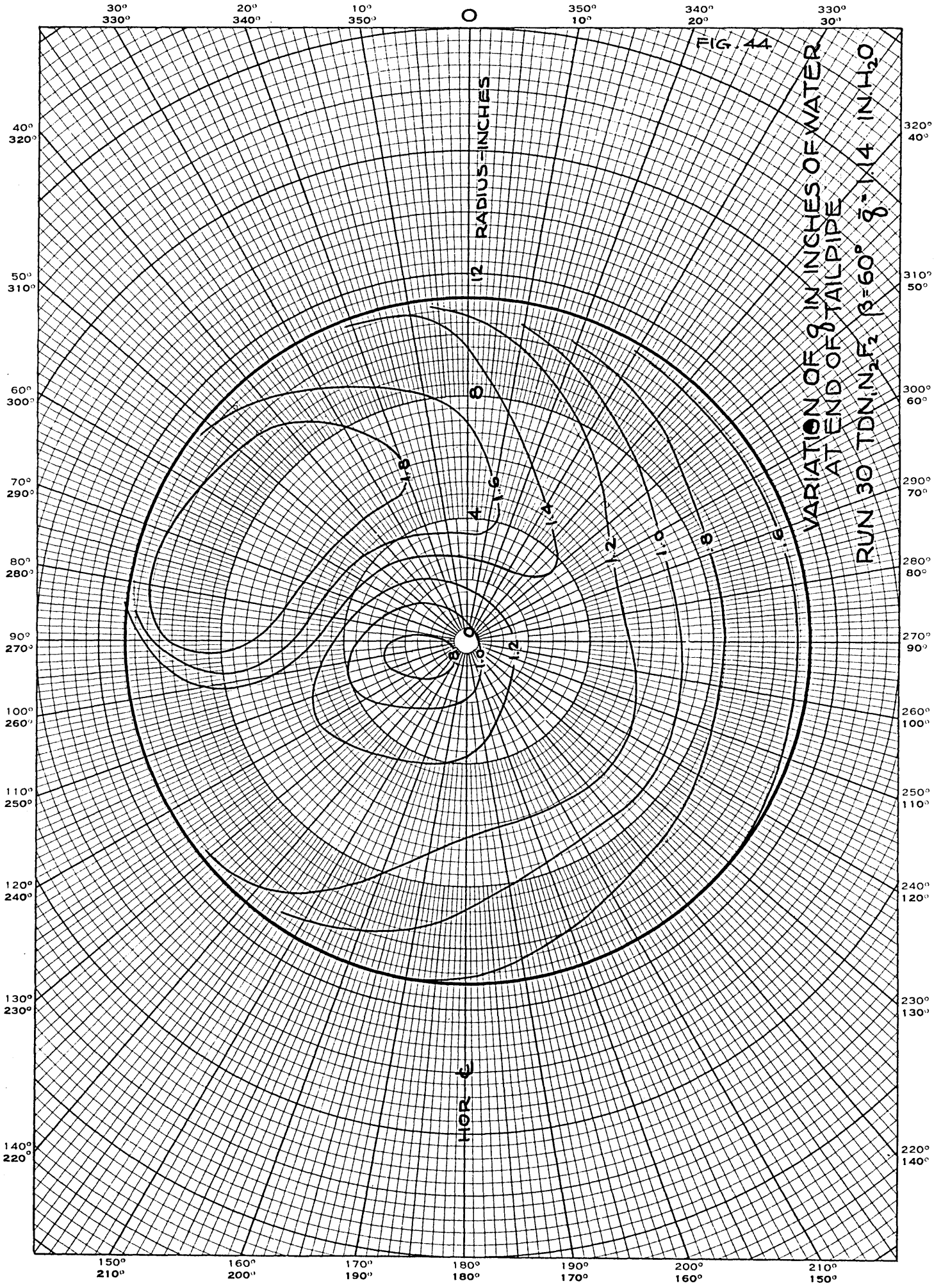
FIG. 44
VARIATION OF q IN INCHES OF WATER AT END OF TAILPIPE
RUN 30 TDN, N_2 P_2 β=60° q=1.4 IN. H_2O
RADIUS=INCHES
12
8
4
HOR. ℄
0
30° 330°
20° 340°
10° 350°
350° 10°
340° 20°
330° 30°
40° 320°
50° 310°
60° 300°
70° 290°
80° 280°
90° 270°
100° 260°
110° 250°
120° 240°
130° 230°
140° 220°
150° 210°
160° 200°
170° 190°
180° 180°
190° 170°
200° 160°
210° 150°
320° 40°
310° 50°
300° 60°
290° 70°
280° 80°
270° 90°
260° 100°
250° 110°
240° 120°
230° 130°
220° 140°

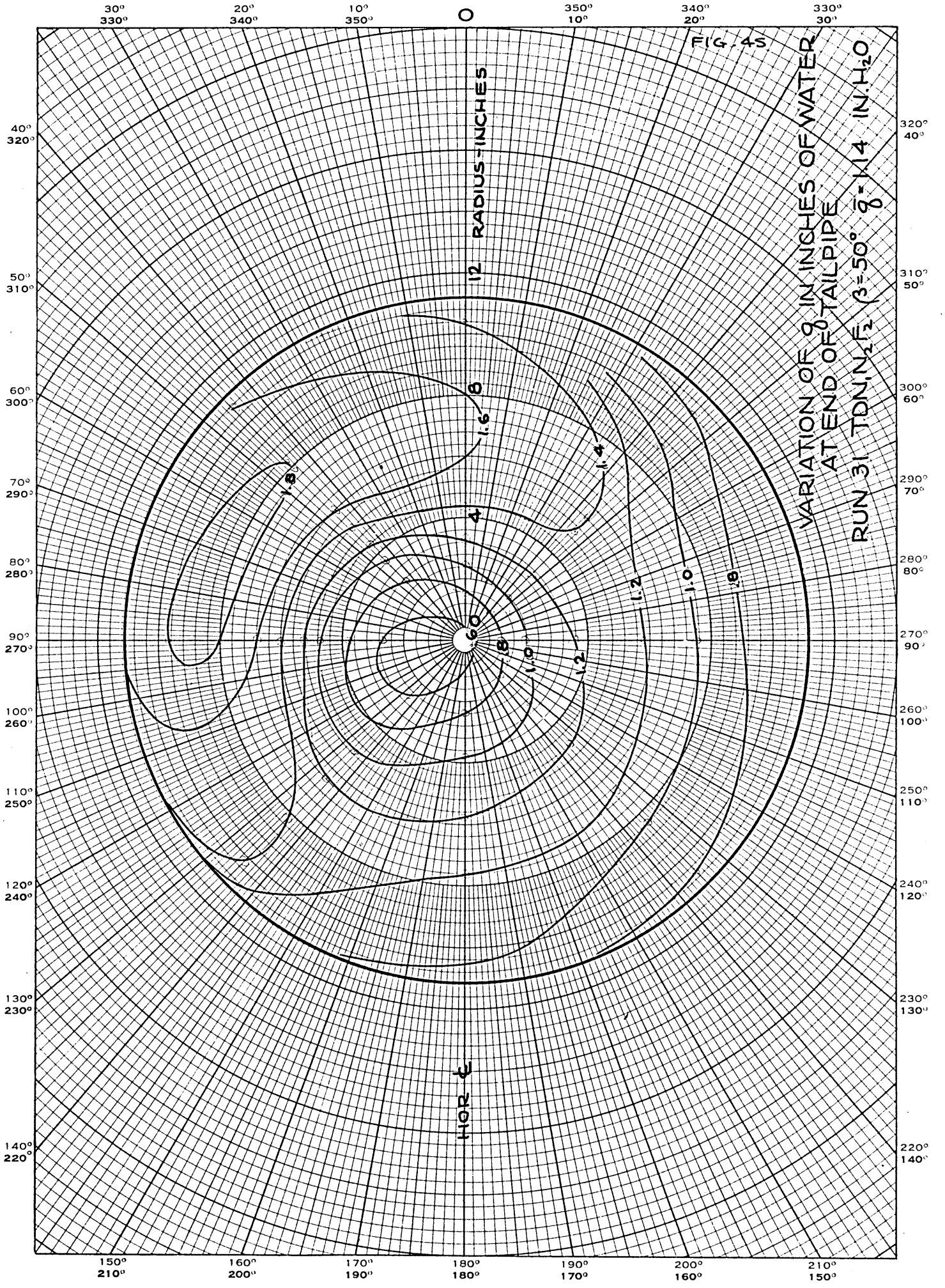
FIG-45
VARIATION OF q IN INCHES OF WATER AT END OF TAILPIPE
RUN 31 TDN, N_2 F_2 (β=50° $\bar{q}$=1.14 IN. H_2O
12 RADIUS-INCHES
8
4
HOR. ℄
1.6
1.4
1.2
1.0
.8
.6
.8
1.0
1.2
0°
30° 330°
20° 340°
10° 350°
350° 10°
340° 20°
330° 30°
40° 320°
50° 310°
60° 300°
70° 290°
80° 280°
90° 270°
100° 260°
110° 250°
120° 240°
130° 230°
140° 220°
150° 210°
160° 200°
170° 190°
180° 180°
190° 170°
200° 160°
210° 150°
320° 40°
310° 50°
300° 60°
290° 70°
280° 80°
270° 90°
260° 100°
250° 110°
240° 120°
230° 130°
220° 140°

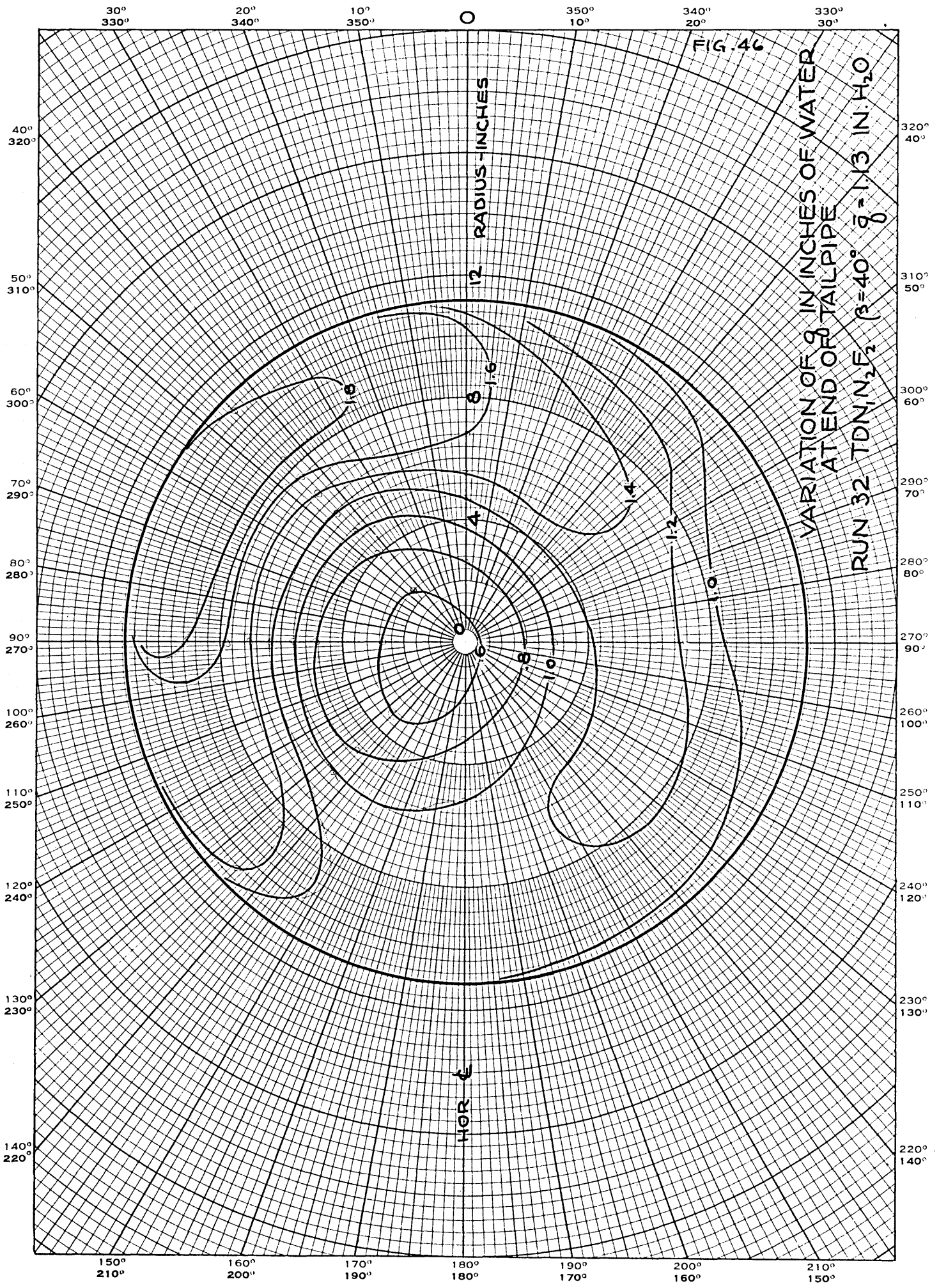
FIG. 46
VARIATION OF q IN INCHES OF WATER AT END OF TAILPIPE
RUN 32 TDN, N2F2 (β=40° q=1.13 IN. H2O
RADIUS-INCHES
HOR
0
4
8
12
1.0
1.2
1.4
1.6
1.8
30° 330°
20° 340°
10° 350°
0°
350° 10°
340° 20°
330° 30°
40° 320°
50° 310°
60° 300°
70° 290°
80° 280°
90° 270°
100° 260°
110° 250°
120° 240°
130° 230°
140° 220°
150° 210°
160° 200°
170° 190°
180°
190° 170°
200° 160°
210° 150°

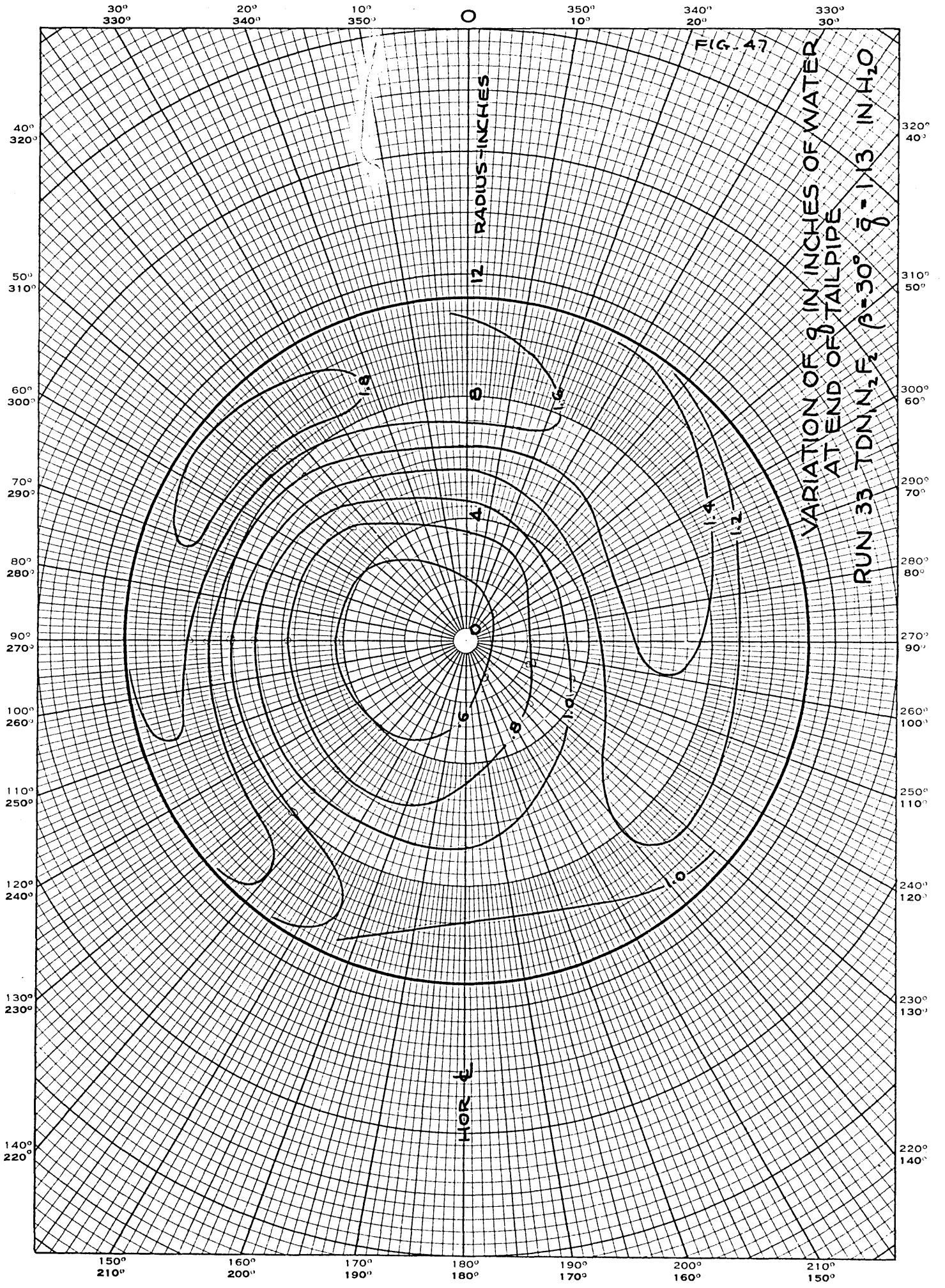
FIG. 47
VARIATION OF q IN INCHES OF WATER AT END OF TAILPIPE
RUN 33 TDN, N_2 F_2 β=30° $\bar{q}$ = 1.13 IN H_2O
RADIUS-INCHES
12
8
4
0
HORIZ
1.8
1.6
1.4
1.2
1.0
.9
.6
30° 330°
20° 340°
10° 350°
0
350° 10°
340° 20°
330° 30°
40° 320°
50° 310°
60° 300°
70° 290°
80° 280°
90° 270°
100° 260°
110° 250°
120° 240°
130° 230°
140° 220°
150° 210°
160° 200°
170° 190°
180° 180°
190° 170°
200° 160°
210° 150°

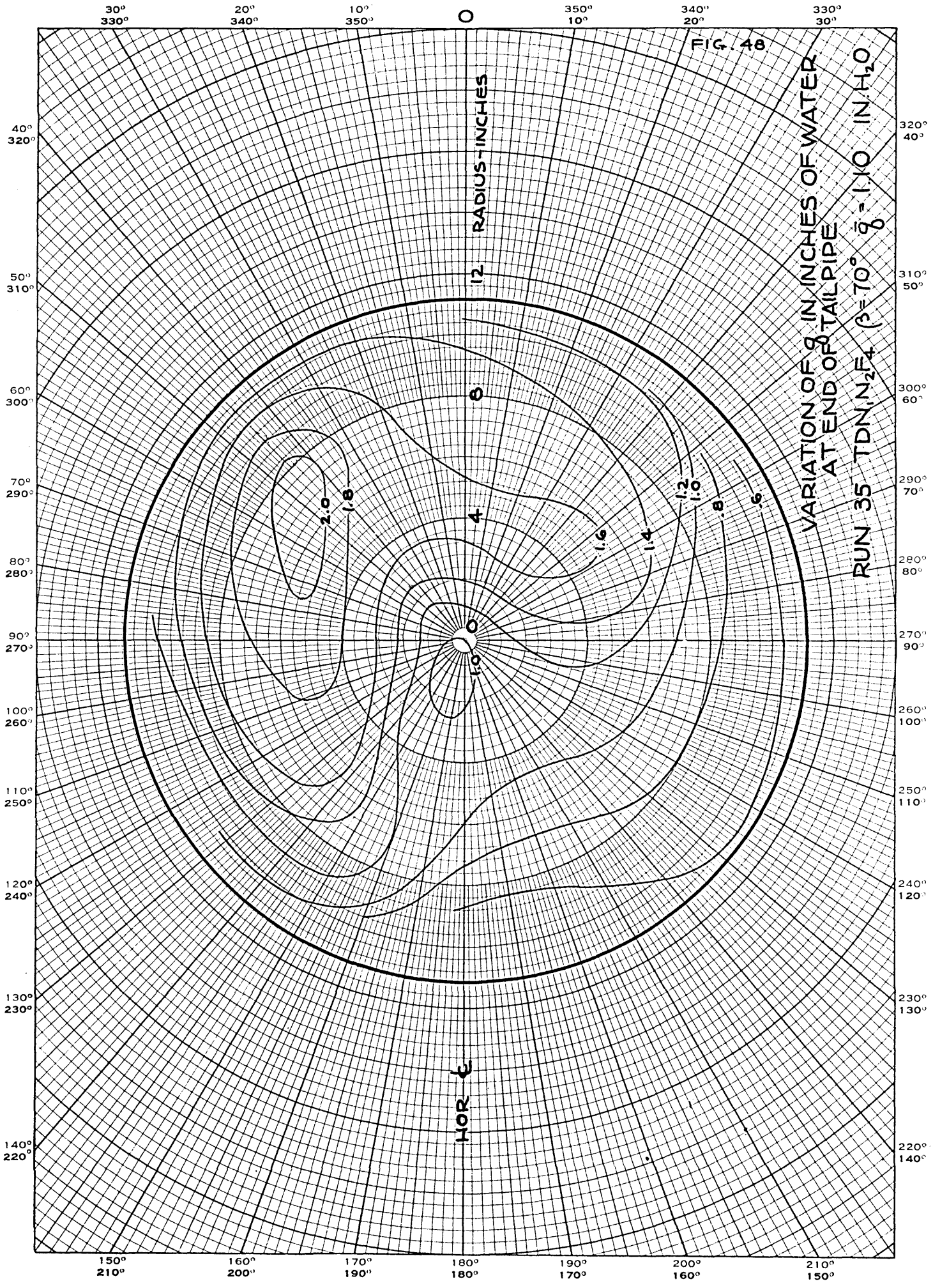
FIG. 48
VARIATION OF q IN INCHES OF WATER AT END OF TAIL PIPE
RUN 35 TDN, N_2F_4 (β=70° $\bar{q}$=1.10 IN H_2O
RADIUS-INCHES
12
8
4
0
HORIZ
2.0
1.8
1.6
1.4
1.2
1.0
.8
.6
1.0
30° 330°
20° 340°
10° 350°
0
350° 10°
340° 20°
330° 30°
40° 320°
50° 310°
60° 300°
70° 290°
80° 280°
90° 270°
100° 260°
110° 250°
120° 240°
130° 230°
140° 220°
320° 40°
310° 50°
300° 60°
290° 70°
280° 80°
270° 90°
260° 100°
250° 110°
240° 120°
230° 130°
220° 140°
150° 210°
160° 200°
170° 190°
180° 180°
190° 170°
200° 160°
210° 150°

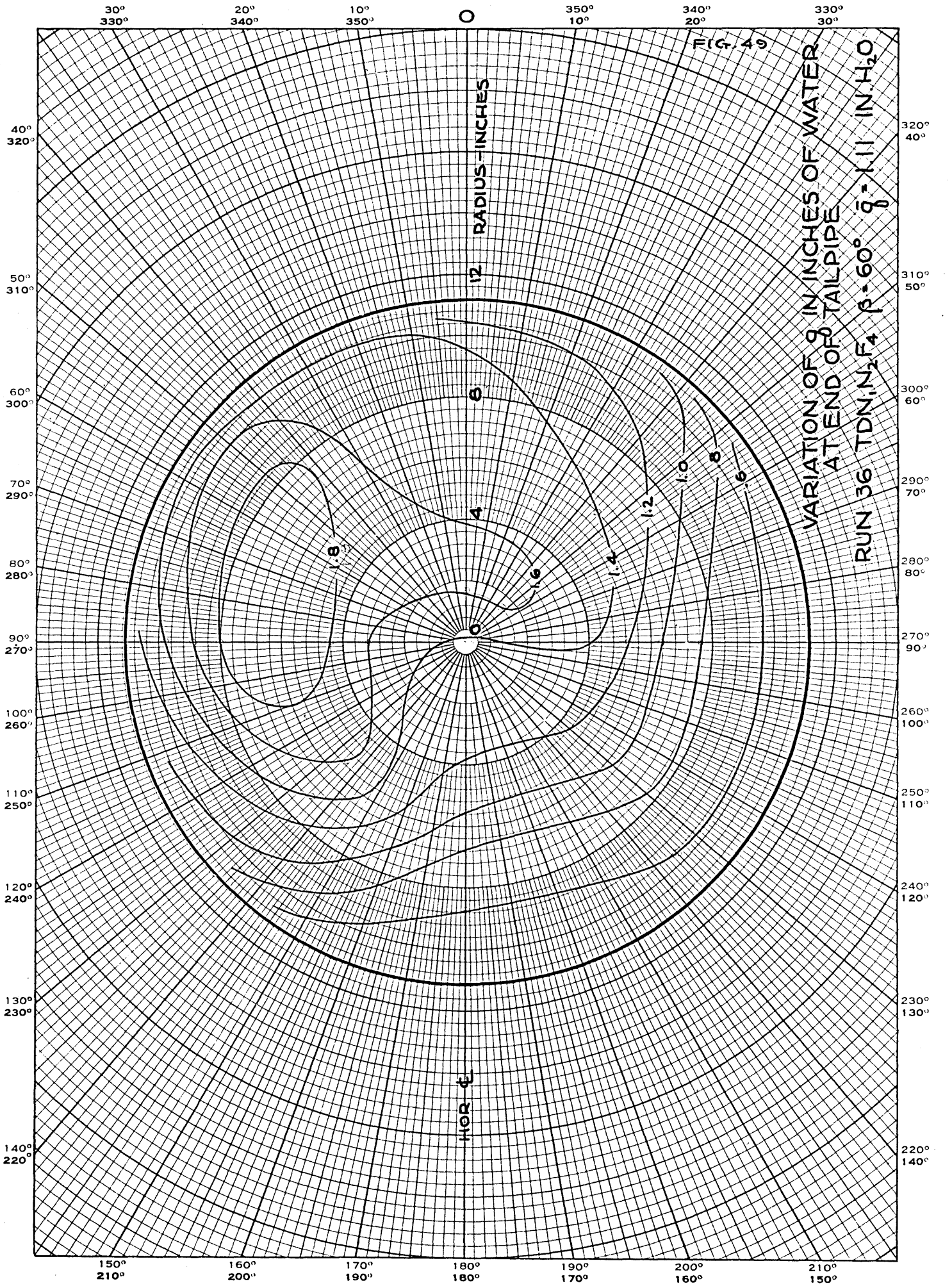
FIG. 49
VARIATION OF q IN INCHES OF WATER AT END OF TAILPIPE
RUN 36 TDN, N2F4 β = 60° q̄δ = 1.11 IN. H2O
RADIUS-INCHES
12
8
4
0
1.8
1.6
1.4
1.2
1.0
.8
.6
HOR ℄
0° 360°
10° 350°
20° 340°
30° 330°
40° 320°
50° 310°
60° 300°
70° 290°
80° 280°
90° 270°
100° 260°
110° 250°
120° 240°
130° 230°
140° 220°
150° 210°
160° 200°
170° 190°
180°
190° 170°
200° 160°
210° 150°
220° 140°
230° 130°
240° 120°
250° 110°
260° 100°
270° 90°
280° 80°
290° 70°
300° 60°
310° 50°
320° 40°

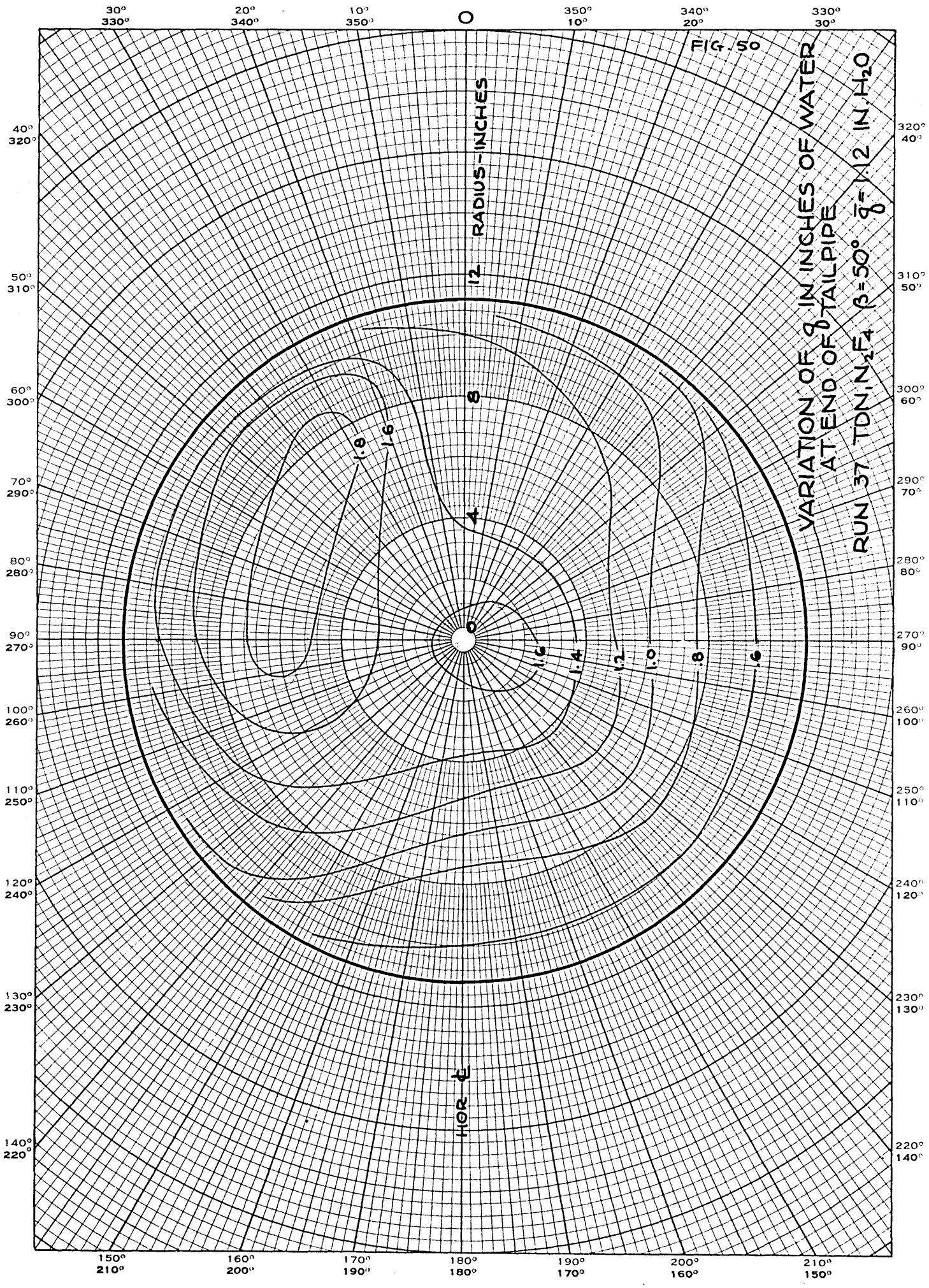
FIG. 50
VARIATION OF q IN INCHES OF WATER AT END OF TAILPIPE
RUN 37 TDN, N_2F_4 $\beta = 50°$ $\bar{q} = 12$ IN. H_2O
RADIUS-INCHES
12
8
4
0
HOR. ℄
1.8
1.6
1.4
1.2
1.0
.8
.6
30° 330°
20° 340°
10° 350°
0°
350° 10°
340° 20°
330° 30°
40° 320°
50° 310°
60° 300°
70° 290°
80° 280°
90° 270°
100° 260°
110° 250°
120° 240°
130° 230°
140° 220°
150° 210°
160° 200°
170° 190°
180°
190° 170°
200° 160°
210° 150°

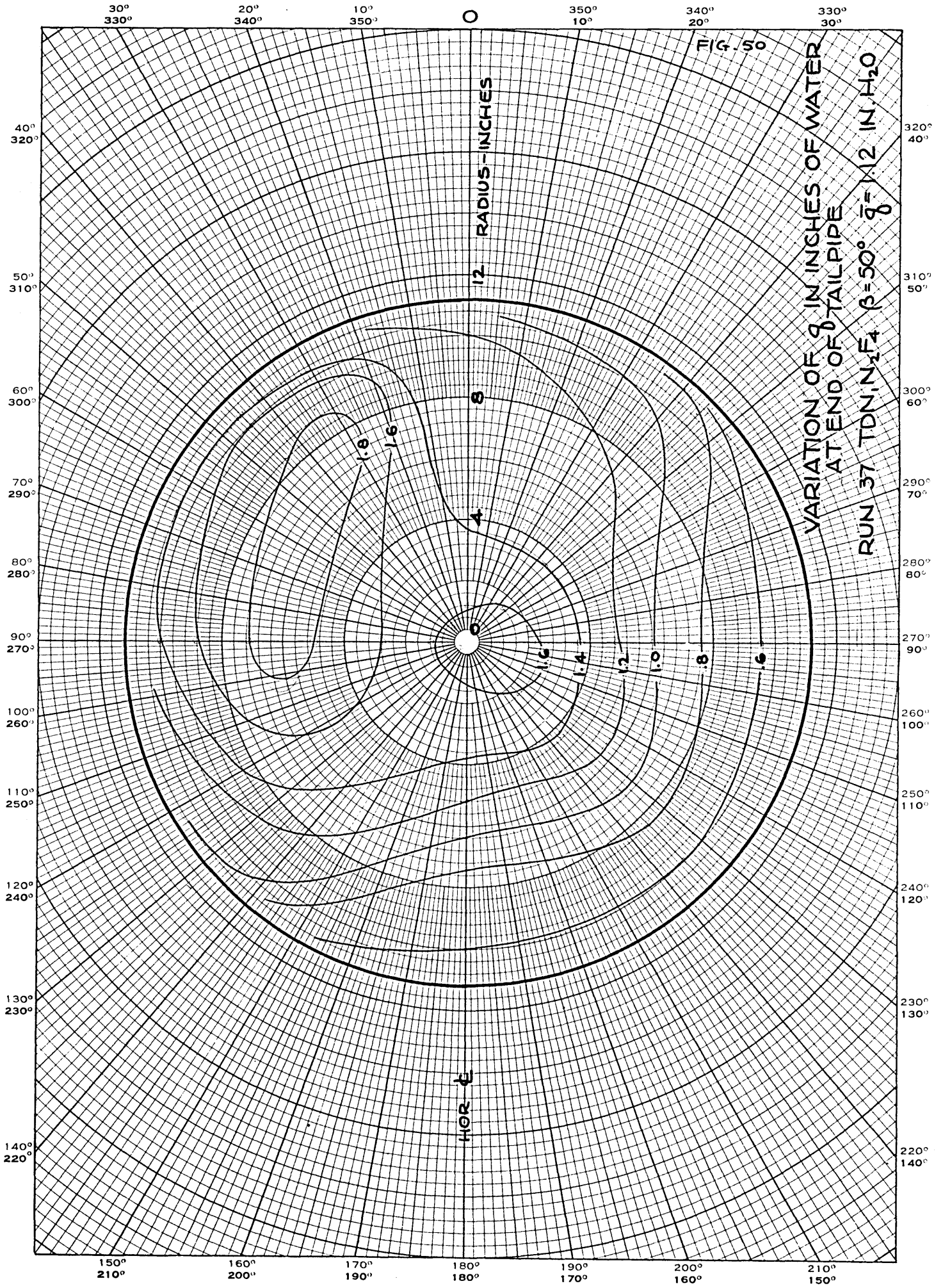
FIG. 50
VARIATION OF q IN INCHES OF WATER AT END OF TAILPIPE
RUN 37 TDN, N2F4 β=50° q̄=12 IN. H2O
12 RADIUS-INCHES
8
4
0
HOR ℄
1.8
1.6
1.4
1.2
1.0
.8
.6
30° 330°
20° 340°
10° 350°
0
350° 10°
340° 20°
330° 30°
40° 320°
50° 310°
60° 300°
70° 290°
80° 280°
90° 270°
100° 260°
110° 250°
120° 240°
130° 230°
140° 220°
320° 40°
310° 50°
300° 60°
290° 70°
280° 80°
270° 90°
260° 100°
250° 110°
240° 120°
230° 130°
220° 140°
150° 210°
160° 200°
170° 190°
180° 180°
190° 170°
200° 160°
210° 150°

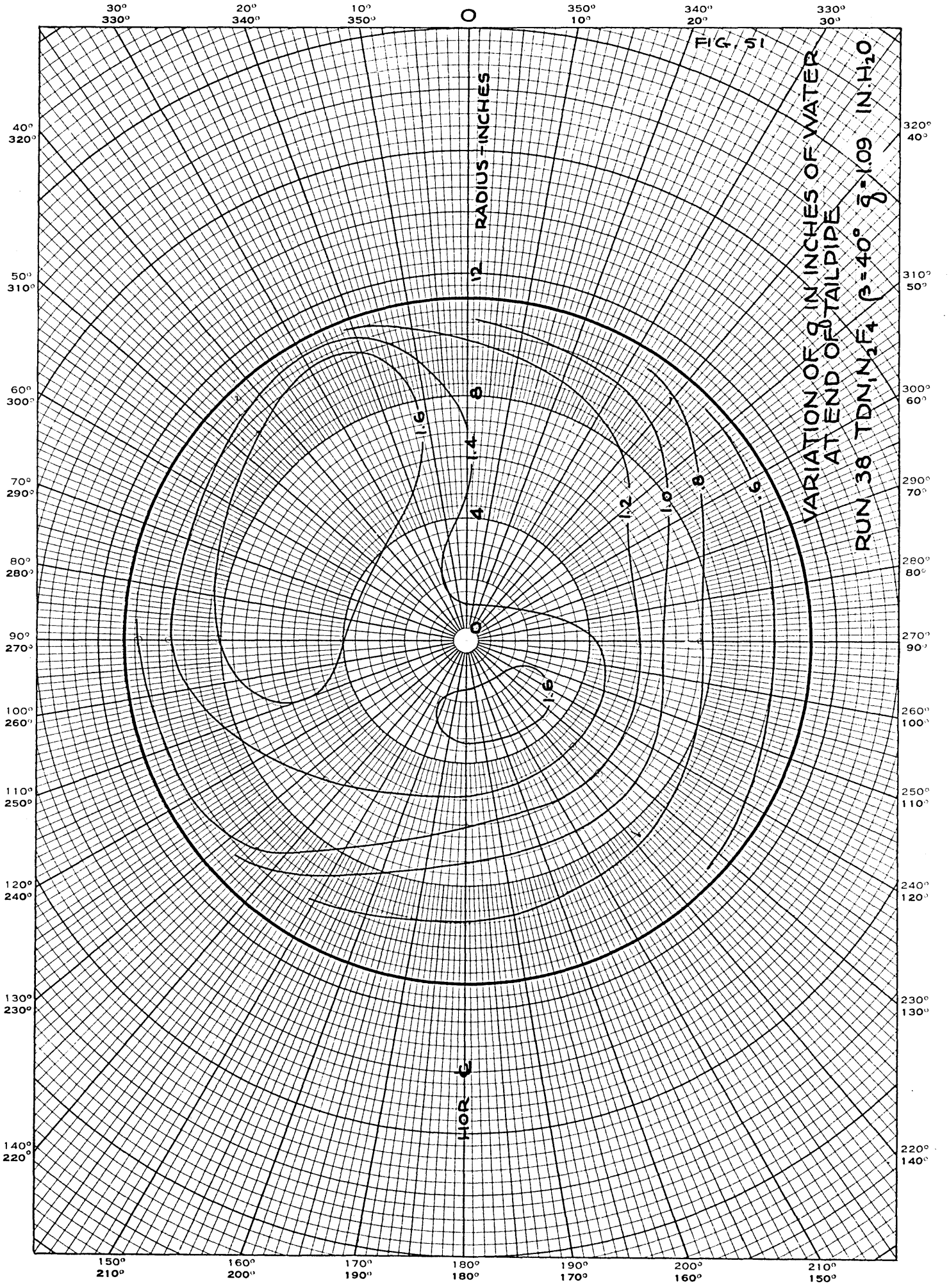
FIG. 51
VARIATION OF q IN INCHES OF WATER AT END OF TAILPIPE
RUN 38 TDN, N_2F_4 β=40° $\bar{q}$=1.09 IN. H_2O
RADIUS-INCHES
12
8
4
0
1.6
1.4
1.2
1.0
.8
.6
HOR
0°
30° 330°
20° 340°
10° 350°
350° 10°
340° 20°
330° 30°
40° 320°
50° 310°
60° 300°
70° 290°
80° 280°
90° 270°
100° 260°
110° 250°
120° 240°
130° 230°
140° 220°
150° 210°
160° 200°
170° 190°
180° 180°
190° 170°
200° 160°
210° 150°
220° 140°
230° 130°
240° 120°
250° 110°
260° 100°
270° 90°
280° 80°
290° 70°
300° 60°
310° 50°
320° 40°

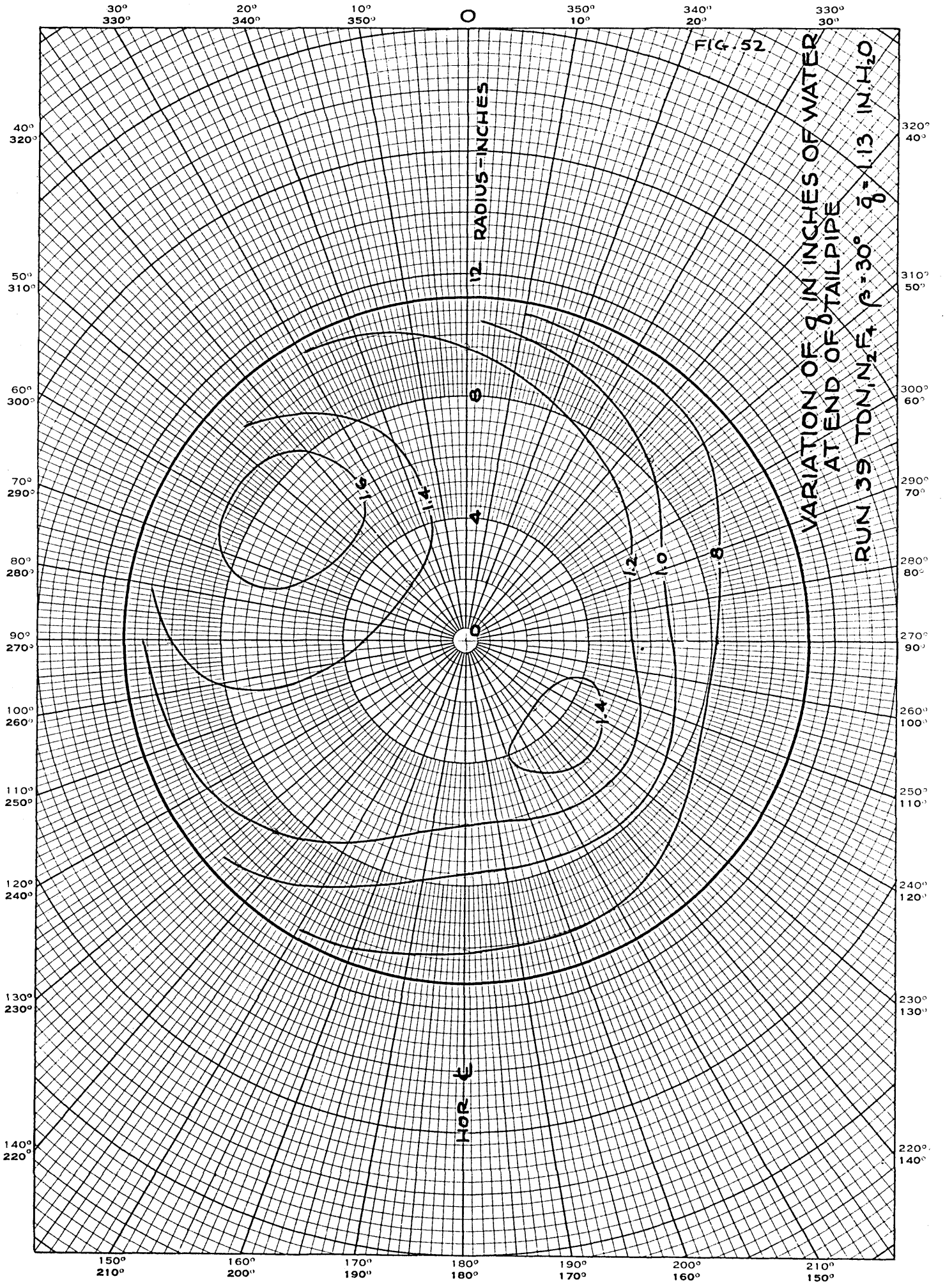
FIG. 52
VARIATION OF q IN INCHES OF WATER AT END OF TAILPIPE
RUN 39 TON, N_2F_4 $\beta = 30°$ $\bar{q}_\theta = 1.13$ IN. H_2O
RADIUS - INCHES
12
8
4
0
1.6
1.4
1.2
1.0
.8
1.4
HORIZ
0° 360°
10° 350°
20° 340°
30° 330°
40° 320°
50° 310°
60° 300°
70° 290°
80° 280°
90° 270°
100° 260°
110° 250°
120° 240°
130° 230°
140° 220°
150° 210°
160° 200°
170° 190°
180° 180°
190° 170°
200° 160°
210° 150°
220° 140°
230° 130°
240° 120°
250° 110°
260° 100°
270° 90°
280° 80°
290° 70°
300° 60°
310° 50°
320° 40°

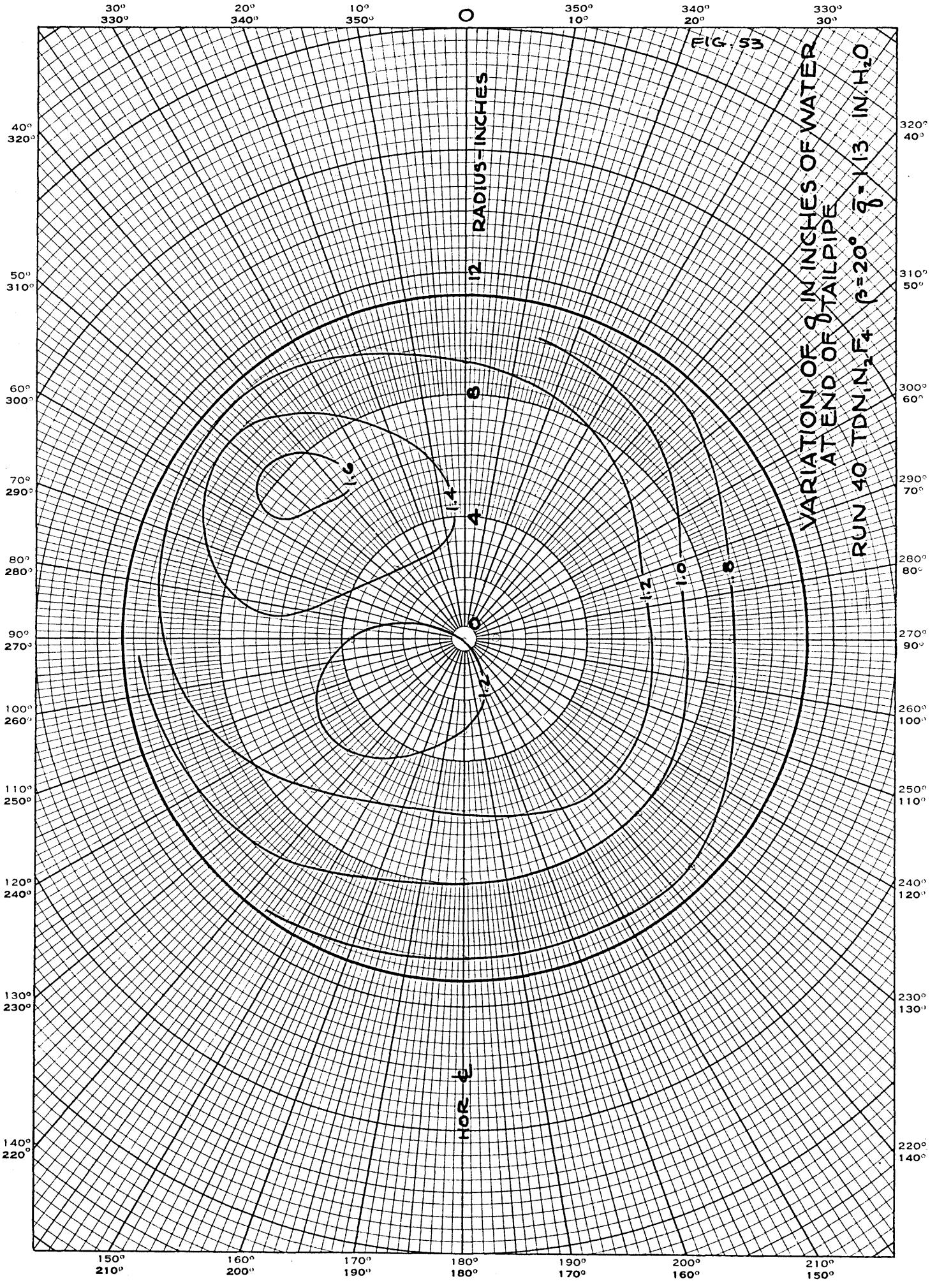
FIG. 53
VARIATION OF q IN INCHES OF WATER AT END OF TAILPIPE
RUN 40 TDN, N_2F_4 $\beta = 20°$ $\bar{q} = 1.13$ IN. H_2O
RADIUS-INCHES
12
8
4
0
1.6
1.4
1.2
1.0
.8
1.2
HOR. ℄
0°
30° 330°
20° 340°
10° 350°
350° 10°
340° 20°
330° 30°
40° 320°
50° 310°
60° 300°
70° 290°
80° 280°
90° 270°
100° 260°
110° 250°
120° 240°
130° 230°
140° 220°
150° 210°
160° 200°
170° 190°
180° 180°
190° 170°
200° 160°
210° 150°

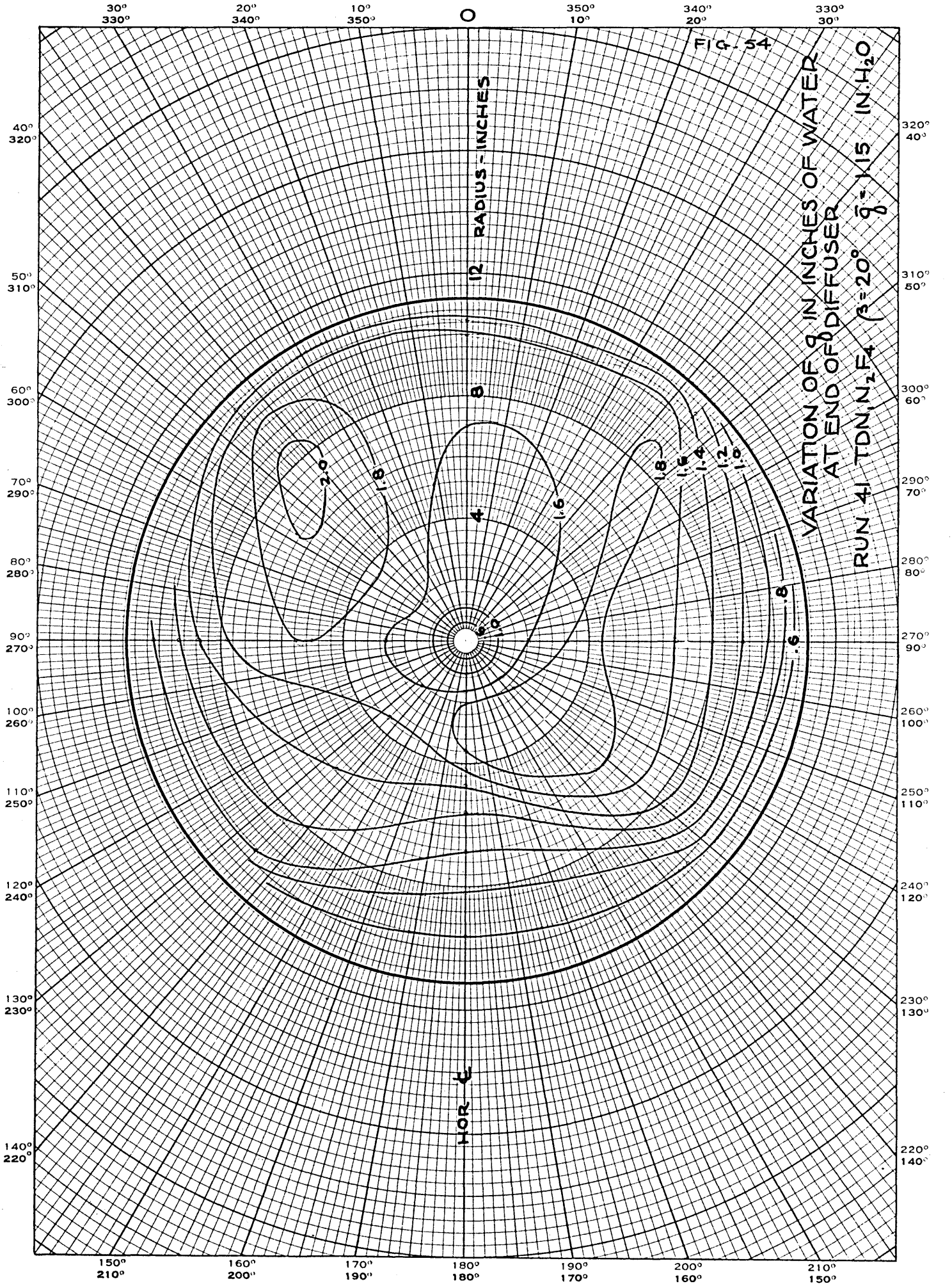
FIG. 54
VARIATION OF q IN INCHES OF WATER AT END OF DIFFUSER
RUN 41 TDN, N_2F_4 (β=20° $\bar{q}$= 1.15 IN. H_2O
12 RADIUS - INCHES
8
4
HOR
O
2.0
1.8
1.6
1.4
1.2
1.0
.8
.6
30° 330°
20° 340°
10° 350°
350° 10°
340° 20°
330° 30°
40° 320°
50° 310°
60° 300°
70° 290°
80° 280°
90° 270°
100° 260°
110° 250°
120° 240°
130° 230°
140° 220°
150° 210°
160° 200°
170° 190°
180° 180°
190° 170°
200° 160°
210° 150°

F. Index of Runs

Run No.	Configuration	Data Obtained
1	T	Pressures
2	T	Pressures
3	T	Pressures
4	TD	Pressures
5	TD	Wind Directions
6	TDN_1	Pressures
7	TDN_1F_1 $\beta=90°$	Pressures
8	TDN_1F_1 $\beta=80°$	Pressures
9	TDN_1F_1 $\beta=70°$	Pressures
10	TDN_1F_1 $\beta=60°$	Pressures
11	TDN_1F_1 $\beta=50°$	Pressures
12	TDN_1F_1 $\beta=40°$	Pressures
13	TDN_1 & TDN_1F_1 All β	Wind Directions
14	TDN_1F_3 $\beta=50°$	Pressures
15	TDN_1F_3 $\beta=40°$	Pressures
16	TDN_1F_3 $\beta=34°$	Pressures
17	TDN_1F_5 $\beta=80°$	Pressures
18	TDN_1F_5 $\beta=70°$	Pressures
19	TDN_1F_5 $\beta=60°$	Pressures
20	TDN_1F_5 $\beta=50°$	Pressures
21	TDN_1F_5 $\beta=40°$	Pressures
22	TDN_1F_5 $\beta=36°$	Pressures
23	TDN_1S, & TDN_1F_5S, $\beta=50°$ TDN_1F_5 All β	Wind Directions
24	TDN_1N_2H	Pressures
25	TDN_1N_2H	Pressures
26	$TDN_1N_2F_2$ $\beta=90°$	Pressures
27	$TDN_1N_2F_2$ $\beta=70°$	Pressures
28	$TDN_1N_2F_2$ $\beta=70°$	Pressures
29	$TDN_1N_2F_2$ $\beta=70°$	Pressures
30	$TDN_1N_2F_2$ $\beta=60°$	Pressures

31	$TDN_1N_2F_2\beta=50°$	Pressures
32	$TDN_1N_2F_2\beta=40°$	Pressures
33	$TDN_1N_2F_2\ \beta=30°$	Pressures
34	$TDN_1N_2F_2$ All β, TDN_1N_2H	Wind Directions
35	$TDN_1N_2F_4\ \beta=70°$	Pressures
36	$TDN_1N_2F_4\ \beta=60°$	Pressures
37	$TDN_1N_2F_4\ \beta=50°$	Pressures
38	$TDN_1N_2F_4\ \beta=40°$	Pressures
39	$TDN_1N_2F_4\ \beta=40°$	Pressures
40	$TDN_1N_2F_4\ \beta=20°$	Pressures
41	$TDN_1N_2F_4\ \beta=20°$	Pressures
42	$TDN_1N_2F_4$ All β	Wind Directions
43	Pitot tube calibrations, Student Tunnel	

G. Figures (Drawings and Photographs)

Figure 55

Forward nacelle N_1 installed in diffuser.

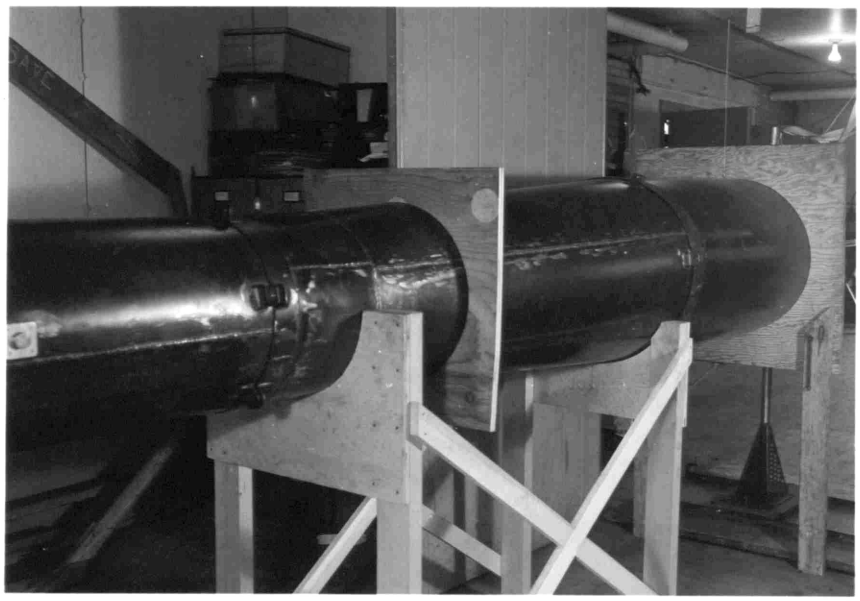

Figure 56

Diffuser and tailpipe -D

Figure 57

Blower and expansion section

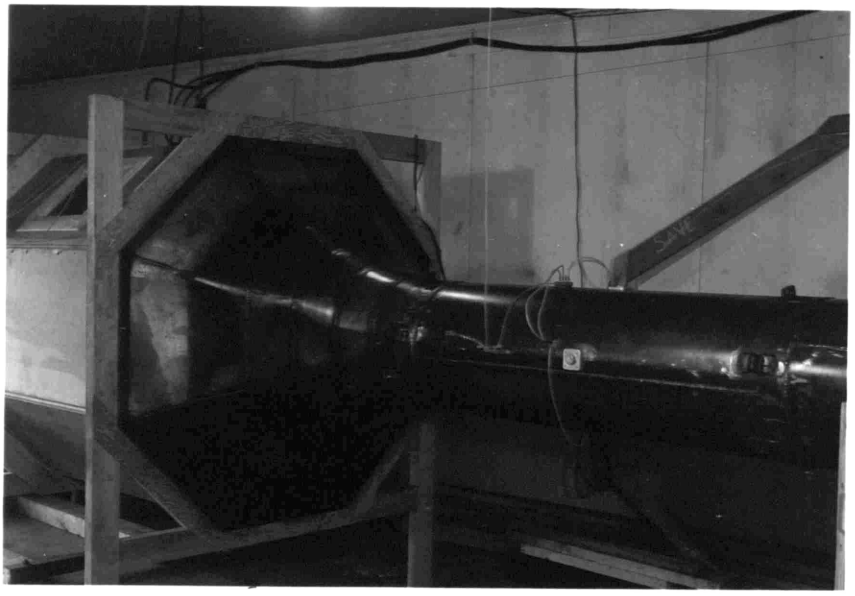

Figure 58

Settling chamber, bell mouth and constant area section.

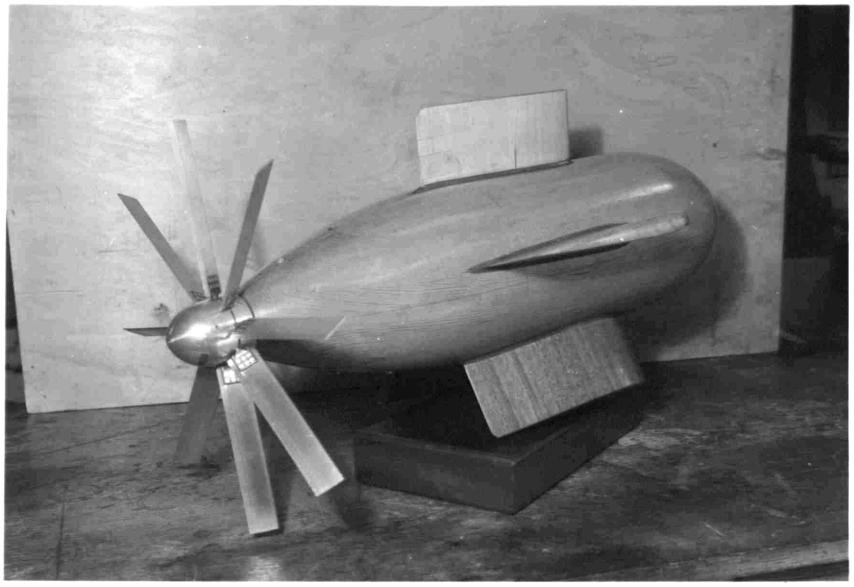

Figure 59

Nacelle N_1 and windmill F_1

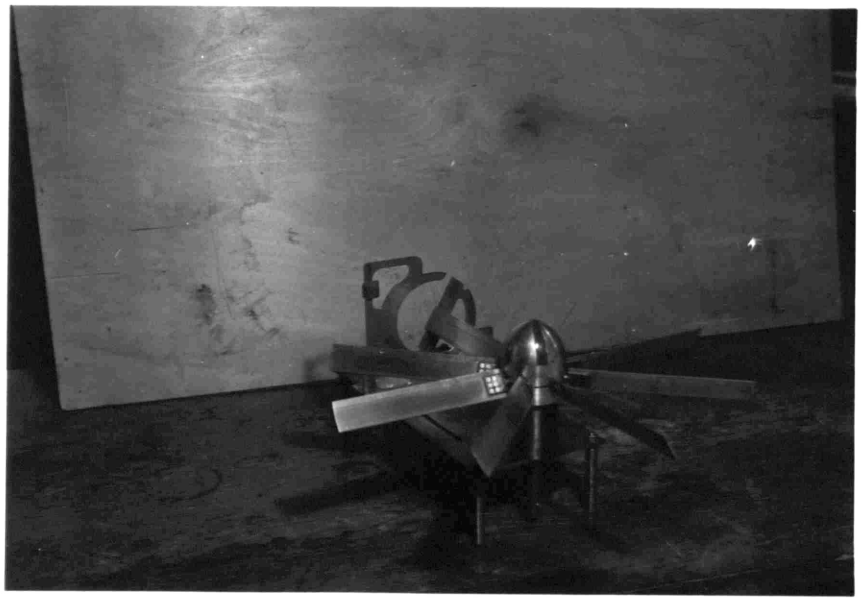

Figure 60

Blade angle check jig and windmill F_1

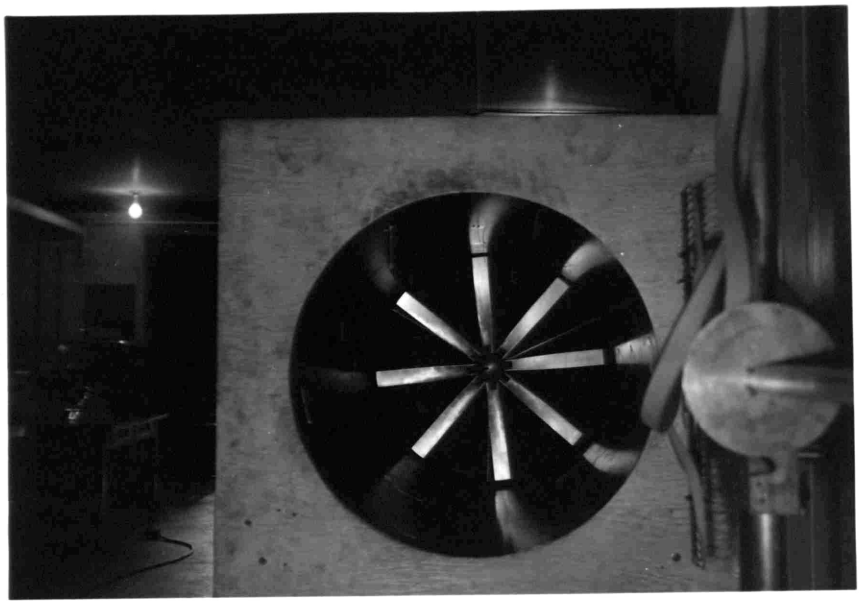

Figure 61

Nacelle N_2 and windmill F_4

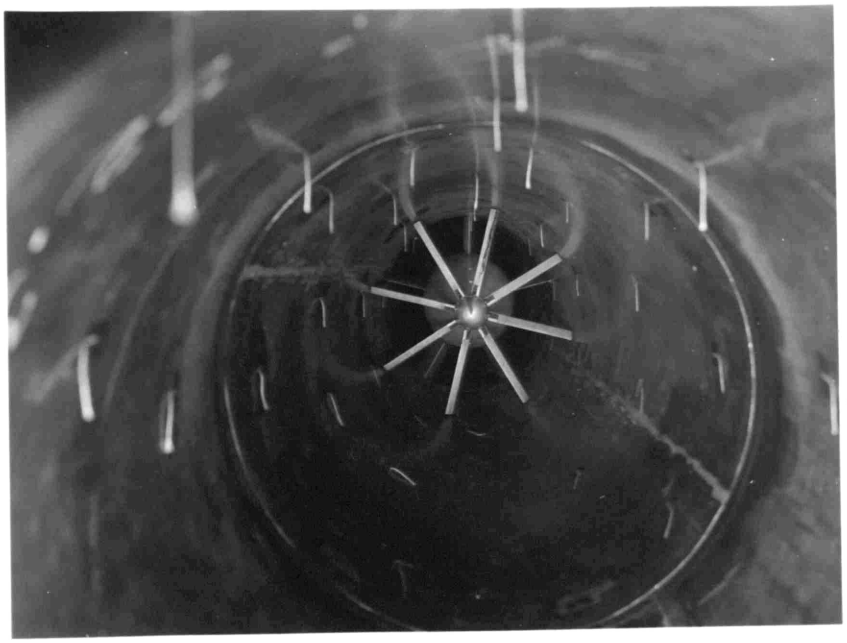

Figure 62

Nacelle N_1, windmill F_1 diffuser and tufts

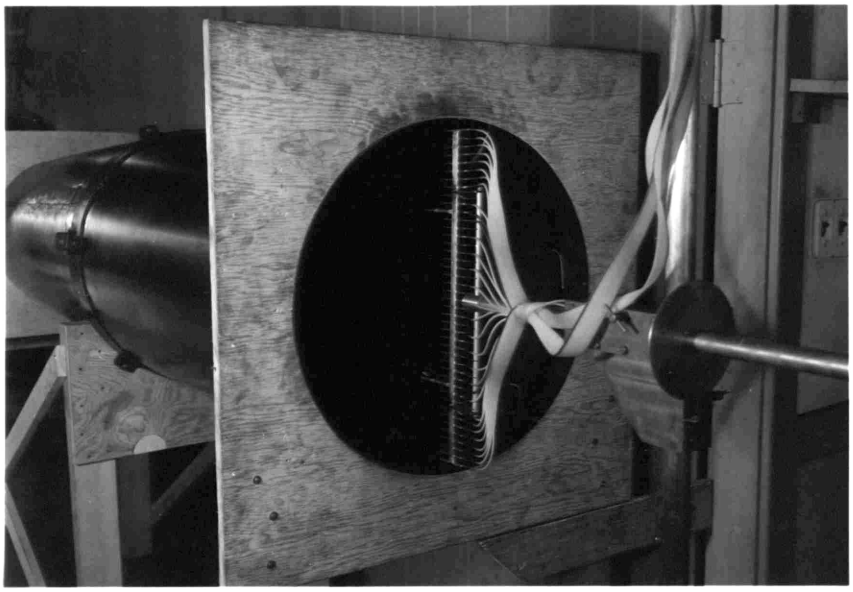

Figure 63

Rake and support

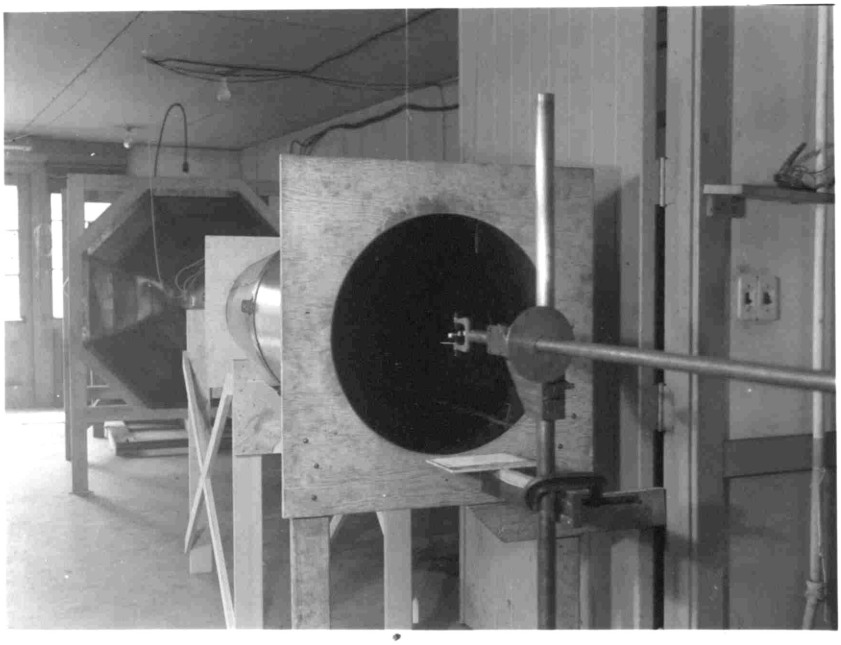

Figure 64

Wind direction indicator and support

Figure 65

Blade twister and blade from windmill F_4

FIGURE-66.

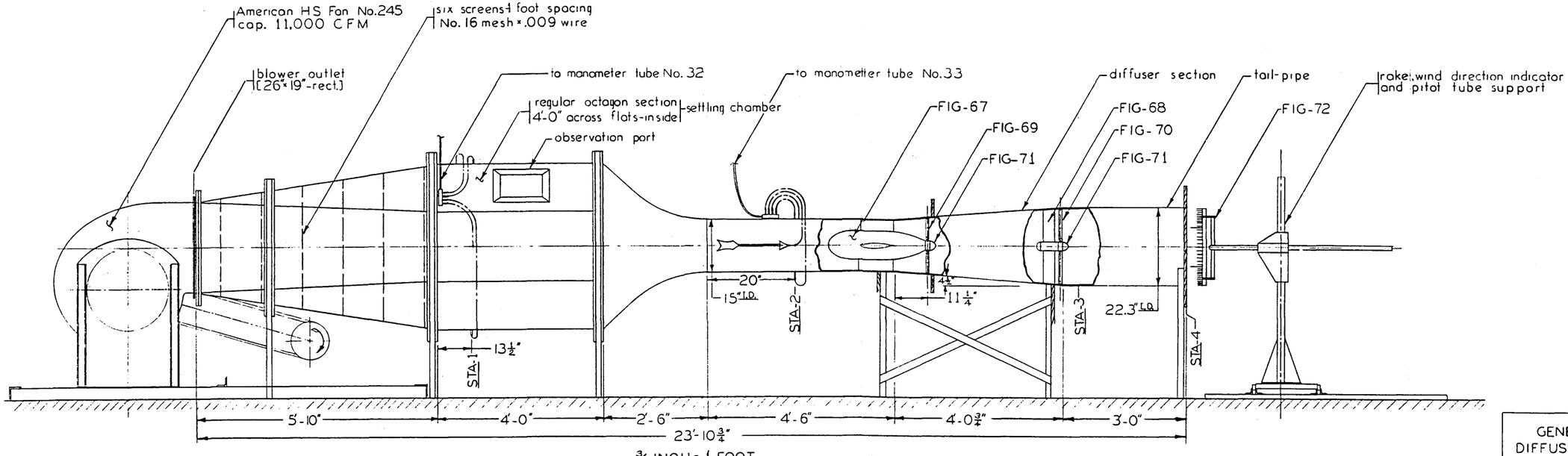

GENERAL ARRANGEMENT
DIFFUSER RESEARCH PROJECT

FIGURE-67

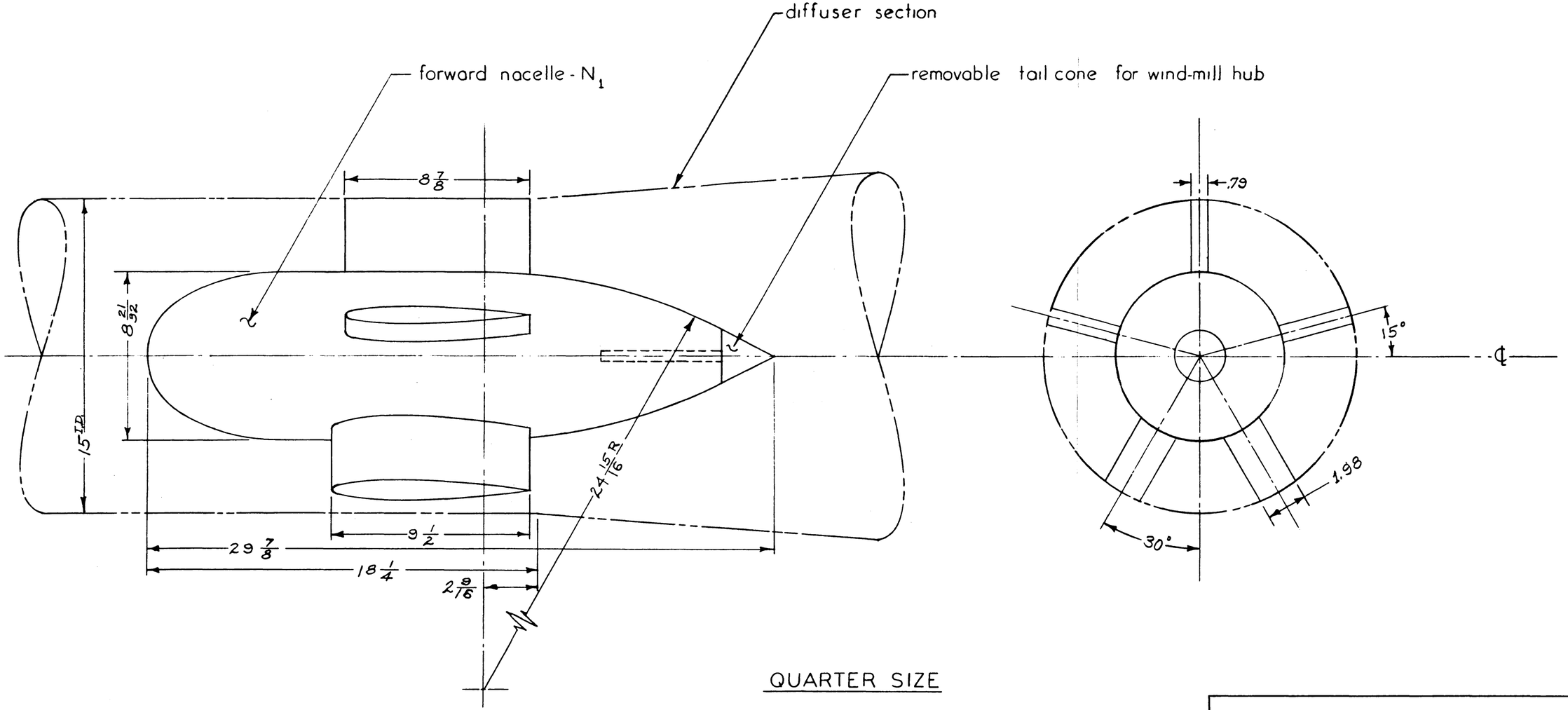

QUARTER SIZE

ref:
wright bros. wind tunnel
dwg. No. D-3-10-6

FORWARD NACELLE
DIFFUSER RESEARCH PROJECT

FIGURE-68

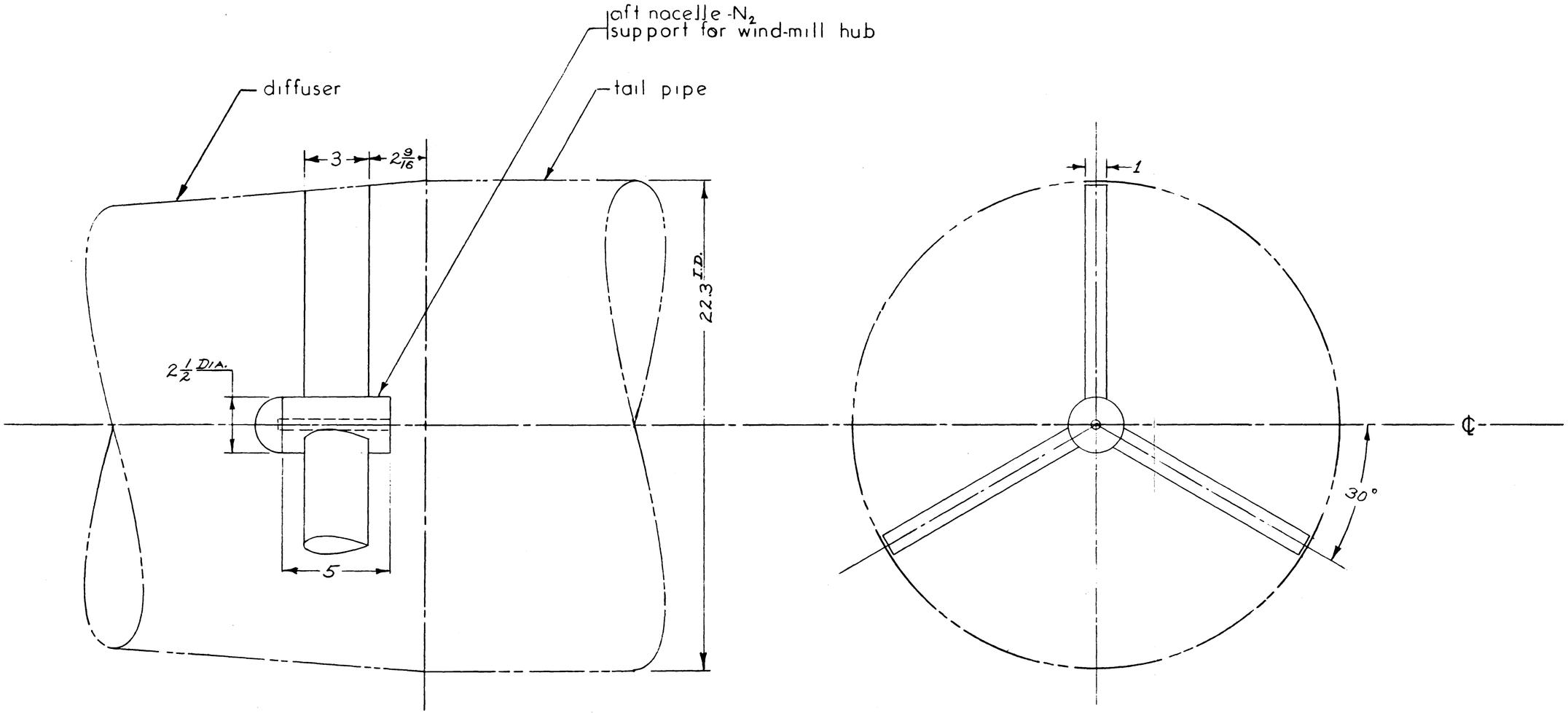

QUARTER SIZE

ref:
wright bros. wind tunnel
dwg. No. D-3-20-7

AFT NACELLE
DIFFUSER RESEARCH PROJECT

blade model	A	B	E	FIGURE
for f'wd nacelle	3/4	1 1/8	6 3/4	69
for aft nacelle	1	1 1/2	9 1/16	70

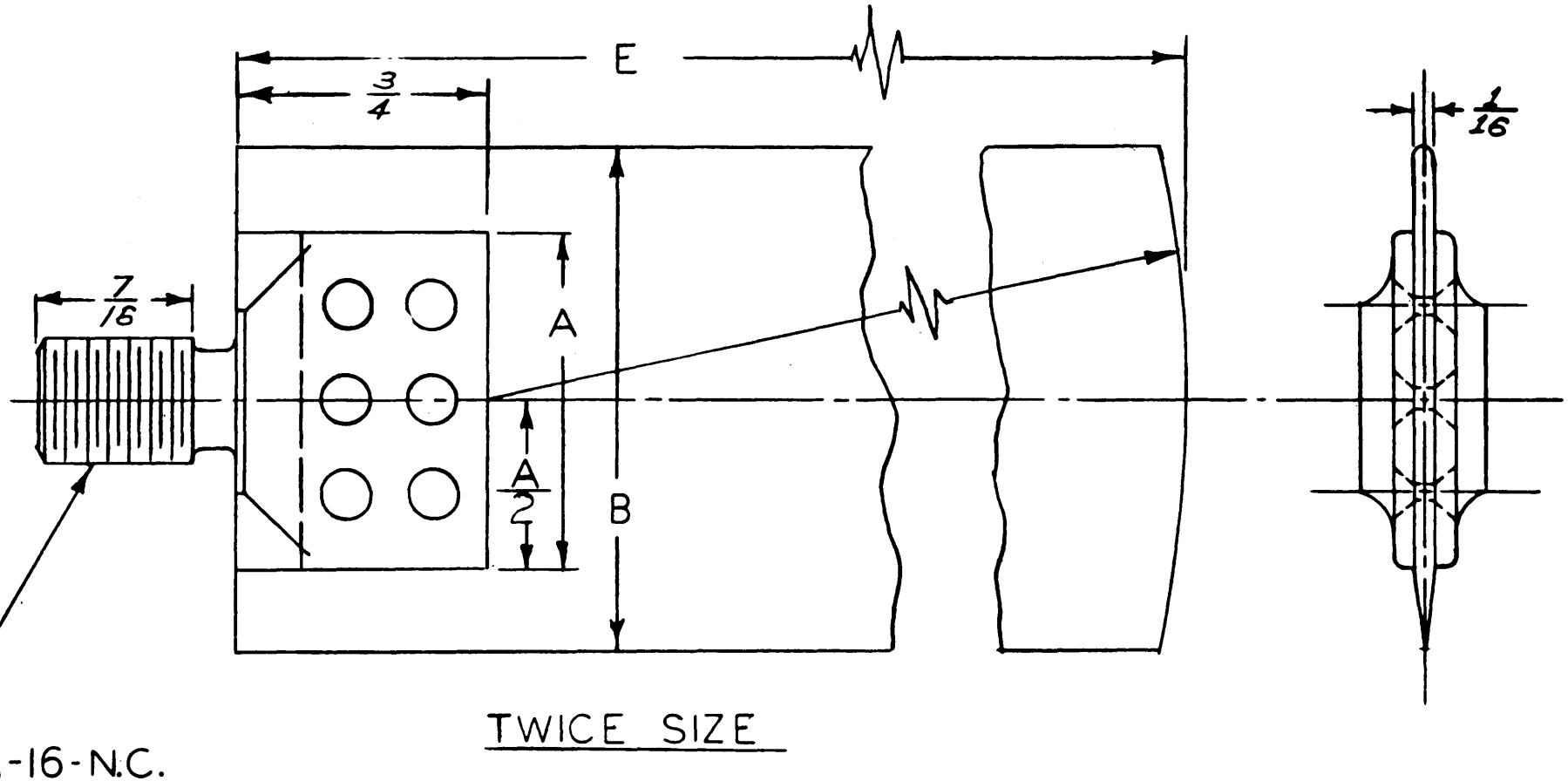

TWICE SIZE

ref:
wright bros. wind tunnel
dwg. No. B-3-20-8

WIND-MILL BLADES
DIFFUSER RESEARCH PROJECT

FIGURE-69&70

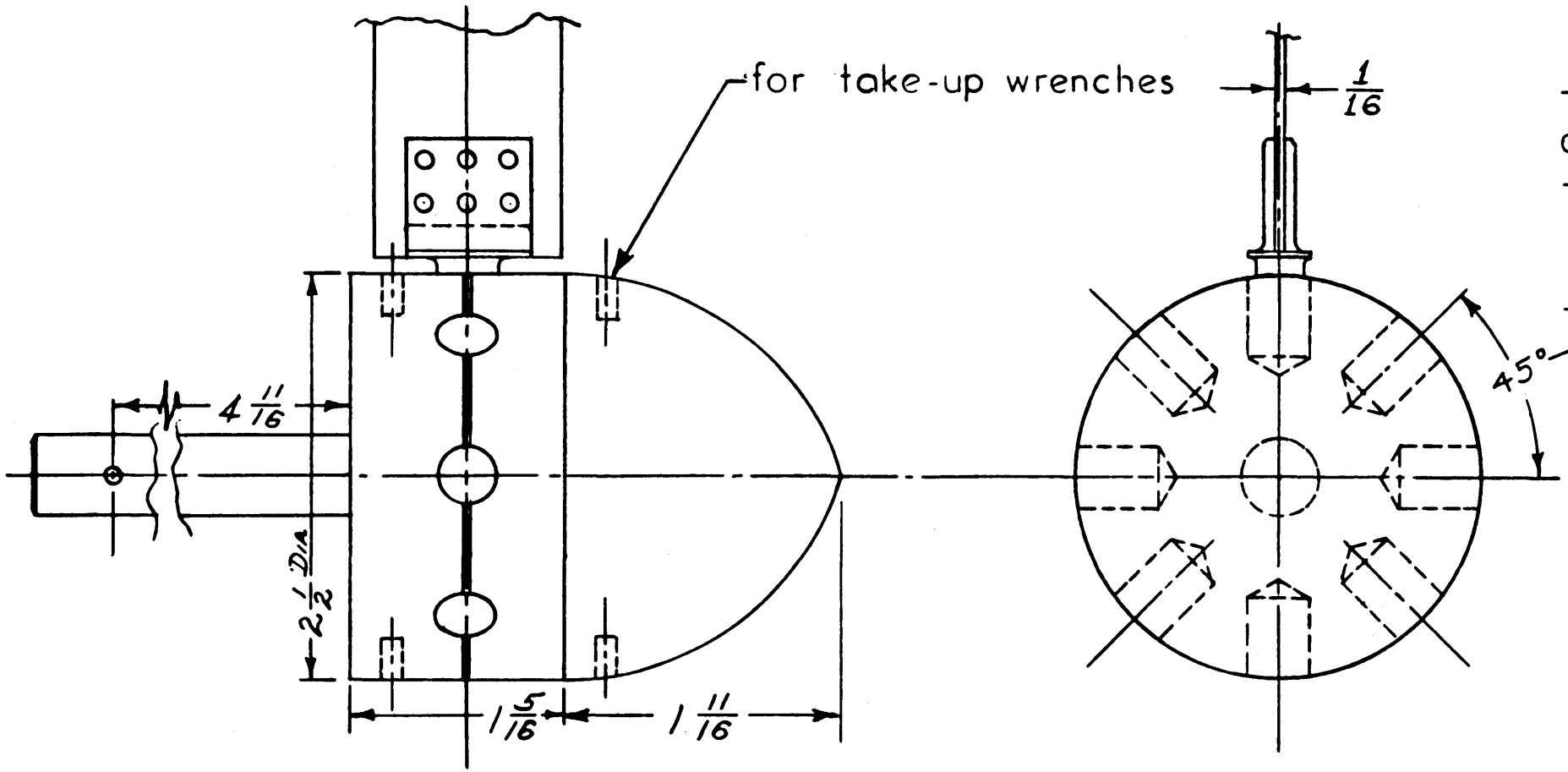

FULL SIZE

ref:
wright bros. wind tunnel
dwg. No. B-3-20-2

WIND-MILL HUB
DIFFUSER RESEARCH PROJECT

FIGURE-71

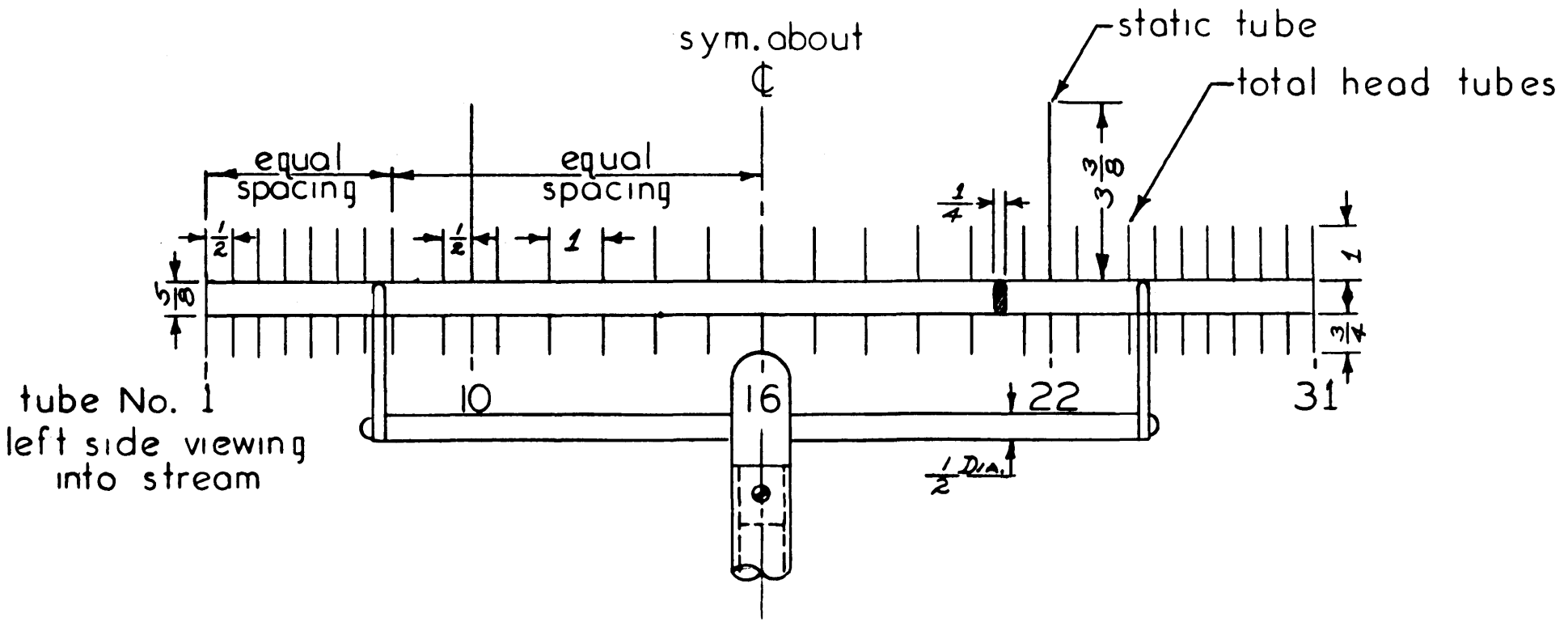

ONE-THIRD SIZE

RAKE
DIFFUSER RESEARCH PROJECT

FIGURE-72

FIGURE- 73

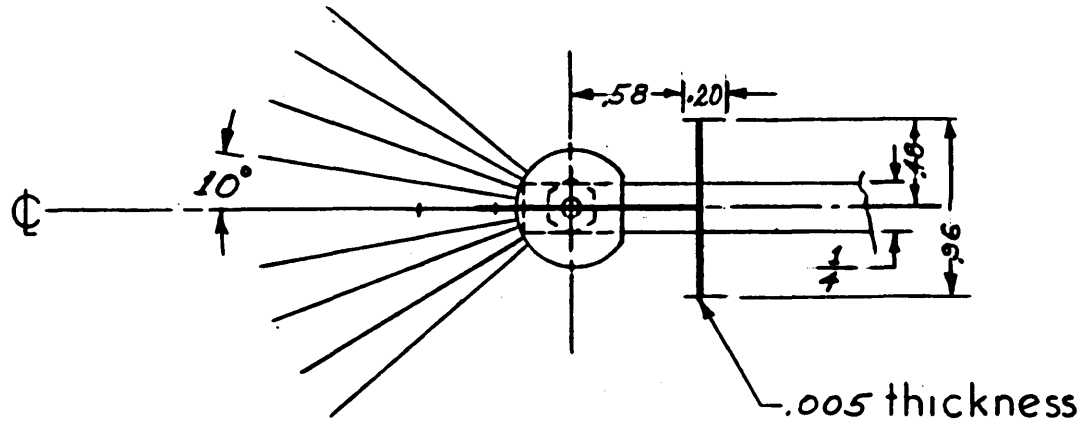

VIEW A-A

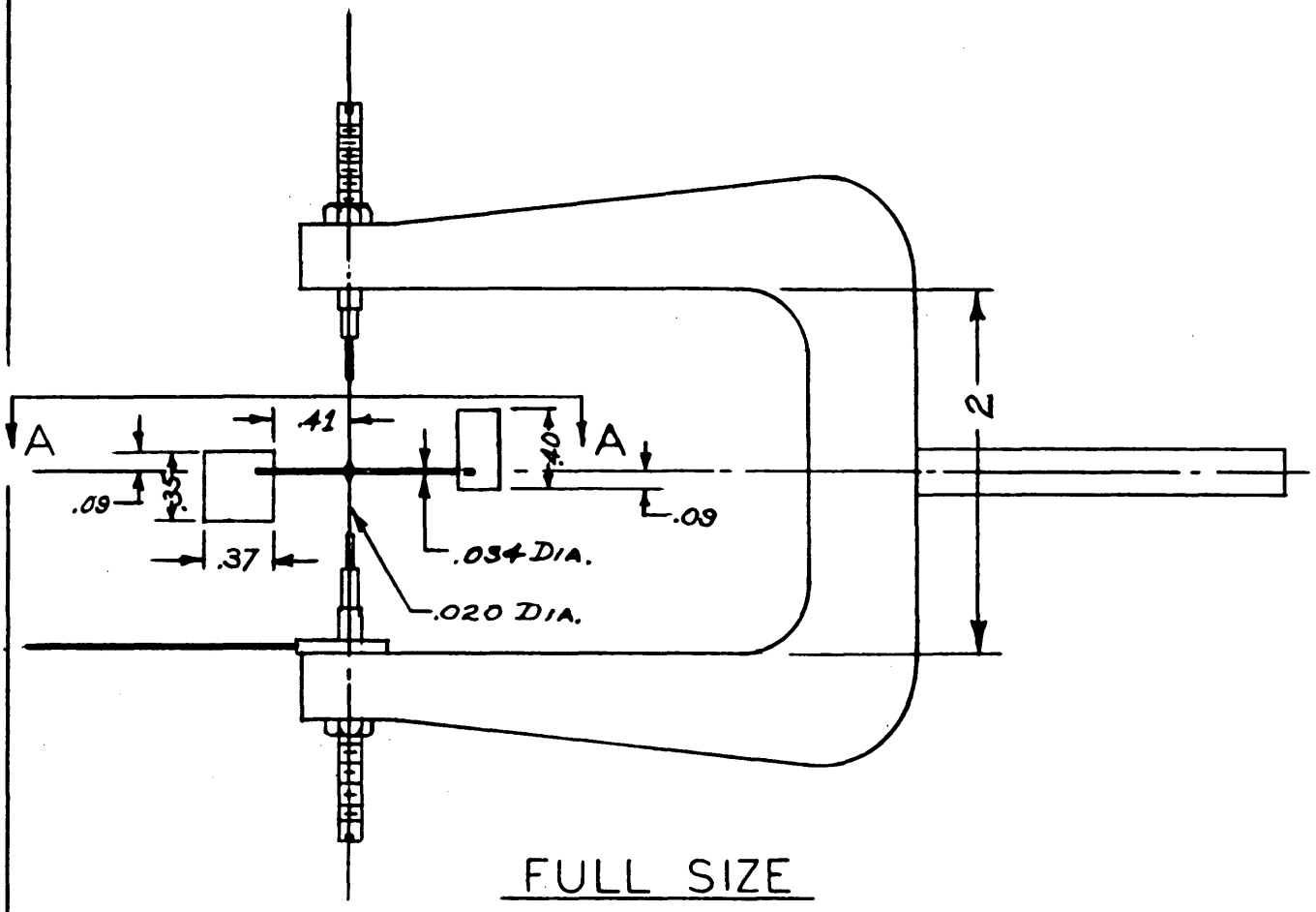

FULL SIZE

WIND DIRECTION INDICATOR
DIFFUSER RESEARCH PROJECT

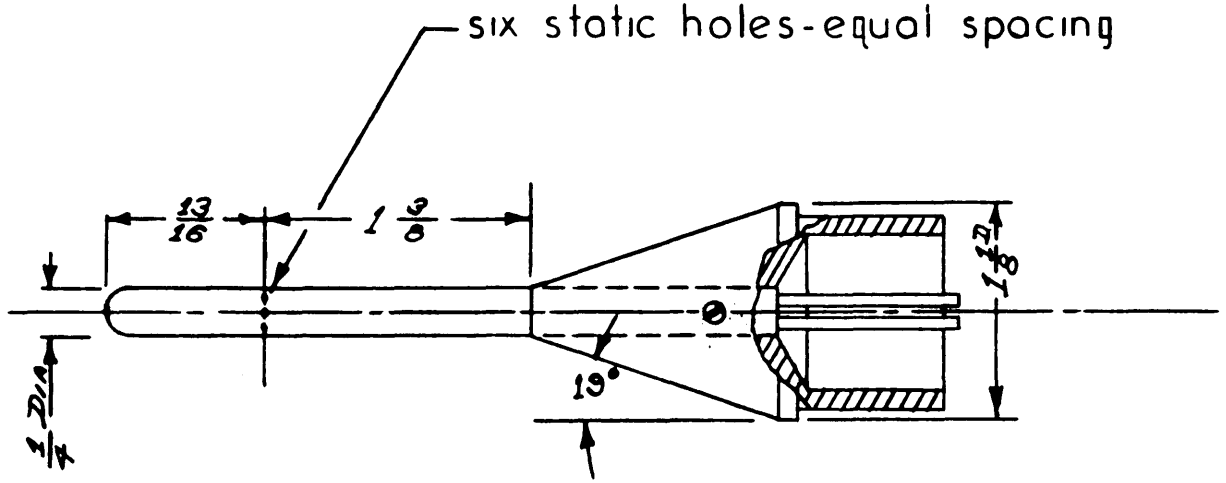

FULL SIZE

PITOT TUBE
DIFFUSER RESEARCH PROJECT

FIGURE-74